Fall 12-11-2020

Synthesis of the Oxidative Metabolites of Di(2-ethylhexyl) phthalate and Analysis of Metabolite Binding with Peroxisome Proliferator-Activated Receptors

Alexis Brooner

Honors Approval Form

Title: Synthesis of the Oxidative Metabolites of Di(2-ethylhexyl) phthalate and Analysis of Metabolite Binding with Peroxisome Proliferator-Activated Receptors

Name: Alexis J. Brooner

Date: December 7th, 2020

Exam Committee:

Dr. E. Davis Oldham, Advisor
Associate Professor of Chemistry

Dr. Kelli M. Slunt
Professor of Chemistry

Dr. Janet A. Asper
Professor of Chemistry

Dr. Sarah E. Smith
Visiting Assistant Professor of Chemistry

Date Approved: 12/11/2020

Synthesis of the Oxidative Metabolites of Di(2-ethylhexyl) phthalate and Analysis of Metabolite Binding with Peroxisome Proliferator-Activated Receptors

By Alexis J. Brooner

Abstract

Di(2-ethylhexyl) phthalate (DEHP) is a persistent organic pollutant that is added to increase the flexibility of soft plastics, such as polyvinyl chloride (PVC). Since DEHP is not bound to the polymer, it leaches into the environment, leading to human exposure. When DEHP is metabolized by the body, it is cleaved into mono-(2-ethylhexyl) phthalate (MEHP). MEHP is then oxidized to produce the secondary-oxidized metabolites mono-(2-ethyl-5-carboxypentyl)phthalate (5cx-MEPP), mono-(2-ethyl-5-oxohexyl)phthalate (5oxo-MEHP), and mono-[2-(carboxymethyl)hexyl]phthalate (2cx-MMHP). DEHP and its metabolites interact with peroxisome proliferator-activated receptors (PPARs), which can alter lipid metabolism. To synthesize 5cx-MEHP, an enolate alkylation was performed with ethyl butyrate to form ethyl 2-ethyl-6-heptenoate. A reduction with $LiAlH_4$ was performed to produce 2-ethyl-6-hepten-1-ol. The alcohol was esterified with phthalic anhydride and subsequently oxidized to produce 5cx-MEHP. This procedure was then repeated to synthesize 2cx-MMHP and 5oxo-MEPP, replacing the enolate alkylation with a malonic ester alkylation and modifying the final oxidation. Binding of the metabolites of DEHP to PPARγ can be assessed using a thermal shift assay. A protocol for the thermal shift assay was developed using the binding of PPARγ and rosiglitazone, a known PPARγ ligand. Information gained surrounding the binding of DEHP and its metabolites to PPARγ may explain the endocrine disrupting effects seen from exposure to phthalate plasticizers by addressing the fundamental question of their cellular targets.

Acknowledgements

I would first like to thank my research advisor, Dr. Davis Oldham, for inviting me to join him on an ongoing project that just so happened to perfectly match my interests in chemistry. Without his email out of the blue I would not have been able to expand my skillset and to explore an area of science in which I had a particular interest. I would also like to thank the members of my committee, Dr. Asper, Dr. Slunt, and Dr. Smith. Dr. Slunt and Dr. Asper served as my organic chemistry professors in semesters one and two, respectively. I discovered a love for organic synthesis through their instruction, for which I am incredibly grateful. The Department of Chemistry as a whole became a family for me, and I have loved the experiences I have been granted at UMW because of the department. I would very much like to thank my fiancé, Noah Swift, for listening to hours of presentations and being a constant support through it all. Finally, I am incredibly thankful for the UMW Summer Science Institute, the UMW Undergraduate Research Grants, and the Mahoney Fellowship, which have funded my research.

Table of Contents

List of Abbreviations

DEHP – Di(2-ethylhexyl) phthalate

MEHP – Mono(2-ethylhexyl) phthalate

2cx-MMHP – Mono-[2-(carboxymethyl) hexyl] phthalate

5cx-MEPP – Mono-(2-ethyl-5-carboxypentyl) phthalate

5oxo-MEHP – Mono-(2-ethyl-5-oxohexyl) phthalate

PVC – Polyvinyl chloride

ADH – Alcohol dehydrogenase

ALDH – Aldehyde dehydrogenase

EDC – Endocrine disrupting chemical

PPAR – Peroxisome proliferator-activated receptor

TSA – Thermal shift assay

LBD – Ligand binding domain

NPC – Protein only control

LOC – Ligand only control

GCMS – Gas chromatography mass spectrometry

NMR – Nuclear magnetic resonance

$LiAlH_4$ – Lithium aluminum hydride

THF – Tetrahydrofuran

DMSO – Dimethyl sulfoxide

DMF – Dimethylformamide

NaHMDS – Sodium bis(trimethylsilyl)amide

qRT-PCR – Quantitative Real-Time Polymerase Chain Reaction

CV – column volume

List of Figures

List of Schemes

I. Introduction

Di(2-ethylhexyl) phthalate and its metabolism

Di(2-ethylhexyl) phthalate (DEHP) (1), is a persistent organic pollutant found ubiquitously in the environment. DEHP (1) is used as a plasticizer in polyvinyl chloride (PVC) plastics.[1,2] A plasticizer is a substance that is used to increase the flexibility of plastics by acting as a molecular lubricant that fits between polymer chains.[3] PVC plastics are frequently found in medical devices and other commercial products. Persistent organic pollutants refer to organic compounds incapable of readily breaking down in the environment. Since DEHP (1) is not chemically bound to the PVC polymer, it can leach into the environment, leading to human exposure via inhalation, ingestion, and absorption through the skin and mucous membranes.[2,4] Toxicological effects of DEHP (1) have been linked to developmental toxicity in animals, hepatocarcinogenesis in rodents, and embryotoxicity in rats and mice, as well as autism spectrum disorders and obesity in humans.[5,6,7,8]

When DEHP (1) is metabolized by the body, it is cleaved into mono-(2-ethylhexyl) phthalate (MEHP) (2) and 2-ethylhexanol (3).[2] This process is catalyzed by esterases and lipases in the pancreas.[9,10] MEHP is then oxidized by several cytochrome P450 (CYP) isoforms, including CYP2C9 and CYP2C19, which are fatty acid omega hydroxylases that act to oxidize organic molecules in the first phase of drug metabolism.[9] This first phase is important for converting the organic molecules to more polar, water-soluble metabolites that can be excreted in the urine.[11] The resulting metabolites are further oxidized by alcohol dehydrogenase (ADH) or aldehyde dehydrogenase (ALDH) to produce the secondary-oxidized metabolites mono-(2-ethyl-5-oxohexyl) phthalate (5oxo-MEHP) (7), mono-(2-

ethyl-5-carboxypentyl) phthalate (5cx-MEPP) (8), and mono-[2-(carboxymethyl) hexyl] phthalate (2cx-MMHP) (9).[2,10] The human metabolism of DEHP (1) is shown in Scheme 1.

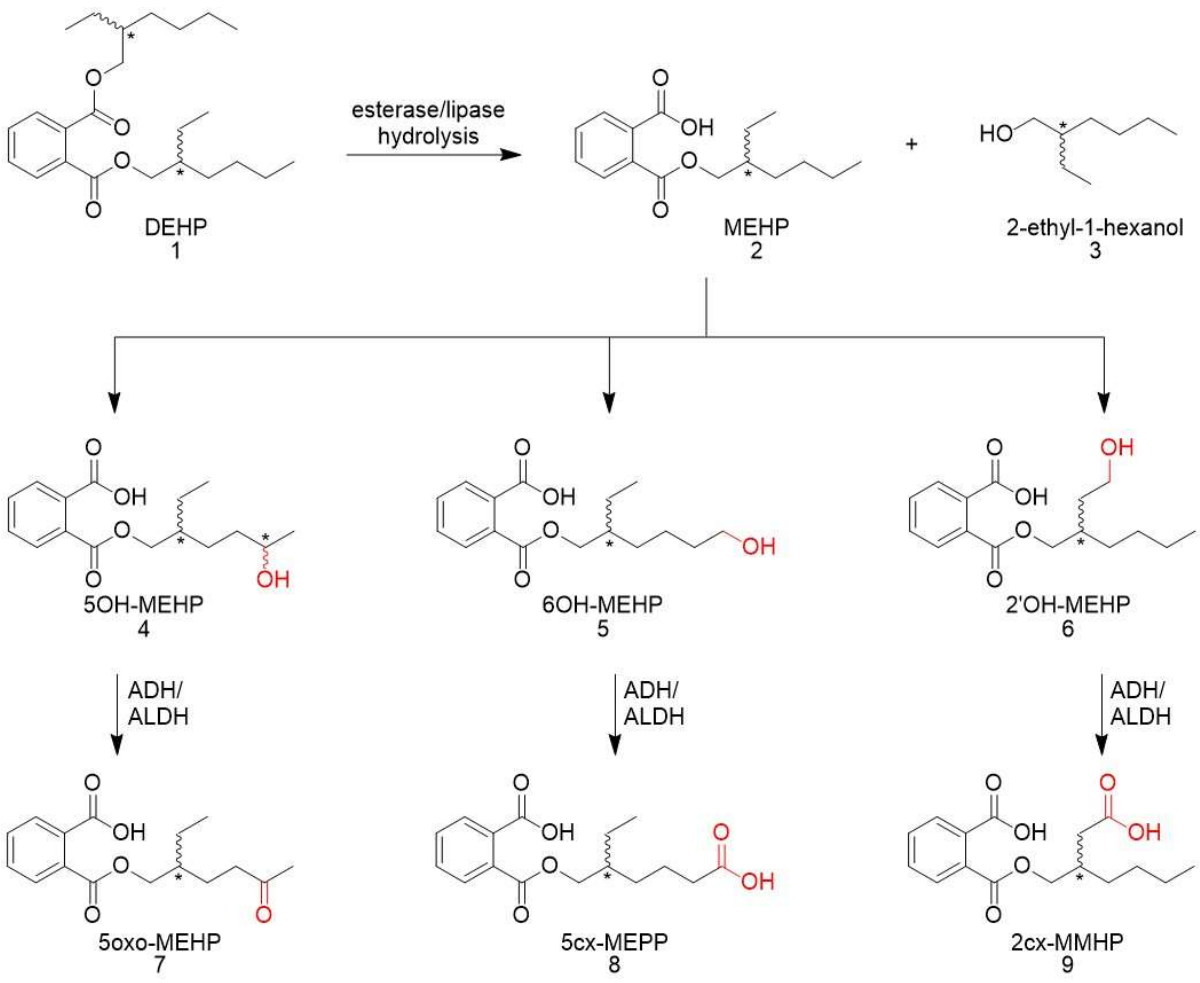

Scheme 1. Human metabolism of DEHP (1). Sites of metabolism are marked in red.

The oxidative metabolites of DEHP (1) have been studied as biomarkers of DEHP (1) exposure.[4,12] It was discovered previously that concentrations of the secondary-oxidized metabolites in human urine is higher than DEHP (1) or MEHP (2) alone.[4,12,13] Additionally, it has been posited that the metabolites themselves may be the cause of the toxic effects of

DEHP (1).[14] However, these previous studies neglect to identify which of the metabolites may have the greatest effect on toxicity.

Phthalate toxicity

DEHP (1) falls under the broader class of chemicals known as phthalates, or phthalate esters, which are esters of phthalic anhydride as seen in Figure 1.

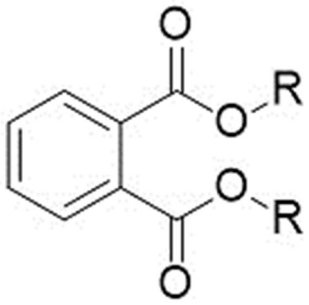

Figure 1. A generic phthalate ester, where R is a branched or linear alkyl chain. The two R groups need not be the same.

Phthalates are known endocrine-disrupting chemicals (EDCs), which are chemicals that alter the function and regulation of the endocrine system.[4,15] EDCs typically function through interaction with nuclear receptors which leads to altered gene expression.[15] Peroxisome proliferator-activated receptors (PPARs) are a type of nuclear receptors with which DEHP (1) is known to interact.[16]

Peroxisome Proliferator-Activated Receptors (PPARs)

Peroxisome proliferator-activated receptors (PPARs) are a family of proteins that are lipid-activated nuclear receptors. Nuclear receptors are a superfamily of transcription factors

that regulate homeostasis and development.[16] PPARs are divided into three subtypes, PPARα, PPARβ/δ, and PPARγ.[17] Each receptor is involved lipid metabolism; therefore disruption of PPAR action can cause an alteration in the regulation of energy maintenance and homeostasis within the body.[5,6,8] PPARα is expressed primarily in the liver, and regulates fatty acid oxidation.[17] PPARβ/δ is expressed ubiquitously in the body, and its primary functions are fatty acid metabolism and the suppression of inflammation caused by macrophages.[17] PPARγ, which was the receptor of focus in this research, is expressed primarily in adipose tissue and regulates adipocyte differentiation and energy storage.[17] The structure of PPARγ is shown in Figure 2A.

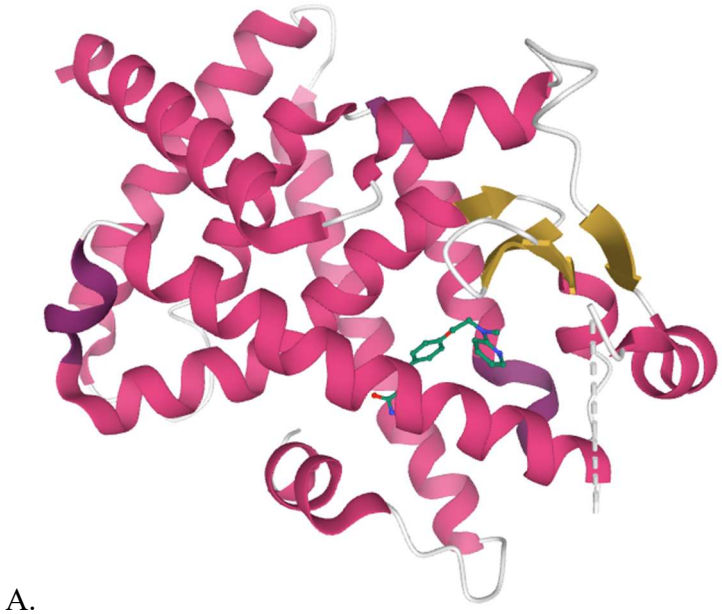

A.

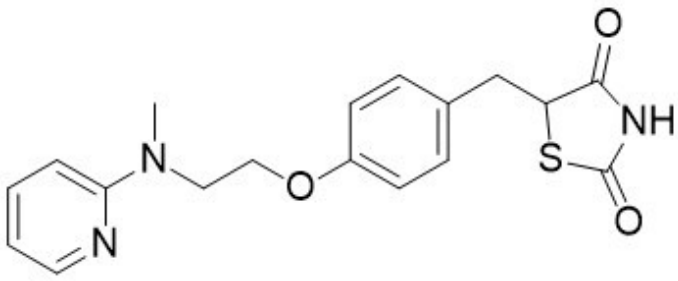

B.

Figure 2. A. Cartoon X-ray diffraction structure of PPARγ ligand binding domain bound to rosiglitazone (PDB code 4EMA).[18] B. Structure of rosiglitazone.

PPARγ is the target of a drug known as rosiglitazone, shown in Figure 2B, which is used to treat diabetes type II and insulin resistance. Rosiglitazone binds to the ligand binding domain of PPARγ and initiates the PPARγ transcriptional cascade, making it a PPARγ agonist.[6] It is known that MEHP (2) binds to PPARγ in a similar manner, acting as a less potent agonist.[6, 19] The predicted binding pocket interactions of PPARγ with MEHP (2) is shown in Figure 3 compared to the binding of rosiglitazone.[19]

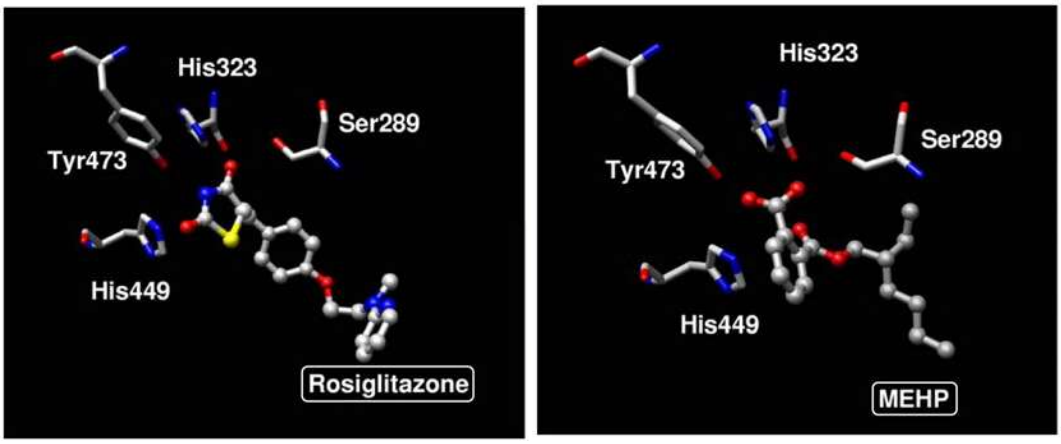

Figure 3. Binding of rosiglitazone to the LBD of PPARγ compared to the predicted binding pocket interactions of MEHP.[19]

It can be predicted that the secondary-oxidized metabolites of DEHP (1) would also bind to PPARγ with similar pathophysiological consequences. This study proposes to examine the binding of PPARγ to rosiglitazone and the secondary-oxidized metabolites of DEHP (1) using a thermal shift assay (TSA).

Synthesis of the oxidative metabolites of DEHP

The purpose of this research is to synthesize the secondary-oxidized metabolites of DEHP (1) and perform a thermal shift assay to assess metabolite binding with the PPARγ ligand binding domain (LBD). This research addresses the need to understand the metabolism of persistent organic pollutants and helps to explain the endocrine disrupting effects seen from exposure to phthalate plasticizers such as DEHP (1) by addressing the fundamental question of their cellular targets. Information gained from this research project surrounding the toxicity of DEHP (1) and its metabolites may be extended to other phthalates and aid in the understanding of the mechanism behind the toxicity of persistent organic pollutants as a whole.

II. Results and Discussion

Synthesis of the secondary oxidized metabolites

Initial attempts to synthesize metabolites 5oxo-MEHP (7), 5cx-MEPP (8), and 2cx-MMHP (9) utilized the malonic ester alkylation. Synthesis of 2cx-MMHP (9) (Scheme 2) was initiated using the procedure outlined by Kelly McDaniel in her previous research on the synthesis of the oxidative metabolites of DEHP (1).

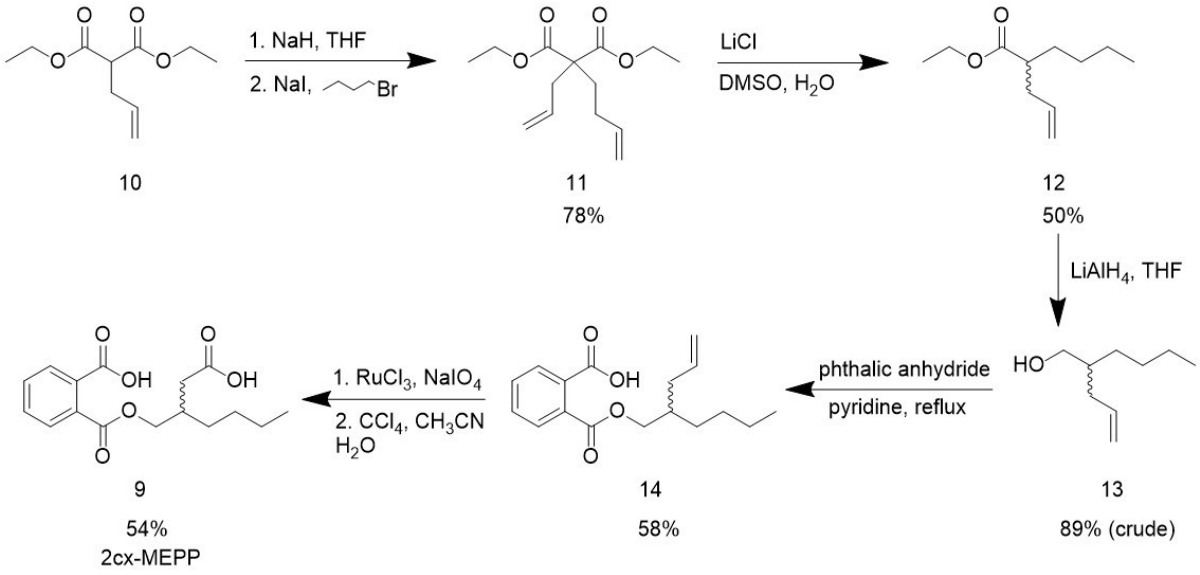

Scheme 2. Synthesis of 2cx-MMHP (9)

The first step is a malonic ester alkylation, which is shown in Figure 4. The synthesis followed a modified procedure in which diethyl allylmalonate (10) was alkylated with allyl bromide.[20] The NaH first deprotonates the malonate and the malonate then performs an S_N2 reaction with the alkyl halide to form a new carbon-carbon bond. Since iodide is a better leaving group than bromide, NaI was added to the reaction to form allyl iodide *in situ*. It was believed this would promote the alkylation of diethyl allylmalonate (10). This reaction

allowed for the production of diethyl allylbutylmalonate (11), the presence of which was verified using ^{1}H NMR (Figure 19).

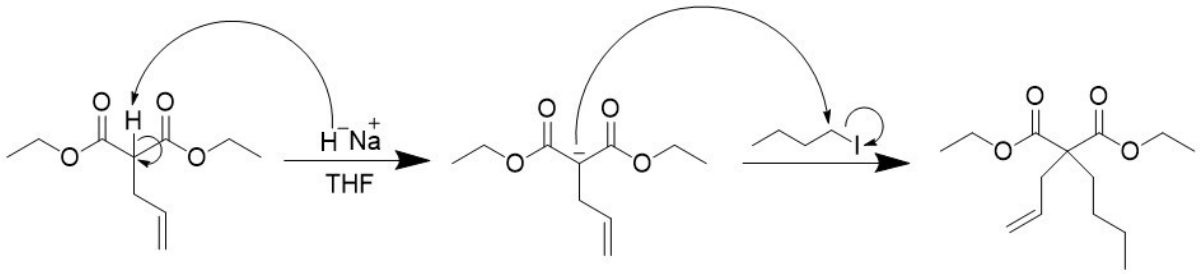

Figure 4. Malonic ester alkylation mechanism

Following the malonic ester alkylation, two possible synthetic methods for the formation of the monoester 2-allyl-hexanoate (12) were proposed. First, a base hydrolysis of the malonic ester (11) using KOH in the presence of H_2O and EtOH with a subsequent decarboxylation was attempted as used previously by Kelly McDaniel. However, several attempts were made using this reaction starting with diethyl allylbutylmalonate (11) with the determination that the hydrolysis was not entirely successful. The hydrolysis produced allylbutylmalonic acid, which was desired, and 2-(allylbutyl)malonic acid ethyl ester (Figure 5), which is only a partial hydrolysis, based on GC-MS of the product (Figure 6). Additionally, the heat involved in the hydrolysis also resulted in the partial decarboxylation of the two hydrolysis products. The full reaction is shown in Scheme 3.

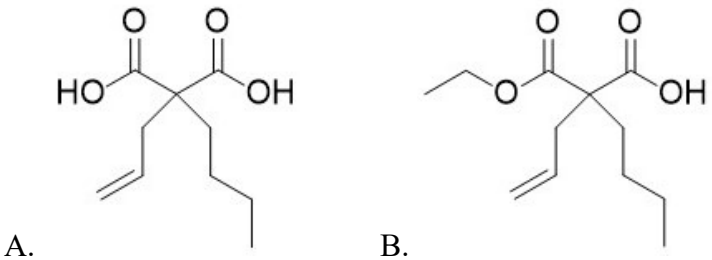

A. B.

Figure 5. Allylbutylmalonic acid (a) and 2-(Allylbutyl)malonic acid ethyl ester (b)

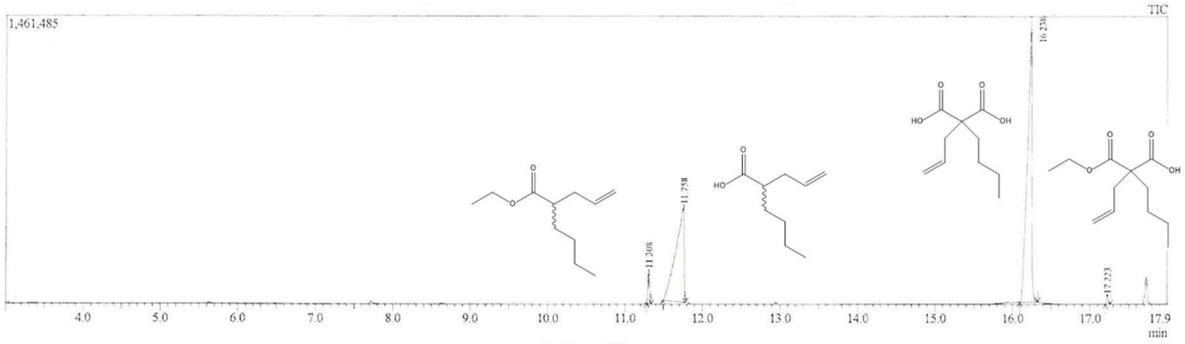

Figure 6. GC-MS of diethyl allylbutylmalonate hydrolysis reaction

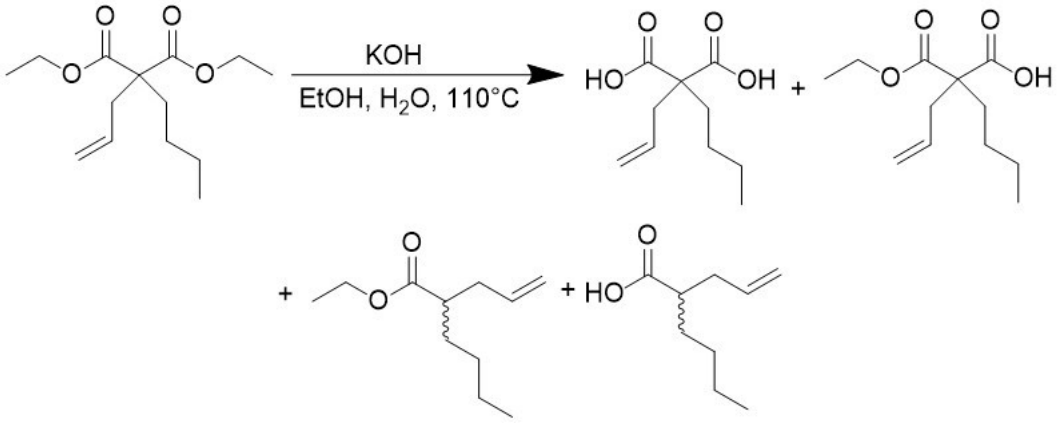

Scheme 3. Hydrolysis and decarboxylation of diethyl allylbutylmalonate (11)

Based on the large mixture of products involved in this reaction, it was determined that the Krapcho decarboxylation would be a suitable replacement, given that it would eliminate the

need for a hydrolysis step. A modified version of the procedure described by Krapcho, et al. was used in which 3 equivalents of LiCl were added per mole of the alkylated diester (11) in a mixture of DMSO and H_2O.[21] The Krapcho decarboxylation, shown in Figure 7, was successful, as evidenced by the production of the monoester ethyl 2-allylhexanoate (12) based on the ^{1}H NMR shown in Figure 20. However, the yield remained low. This issue could be alleviated in the future with the use of a methyl ester rather than ethyl ester as the reaction takes place as an S_N2 reaction in which the chloride ion acts as a nucleophile and attacks the electrophilic carbon in the ester resulting in an electron rearrangement that causes the loss of one of the carboxyl groups in the malonate. The steric hindrance of the methyl ester is lower than that of the ethyl ester which would increase the likelihood of the occurrence of an S_N2 reaction.

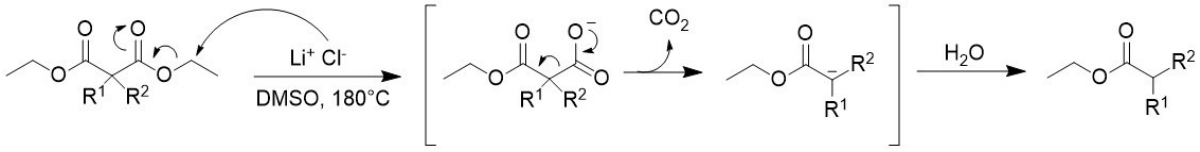

Figure 7. Krapcho decarboxylation of malonic esters

Following the Krapcho decarboxylation, a $LiAlH_4$ reduction was used to form 2-allyl-1-hexanol (13) (Figure 8). The resulting alcohol was analyzed with ^{1}H NMR (Figure 21).

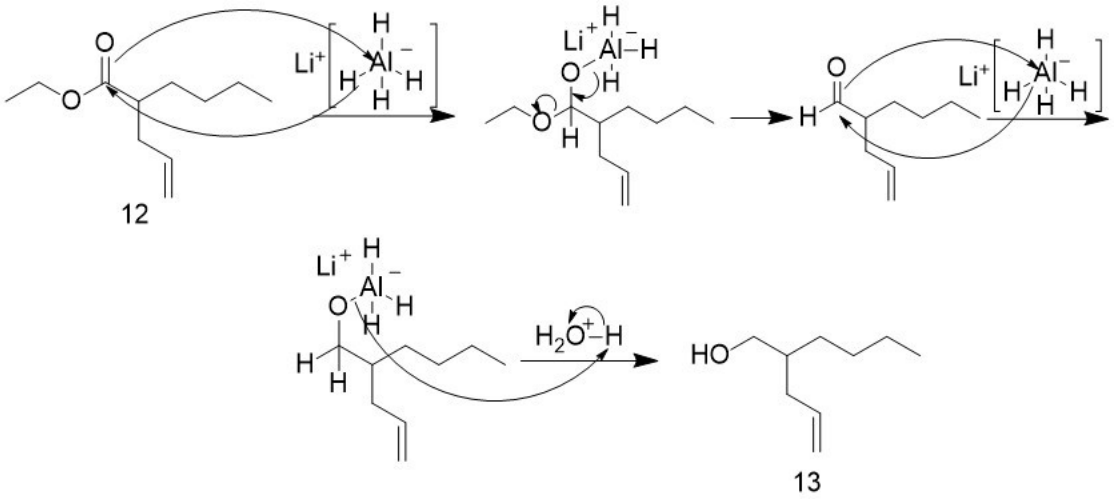

Figure 8. $LiAlH_4$ reduction of ethyl 2-allylhexanoate (12)

A subsequent esterification of the resulting alcohol from the $LiAlH_4$ reduction was performed using phthalic anhydride in pyridine. Then, a ruthenium catalyzed oxidation of the allyl double bond was performed to form 2cx-MMHP (9) (Scheme 4).

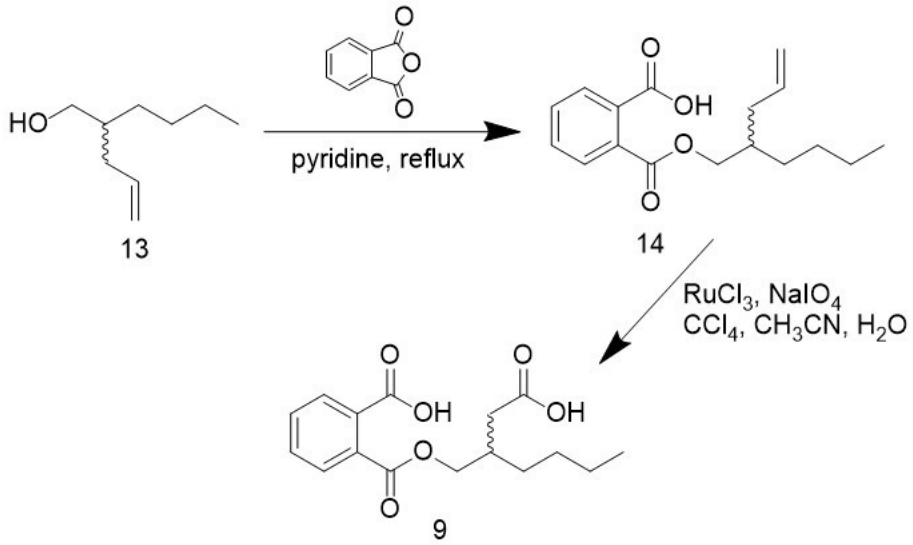

Scheme 4. Esterification and oxidation of 2-allyl-1-hexanol (13)

As shown in Scheme 5, the synthesis of 5oxo-MEHP (7) followed a similar pattern, with the substitution of the starting material with diethyl ethylmalonate (15) and the replacement of the final oxidation with a Wacker oxidation catalyzed by palladium (II) chloride.

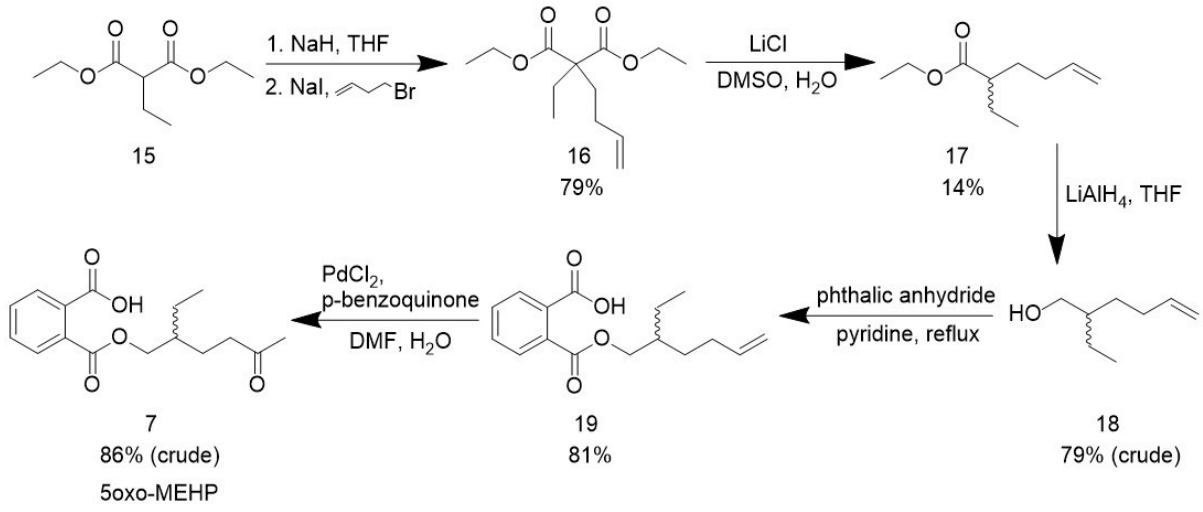

Scheme 5. Synthesis of 5oxo-MEHP (7)

The Wacker oxidation is shown in Scheme 6. This reaction oxidized the double bond in mono(2-ethyl-5-hexenyl) phthalate (19) to form 5oxo-MEHP (7).

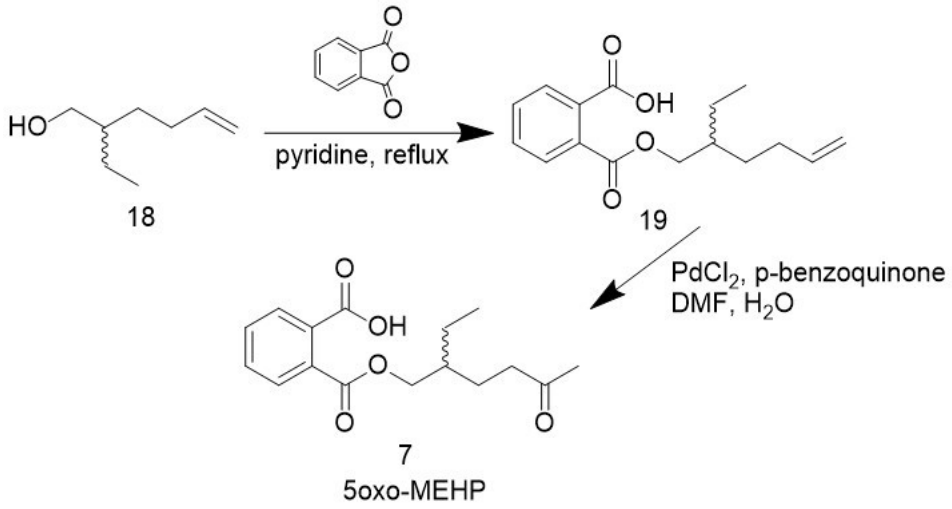

Scheme 6. Esterification and oxidation of 2-ethyl-5-hexenol (18)

The presence of 2cx-MMHP (9) and 5oxo-MEHP (7) were verified with ^{1}H NMR (Figures 23 and 28). The structures of 2cx-MMHP (9) and 5oxo-MEHP (7) with their respective ^{1}H NMR peaks labeled are shown in Figures 9 and 10.

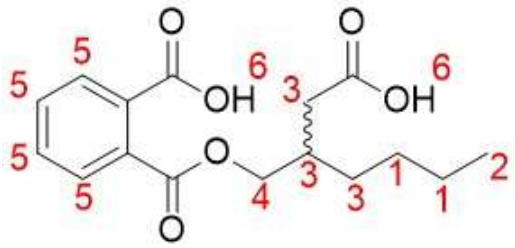

Figure 9. 2cx-MMHP (9) with labeled ^{1}H NMR peaks

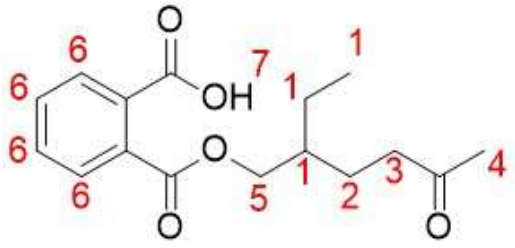

Figure 10. 5oxo-MEHP (7) with labeled ^{1}H NMR peaks

The ^{1}H NMR of 2cx-MMHP (9) shows some contamination with n-hexanes based on the triplet peak at 0.89 ppm. The carboxylic acid peak, which contains both carboxylic acids in the structure, is far lower than a typical carboxylic acid peak at 8.38 ppm. The increased shielding of the hydrogen atoms on the carboxylic acids that caused a lower shift than the expected peak is potentially caused by an intramolecular interaction that must be studied further. The ^{1}H NMR of 5oxo-MEHP (7) was significantly contaminated with dimethylformamide (DMF), which was the solvent used in the Wacker oxidation of mono(2-ethyl-5-hexenyl)phthalate. The peaks of DMF are present at 8.01 ppm, 2.99 ppm, and 2.88 ppm, each of which also corresponds to the chemical shifts of protons on 5oxo-MEHP (7), specifically the carboxylic acid on the aromatic ring, the protons of the terminal alkane, and those of a methylene group internal to the structure.[22] The lower chemical shift caused by the increased shielding of the carboxylic acid protons that resulted in a peak at 8 ppm instead of the expected chemical shift of 10-12 ppm also occurred in 5oxo-MEHP (7). Once again, this may be due to an intramolecular interaction that results in the shielding of the carboxylic acid proton. Additionally, there appears to be residual diethyl ether based on the peaks at 3.48 ppm and 1.21 ppm.[22] The peaks near 1.21 ppm correspond to the ethyl group on 5oxo-MEHP as well.

A synthesis similar to that used in the formation of 2cx-MMHP (9) and 5oxo-MEHP (7) was initiated to form 5cx-MEPP (8). Scheme 7 details the approach used in the previous synthesis attempts of 5cx-MEPP (8) that follows the model of 2cx-MMHP (9) and 5oxo-MEHP (8) in which a malonic acid alkylation (20) is followed by the Krapcho

decarboxylation (21a) before performing a $LiAlH_4$ reduction (22) followed by esterification (23) and oxidation (8).[23]

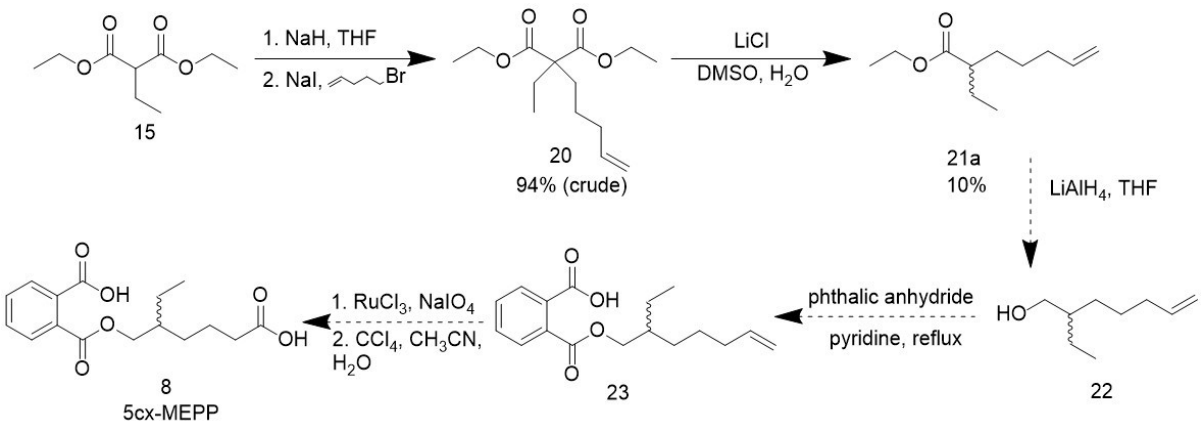

Scheme 7. Proposed synthesis of 5cx-MMHP (8)

Most similar to 5oxo-MEHP (7), diethyl ethylmalonate (15) was used as the starting material, with 5-iodo-1-pentene (24) as the alkyl halide, which was synthesized as shown in Scheme 8.

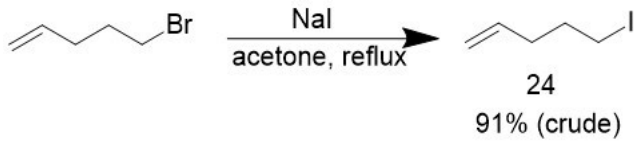

Scheme 8. Synthesis of 5-iodo-1-pentene (24)

The malonic acid alkylation occurred without complication; however, the Krapcho decarboxylation suffered significant difficulties. The reaction time, already long in the formation of monoesters (12) and (17), was increased in an effort to increase the yield of the reaction, but it resulted in the decomposition of the materials of the reaction as shown in Figure 11.

A.

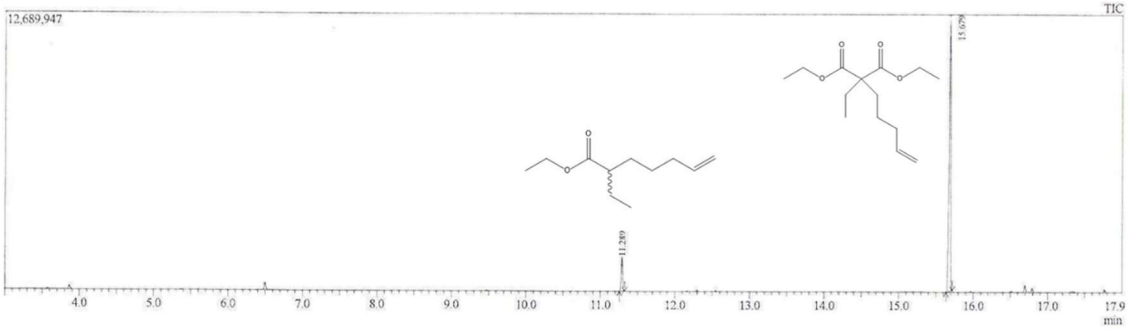
TIC
12,689,947
11.289
15.679
4.0
5.0
6.0
7.0
8.0
9.0
10.0
11.0
12.0
13.0
14.0
15.0
16.0
17.0
17.9
min

B.

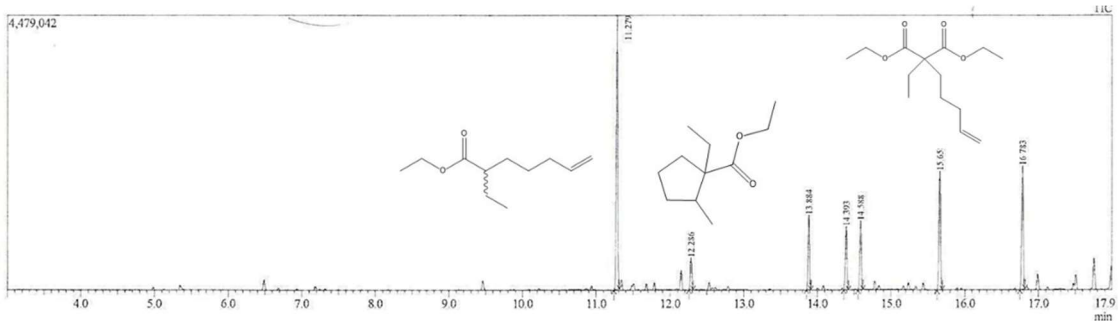
4,479,042
11.279
12.256
13.884
14.393
14.588
15.65
16.783
4.0
5.0
6.0
7.0
8.0
9.0
10.0
11.0
12.0
13.0
14.0
15.0
16.0
17.0
17.9
min

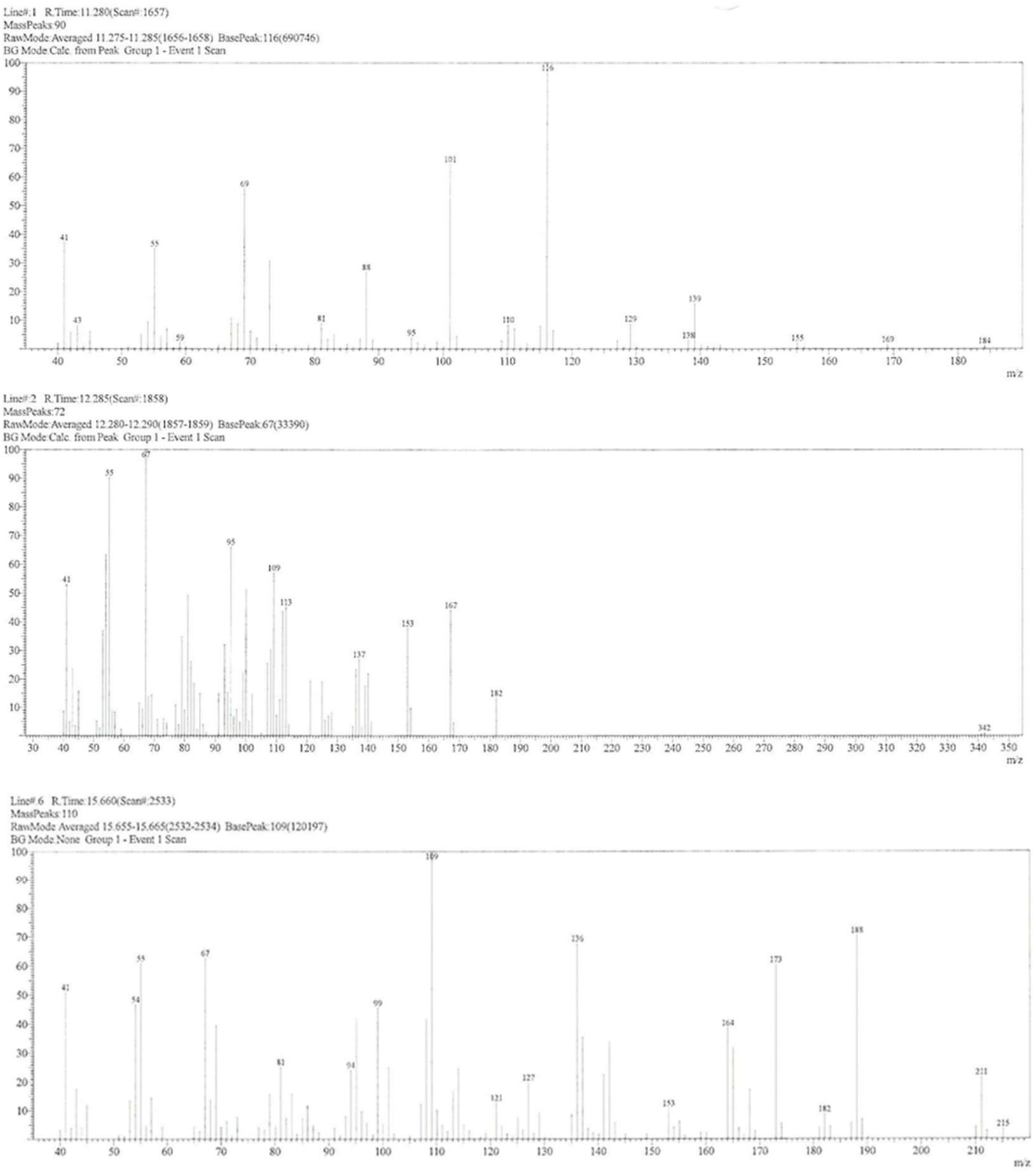

C.

Figure 11. GC-MS of Krapcho decarboxylation reaction progress. A. GC of the Krapcho decarboxylation after 8 hours. B. GC of the Krapcho decarboxylation after 24 hours. C. MS of selected peaks from the GC shown in 11B.

The expected monoester ethyl 2-ethyl-6-heptenoate (21a) failed to form in any significant quantity. As can be seen in Figure 11A, after 8 hours at 180 ℃, only a small amount of product had formed, while a large amount of starting material remained. Figure 11B shows the reaction after 24 hours on heat and shows that several other products were present in the

mixture of product and starting material. This was unanticipated, as the sole difference between the alkylation products (16) and (20) was the alkyl chain of the alkyl halide. The five-carbon chain that originated in 5-iodo-1-pentene (24) appeared to either cause a significant disruption to the mechanism of the Krapcho decarboxylation or to cause the rapid decomposition of the product. One of the decomposition peaks was identified as a potential cyclization reaction referred to as the Conia-Ene reaction shown in Figure 12. A four-carbon chain would form too unstable a ring, which is why that would be unlikely to occur in the formation of 2-ethyl-5-hexenoate (17). The five-carbon chain in ethyl 2-ethyl-6-heptenoate (21a) would, on the other hand, potentially form a ring structure from the pentene chain in the presence of heat.[24]

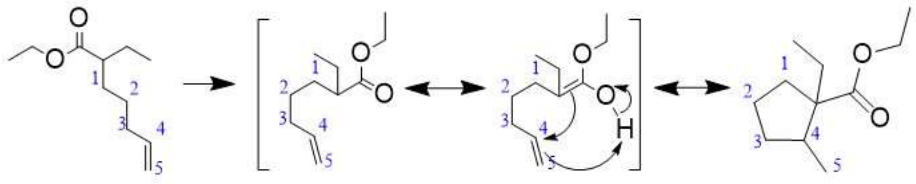

Figure 12. Conia-Ene reaction of ethyl 2-ethyl-6-heptenoate (21a)

Although the MS of the second peak present in the GC does not appear to contain the expected mass peak of the Conia-Ene reaction product at 184 m/z as shown in Figure 11C, the fragments shown may correspond with the Conia-Ene five carbon ring. The peak at 182 m/z would be the M – H_2 peak, and the peak at 153 m/z would be the fragmentation of the ethyl group on the ester. The lack of a corresponding M peak is does not necessarily rule out the Conia-Ene reaction, but it does indicate that further study may be needed to understand the intramolecular rearrangement that resulted in the loss of H_2. Additionally, a peak that was

characteristic in all other derivatives of the Krapcho reaction with diethyl (3-pentenyl)ethylmalonate (20) was at 116 m/z, which is the McLafferty rearrangement that results in the loss of the pentenyl group as shown in Figure 13.

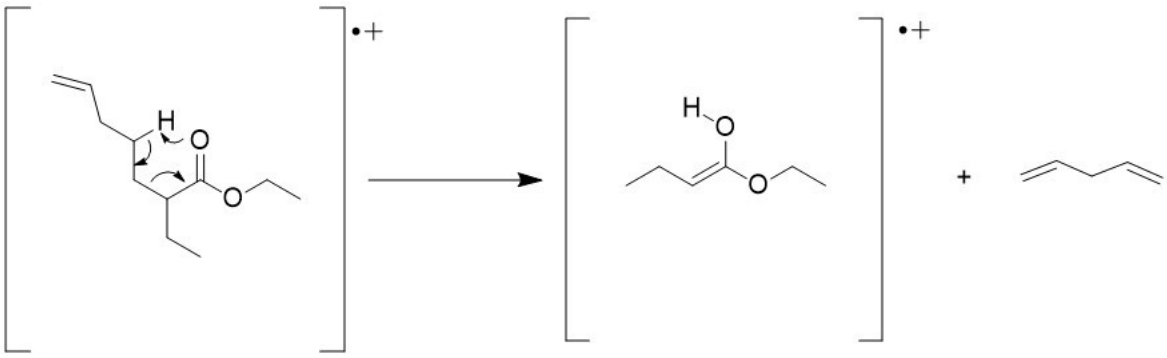

Figure 13. McLafferty rearrangement of diethyl 2-ethyl-6-heptenoate (21a)

This peak was not present in this fraction of the GC-MS, which indicates that the pentenyl group was not present for the McLafferty rearrangement to occur. The failure of the Krapcho decarboxylation as a result of the decomposition of the product of the decarboxylation before a sufficient amount could be recovered, lead to the decision to pursue a new synthesis pathway that would allow the direct formation of the desired monoester ethyl 2-ethyl-6-heptenoate (21a).

An alternative approach for the synthesis of 5cx-MEPP (8) was proposed as shown in Scheme 9. In this procedure, the monoester starting material is first deprotonated by sodium bis(trimethylsilyl)amide (NaHMDS) to form an enolate which can then be attacked by an alkyl halide to bypass the Krapcho decarboxylation in the formation of the desired ester (21b).[25]

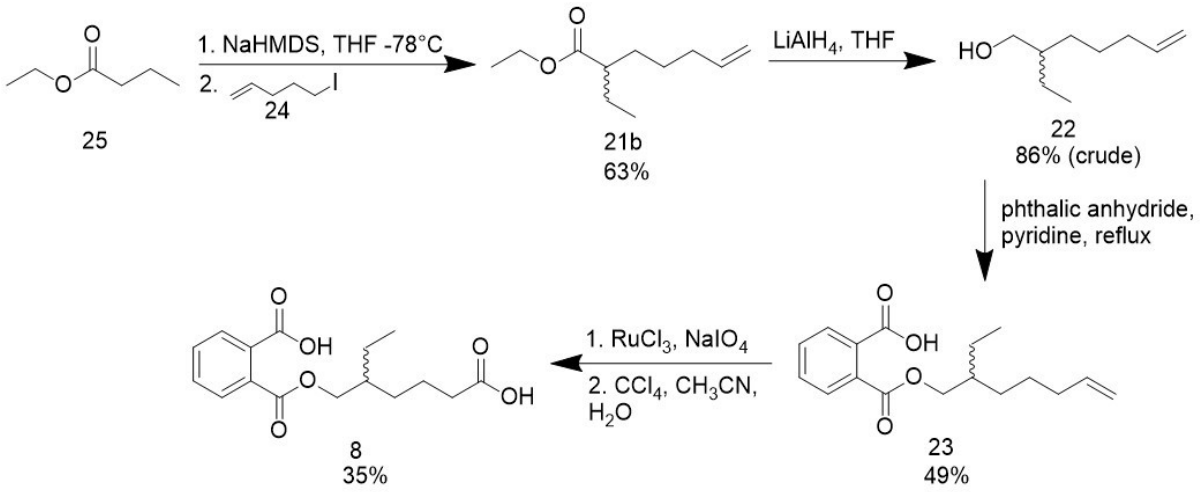

Scheme 9. Alternative synthesis of 5cx-MEPP (8)

The rest of the synthesis is identical to that shown in Scheme 2, where the ester (21b) is reduced by $LiAlH_4$ to form 2-ethyl-6-heptenol (22). The alcohol is then esterified in reaction with phthalic anhydride, with pyridine acting as a base. Oxidation of mono(2-ethylheptenyl) phthalate (23) with ruthenium trichloride and sodium periodate results in the cleavage of the terminal alkene to a carboxylic acid, forming 5cx-MEPP (8).

This enolate alkylation allows for the direct synthesis of ethyl 2-ethyl-6-heptenoate (21b) from ethyl butyrate (25) and 5-iodo-1-pentene (24) in the presence of NaHMDS in THF at -78°C. A modified literature procedure in which 1.2 equivalents of NaHMDS were used was followed as shown in Scheme 10.[25]

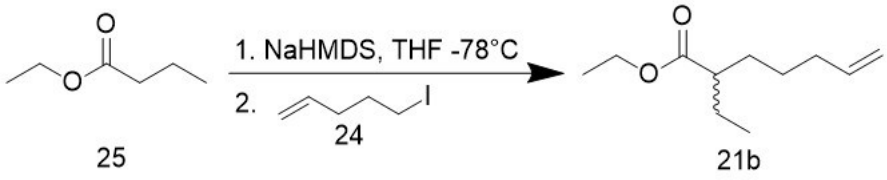

Scheme 10. Enolate alkylation of ethyl butyrate (25)

After the enolate alkylation of ethyl butyrate (25), the rest of the synthesis was identical to that shown for 2cx-MMHP (9) and 5oxo-MEHP (7) where the monoester (21b) was reduced by $LiAlH_4$ producing 2-ethyl-6-heptenol (22). The alcohol was esterified with phthalic anhydride to produce mono(2-ethyl-6-heptenyl) phthalate (23) and subsequently oxidized using a ruthenium-catalyzed reaction to produce 5cx-MEPP (8) as shown in Scheme 15.

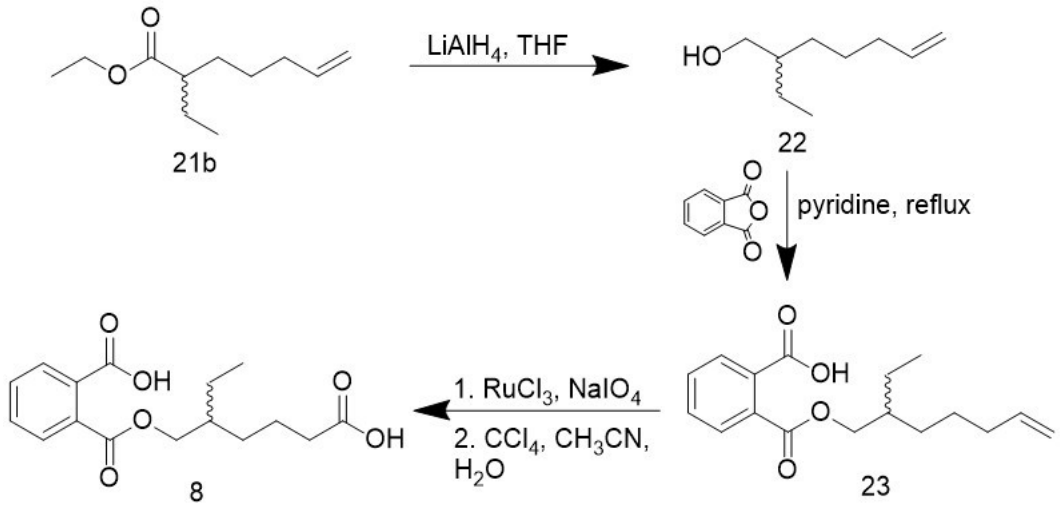

Scheme 11. $LiAlH_4$ reduction, esterification with phthalic anhydride, and oxidation of ethyl 2-ethyl-6-heptenoate (21b)

The presence of 5cx-MEPP (8) was verified with ^1H NMR shown in Figure 32. The structure of 5cx-MEPP (8) with the ^1H NMR peaks labeled is shown in Figure 14.

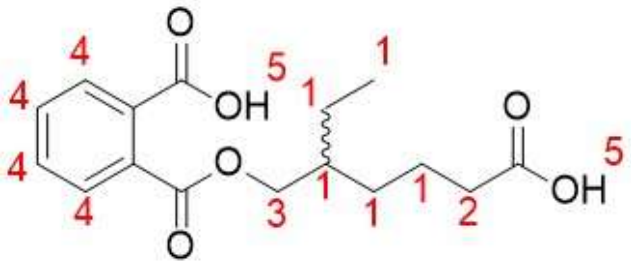

Figure 14. 5cx-MEPP (8) with labeled ^{1}H NMR peaks

The carboxylic acid peaks of 5cx-MEPP (8), similar to the other two secondary oxidized metabolites, are shielded and appear at a lower shift of 8.5 ppm. The peak is broad, and therefore was not integrated as the integral would not be accurate. The reason behind the shielding of the carboxylic acid peaks for all three secondary oxidized metabolites must be investigated further. The sample was also contaminated with dichloromethane (DCM), with a singlet peak at 5.24 ppm, methanol, with a peak at 3.49 ppm, and acetic acid, with a peak at 2.05 ppm.[22] These solvents were used to purify the sample but were difficult to remove following purification. Additionally, there appeared to be some n-hexanes that remained in the sample based on the triplet peak at 0.86 ppm and the multiplet at 1.38 ppm.[22]

Thermal shift assay

The binding of the metabolites of DEHP to PPARγ can be studied through the use of a thermal shift assay (TSA).[26] A common TSA protocol and results are shown in Figure 15. Proteins, such as PPARs, have a characteristic melting point (T_M) at which the temperature is high enough to result in denaturation of 50% of the protein and the loss of protein tertiary structure.[26] When a ligand binds to a protein, the melting point of the protein may change. The melting point will typically increase, given that proteins are generally stabilized by

ligand binding, and the change is directly proportional to the ligand-binding affinity.[26,27,28] TSAs rely on fluorescence; changes in fluorescence are measured as the temperature is increased using the melt curve function of a qPCR instrument following the binding of a fluorescent dye.[29,30]

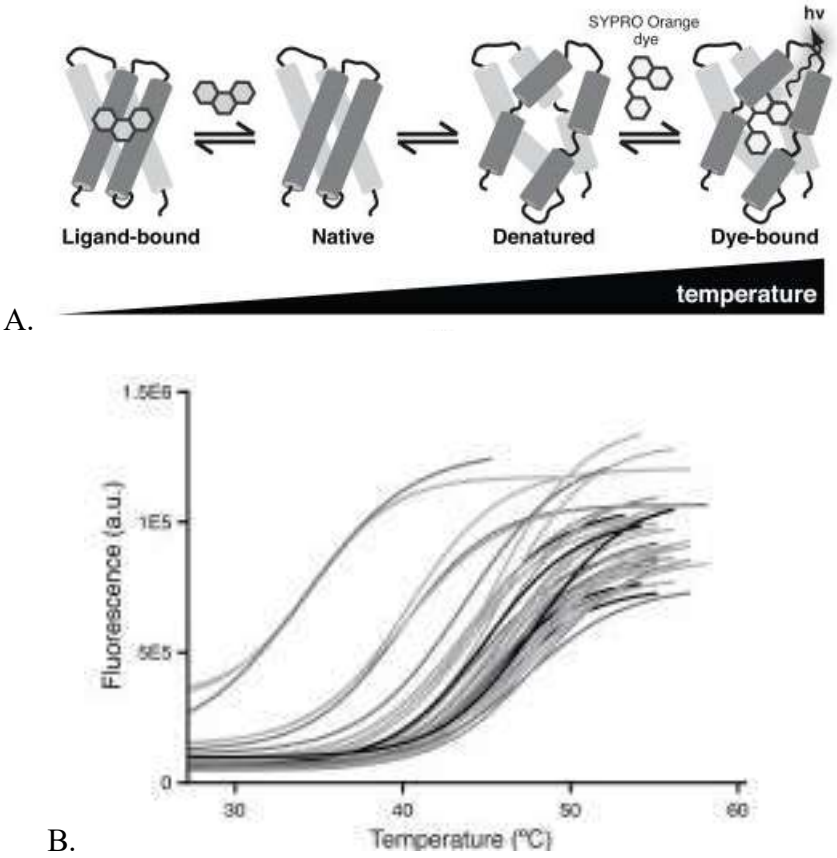

Figure 15. A. The effect of temperature on the denaturation of a ligand-bound protein and the fluorescence of SYPRO Orange dye. B. Sample melt curve plot of fluorescence versus temperature. The curve ends at the T_M.[31]

Protein tertiary structure formation relies on hydrophobic collapse, which refers to the tendency of the hydrophobic regions of the protein to fold together to the interior of the protein and is a result of the interactions between the hydrophobic amino acids of the protein.

This causes the internal regions of the protein to be primarily hydrophobic. As the protein is denatured, the hydrophobic interior is exposed, allowing the binding of the fluorescent dye to this hydrophobic core as shown in image A of Figure 15, which results in a significant increase in fluorescence at that point.[26] Therefore, the protein-dye complex fluoresces at the temperature at which the protein denatures and the fluorescence can be plotted versus the increasing temperature to produce a melt curve analysis such as that shown in Figure 15B. The melt curve analysis can then be used to determine the shift in the melting temperature of the native, unbound protein compared to the ligand-bound protein. A significant increase in the melt temperature of the ligand-bound protein indicates that the stability of the protein is increased by its binding to the ligand. The ligand-protein interaction is therefore considered favorable. Within the context of this study, the oxidative metabolites of DEHP (1) would be predicted to bind to PPARγ and increase its melting temperature relative to the unbound PPARγ, indicating that the ligands are likely to bind to PPARγ and affect its transcription activity.

Thermal Shift Assay using PPARγ and Rosiglitazone

The thermal shift assay was expected to provide information regarding the binding of DEHP (1), MEHP (2), and the secondary-oxidized metabolites 2cx-MMHP (9), 5oxo-MEHP (7), and 5cx-MEPP (8) to PPARγ LBD. In order to optimize the conditions required for PPARγ binding, the assay was first performed with known PPARγ ligand rosiglitazone. Rosiglitazone is used as an antidiabetic drug, and functions by stimulating PPARγ to activate the transcriptional cascade involved in adipogenesis.[32] Since binding of a ligand to a protein typically stabilizes the structure of the protein and increases its melting temperature, this was

expected to be seen in the melt curve of PPARγ and rosiglitazone. Previous research suggested that PPARγ binding to rosiglitazone was optimal with rosiglitazone at a concentration of 200 µM; therefore, trials were performed with rosiglitazone at that concentration and above.[33] Initially, given that PPARγ LBD was received in a buffer containing 50 mM Tris HCl, 100 mM NaCl, 1 mM TCEP, and 20% glycerol at pH 8.0, the entire assay was conducted using this buffer. Each well in use contained 5 µL of this buffer, along with 2.5 µL of dye, which was a proprietary mixture by ThermoFisher that emits/excites at ROX optical filter parameters, while experimental wells contained 3 µL, or 2 µM of PPARγ LBD and varying concentrations of rosiglitazone between 100 µM and 200 µM. The wells were then filled to 20 µL total with DI H_2O. The melt curve of the assay conducted using the 50 mM Tris HCl, 100 mM NaCl, 1 mM TCEP, and 20% glycerol buffer at pH 8.0 is shown in Figure 16.

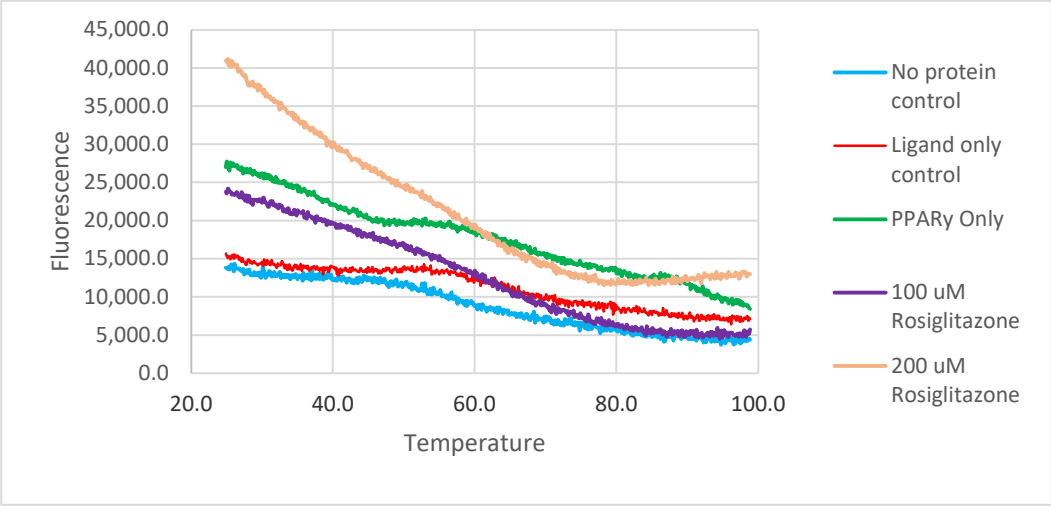

Figure 16. Melt curve of PPARγ with rosiglitazone using buffer containing glycerol

As can be seen in Figure 16, the fluorescence emission was at too high an initial level and the emission expected from the denaturation of the protein was not able to be measured both without ligand and in the presence of ligand. There was no melt curve, which means the dye did not bind to the protein. This was potentially due to the fact that the proprietary dye mixture provided by ThermoFisher in the thermal shift assay kit was not designed to bind with membrane proteins or proteins in buffer containing hydrophobic elements.[34]

Since the buffer used in the assay contained 20% glycerol, which is a hydrophobic molecule that may have interacted with the dye, it was determined that a 0.1 M phosphate buffer at pH 7.0 would be used in future assays. Additionally, given that that the dye mixture did not appear to bind sufficiently with the hydrophobic core of the PPARγ LBD when denaturation occurred, a new dye, SYPRO Orange, was selected, given that SYPRO Orange is a standard dye used in thermal shift assays.[31] A second thermal shift assay was performed using PPARγ and rosiglitazone, but with the newly selected buffer and dye. The melt curve of this assay can be seen in Figure 17.

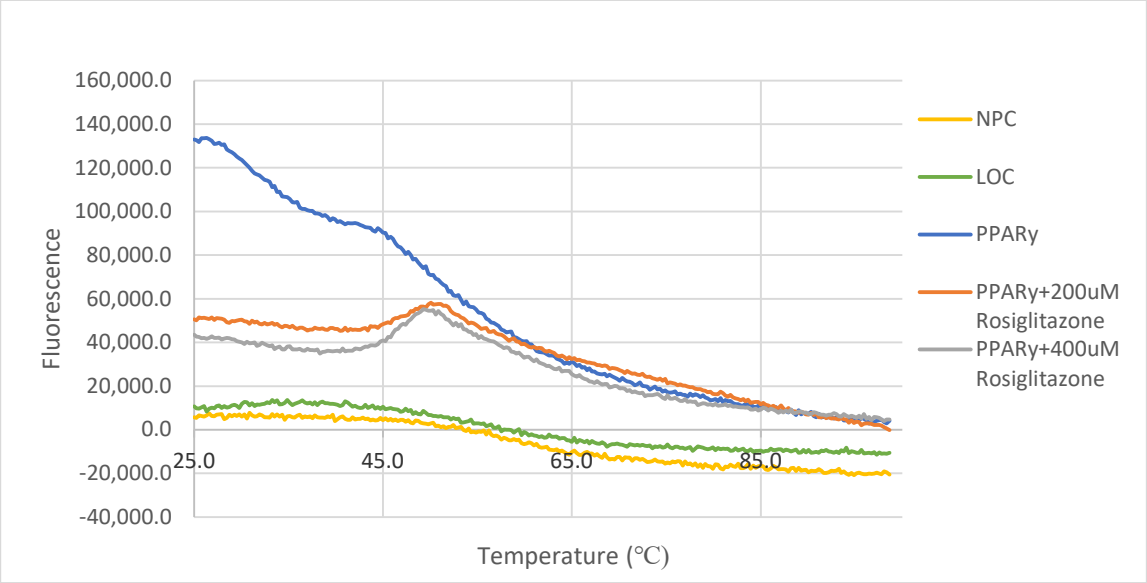

Figure 17. Melt curve of PPARγ with rosiglitazone in phosphate buffer and SYPRO Orange.

The melt curve shown in Figure 17 demonstrates the expected increase in fluorescence emission when the PPARγ LBD was denatured. Although the melt curve of the wells containing only PPARγ was out of proportion initially with the rest of the fluorescence, the obvious peaks in the wells containing rosiglitazone indicate that the protocol designed was effective. It is possible that the PPARγ began denaturing at a temperature below 25°C, which would explain the high fluorescence prior to reaching its expected T_M, or the PPARγ LBD may have native fluorescence, so in the future it may be valuable to perform a TSA with the PPARγ unbound to SYPRO orange dye. The lack of a melt curve in the NPC and LOC wells indicates a lack of contamination as well as that there were no other fluorescence emitting substances besides the protein that would have skewed the results in the experimental wells. Using the first derivative of the fluorescence with respect to the temperature, the melt temperature of the protein in the absence and presence of rosiglitazone

could be determined. Where the graph shows peaks and the slope is equal to zero is considered to be the T_M. The first derivative graph is shown in Figure 18.

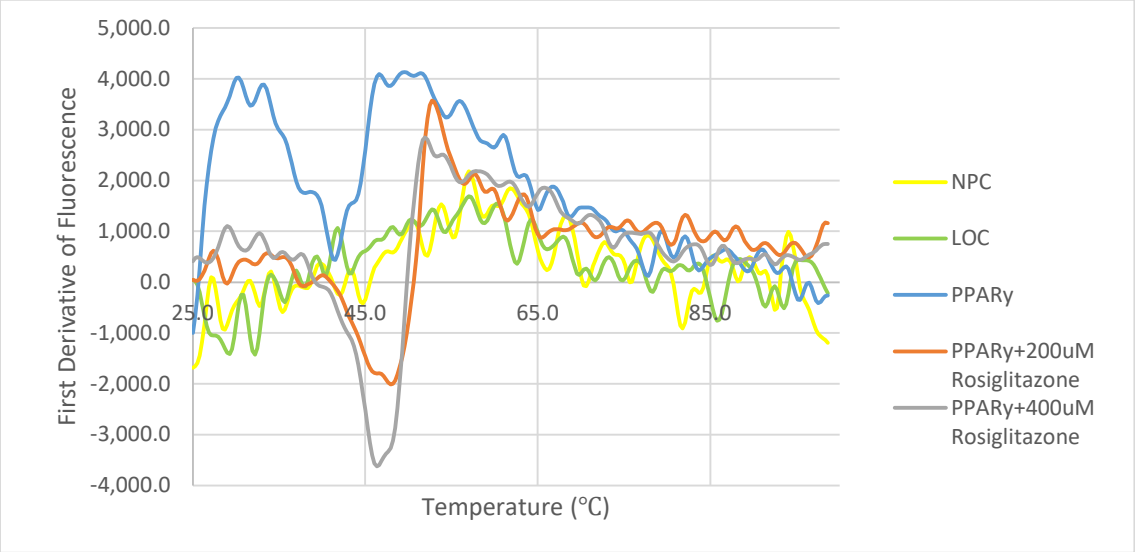

Figure 18. Graph of the first derivative of the fluorescence with respect to the temperature.

The graph of the first derivative indicates the melting temperature of the protein. It can be seen that the PPARγ only well showed two melting points, the first of which had a greater fluorescence intensity. The first T_M of the PPARγ not in the presence of rosiglitazone was 30.20°C, while the second T_M was found to be 49.52°C. These temperatures were then used for comparison with the melting temperature of the protein in the presence of ligand. The first temperature determined from the assay is lower than that found in the literature, 48.75 ± 0.08°C; however, the literature values were obtained using a TSA in a different buffer.[35] The second T_M of 49.52°C is very similar to the literature. The first T_M obtained is more similar to that determined by David Nunez and Dr. Kelli Slunt in their research on PPARγ binding to rosiglitazone, which was 31.83°C.[33] In the future, it may be valuable to

experiment using the buffer cited in the literature in order to obtain temperatures that may be better analyzed.

In the experimental wells containing rosiglitazone, an increase in the T_M can be seen. Based on the first derivative graph, it was determined that the T_M of PPARγ in the presence of rosiglitazone increased to 52.87℃ for 200 μM and 51.94℃ for 400 μM added rosiglitazone. This indicated that the assay designed was successful in demonstrating the effect of ligand binding on the stability of PPARγ, which would allow further testing of ligands, such as DEHP (1), MEHP (2), and the secondary-oxidized metabolites (7-9) using this protocol.

III. Conclusion and Future Work

All three secondary-oxidized metabolites were synthesized; however, analysis of the binding of the secondary oxidized metabolites (7-9) and MEHP (2) to PPARγ remains to be performed. Synthesis of the metabolites on a larger scale should be completed. Therefore, the synthetic scheme used to synthesize 5cx-MEPP (8) using the enolate alkylation, is more efficient than using the malonic ester alkylation combined with the Krapcho decarboxylation. The length of time involved in the Krapcho decarboxylation is extensive, and often resulted in a product with significant impurities that were difficult to fully remove as shown in the ^{1}H NMRs taken of 2-allylhexanoate (12) and 2-ethyl-5-hexenoate (17). While the Krapcho was an improvement on the KOH hydrolysis and subsequent decarboxylation with heat in terms of generating the desired product, the yield was usually low following purification, which would prove a hindrance in scaling up the reactions. Therefore, proposed synthetic mechanisms for 2cx-MMHP (9) and 5oxo-MEHP (7) using the enolate alkylation are shown in Scheme 12 and 13, respectively.

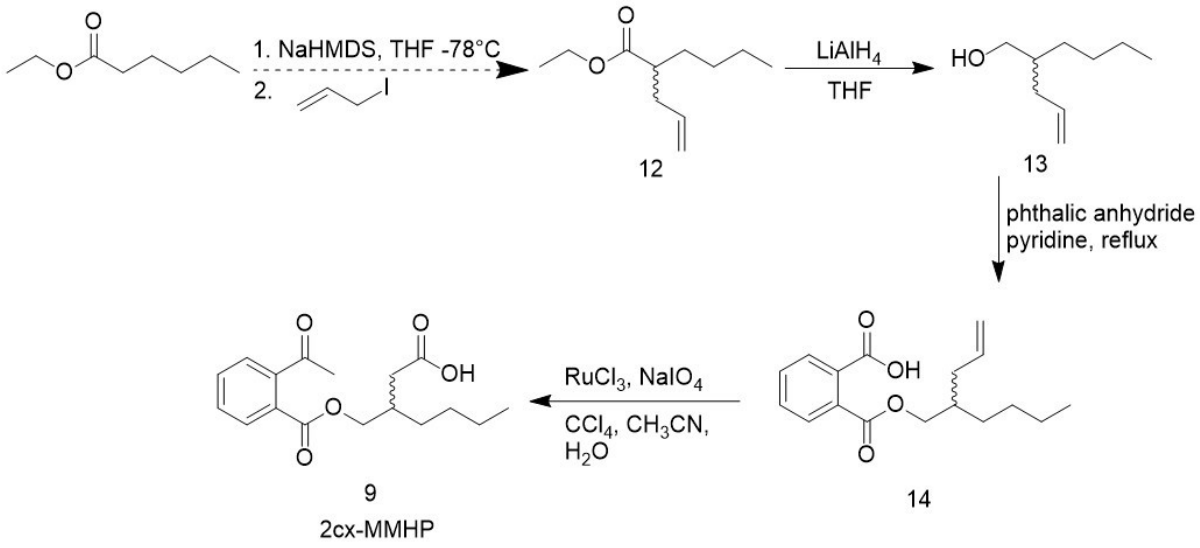

Scheme 12. Synthesis of 2cx-MMHP (9) using the enolate alkylation

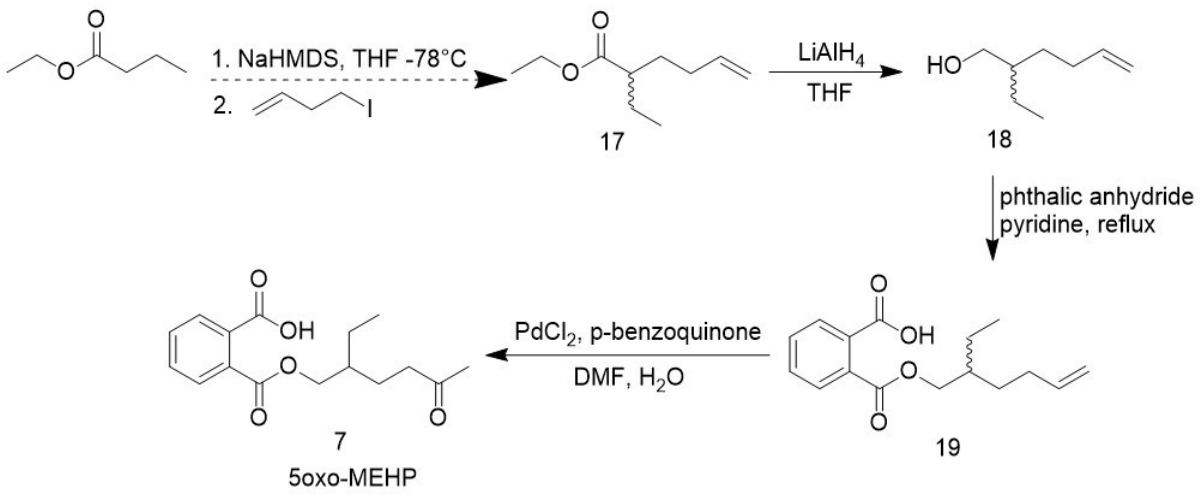

Scheme 13. Synthesis of 5oxo-MEHP (7) using the enolate alkylation

Once the metabolites have been synthesized in greater quantity, their binding with PPARγ can be tested using the TSA protocol developed. The dose response of PPARγ binding to the metabolites would be interesting to examine by performing the TSA with a variety of concentrations of the secondary-oxidized metabolites.

Additionally, since DEHP (1) is a chiral molecule, in the future it would be important to consider the effect of chirality on the binding of PPARγ and the secondary-oxidized metabolites. Enzymes, including PPARγ, are chiral molecules, and often show preference for one enantiomer of a chiral ligand over the other. The synthesis used to form 2cx-MMHP (9), 5oxo-MEHP (7), and 5cx-MEPP (8) is racemic, meaning there is a mixture of the two possible enantiomers of the metabolites. In order to synthesize enantiomerically pure secondary-oxidized metabolites, an enzymatic resolution could be performed on the alcohol intermediates, 2-allylhexanol (13), 2-ethyl-5-hexen-1-ol (18), and 2-ethyl-6-hepten-1-ol (22). This could be done using *Candida antarctica* lipase to enantioselectively acylate the alcohol intermediates.[36] The (*S*) enantiomer of the alcohol would be acylated with vinyl acetate,

yielding the (*R*) alcohol and (*S*) acetate. These would be separated using column chromatography and the (*S*) acetate would be reduced using $LiAlH_4$ to produce the (*S*) alcohol. A proposed enzymatic resolution using 2-allylhexanol (13) is shown in Scheme 14.[36]

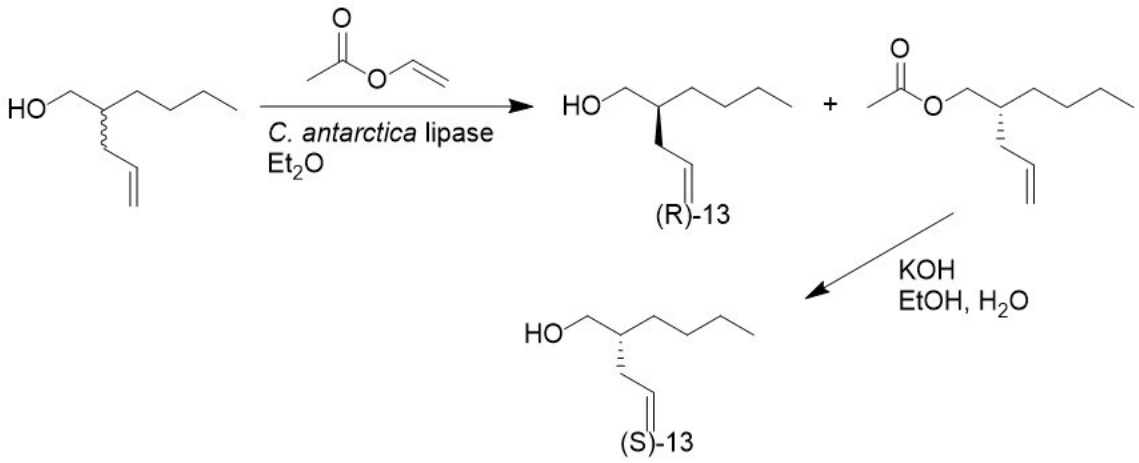

Scheme 14. Enzymatic resolution of 2-allylhexanol (13)

The enantiomerically pure resolved alcohol intermediates would then be used to synthesize enantiomerically pure secondary-oxidized metabolites that could be used to determine the effect of chirality on the binding of the metabolites to PPARγ.

IV. Experimental

The suppliers of all reagents and their purities are listed in the Materials subsection. Anhydrous tetrahydrofuran was dispensed from an MBraun Solvent Purification System. All chemicals were used as supplied unless otherwise specified. Purification of products was performed using column chromatography in a Biotage Isolera One flash chromatography system with Biotage silica gel columns. Gas Chromatography Mass Spectrometry (GC-MS) was performed on a Shimadzu GCMS-QP5050A. Nuclear Magnetic Resonance (NMR) of the oxidative metabolites was performed on a 400 MHz aOne NMR in $CDCl_3$.

Materials

Reagent	Supplier	Purity
Ethyl Ether	Fisher Chemical	Laboratory Grade
Hexanes	Fisher Chemical	99.9%
Ethyl Acetate	Honeywell	>99.5%
Methylene Chloride	Fisher Chemical	99.9%
Pyridine	Fisher Chemical	99.9%
Acetone	Fisher Chemical	99.5%
Methyl Sulfoxide	ACROS Organics	99.9%
Carbon Tetrachloride	ACROS Organics	99.5%
N,N-Dimethylformamide	ACROS Organics	99.5%
Iodoethane	ACROS Organics	98%
1-Iodobutane	ACROS Organics	98%
Diethyl allylmalonate	Alfa Aesar	97%
Ruthenium (III) Chloride	Aldrich	99.98%
Ethyl Butyrate	ACROS Organics	99%
Diethyl ethylmalonate	ACROS Organics	99%
Sodium Iodide	ACROS Organics	98%
Palladium (II) Chloride	ACROS Organics	59% Pd

Lithium Chloride	ACROS Organics	99+%
p-Benzoquinone	Alfa Aesar	98+%
Phthalic Anhydride	ACROS Organics	99%
Sodium Meta Periodate	Fisher Scientific Company	98%
4-Bromo-1-butene	ACROS Organics	98+%
Lithium Aluminum Hydride Solution	Aldrich	1.0 M in THF
Sodium bis(trimethylsilyl)amide	Aldrich	1.0 M in THF
Sodium Hydride	Aldrich	60% dispersion in mineral oil
Magnesium Sulfate Anhydrous	Fisher Chemical	
SYPRO Orange Protein Gel Stain	SIGMA-ALDRICH	5000X concentration in DMSO
PPARγ (LBD) Human Recombinant (His-tagged)	BioVision	>90%

Diethyl allylbutylmalonate (11). A round bottom flask and stir bar were dried in the oven and cooled under nitrogen. NaH (60% dispersion in mineral oil, 1.15 g, 28.8 mmol) was added and the flask was fitted with a septum before placing under nitrogen. THF (92 mL) was added and the flask was placed on an ice bath. The flask was cooled for 15 minutes before adding diethyl allylmalonate (4.81 g, 4.77 mL, 24 mmol). Bromobutane (4.93 g, 3.8 mL, 36 mmol) was added after stirring the flask for 30 minutes at 0°C. The flask was then removed from the ice bath and nitrogen. NaI (1.8 g, 12 mmol) was added. The round-bottom flask was then placed under a condenser with a drying tube filled with glass wool and anhydrous calcium sulfate placed on top. The reaction was then refluxed at 65°C overnight. The reaction was then quenched with DI H_2O (100mL) and extracted with diethyl ether (3x

with 40 mL). The organic layers were combined and dried with $MgSO_4$ and concentrated under vacuum. The resulting liquid was purified using flash column chromatography in hexanes/ethyl acetate with 5% ethyl acetate for 1 column volume (CV) followed by a gradient of 5-40% ethyl acetate for 10 CV and a final 40% ethyl acetate for 2 CV. Diethyl allylbutylmalonate (11) (5.75 g, 22.4 mmol, 78%) was obtained as a pale-yellow liquid. 1H NMR (400 MHz, CDCl3) δ 5.65 (dt, J = 16.9, 8.7 Hz, 1H), 5.07 (p, J = 8.6, 7.3 Hz, 2H), 4.17 (p, J = 8.7, 7.9 Hz, 4H), 2.65 (t, J = 7.8 Hz, 2H), 1.87 (dq, J = 10.6, 6.9, 6.3 Hz, 2H), 1.66 – 1.47 (m, 10H), 1.05 – 0.70 (m, 3H).

2-Allylhexanoate (12). Diethyl allylbutylmalonate (11) (4.31 g, 16.8 mmol) was added to a 250 mL round-bottom flask with a stir bar. DMSO (43 mL), LiCl (2.14 g, 50.4 mmol), and H_2O (0.70 mL) were combined with diethyl allylbutylmalonate (11) and the flask was heated to 180°C with stirring. The flask was heated for 10 hours and allowed to stir overnight. The reaction was quenched with H_2O (150 mL) before extracting with ethyl acetate (3x with 100 mL). The organic layers were combined and washed with brine (150 mL) and dried over $MgSO_4$. The organic layers were then concentrated under vacuum. The resulting liquid was purified using flash column chromatography in hexanes/ethyl acetate with 5% ethyl acetate for 1 column volume (CV) followed by a gradient of 5-40% ethyl acetate for 10 CV and a final 40% ethyl acetate for 2 CV. 2-Allyl-hexanoate (2.91 g, 15.7 mmol, 50%) was obtained as a dark brown liquid. ^{1}H NMR (400 MHz, CDCl3) δ 5.74 (ddt, J = 16.8, 10.2, 6.8 Hz, 1H), 5.09 – 4.96 (m, 2H), 4.30 – 3.93 (m, 1H), 2.46 – 2.29 (m, 2H), 2.27 – 2.14 (m, 1H), 1.60 (qd, J = 9.7, 8.2, 4.4 Hz, 2H), 1.49 (pt, J = 7.6, 3.7 Hz, 2H), 1.40 – 1.08 (m, 7H), 0.88 (t, J = 6.8 Hz, 3H).

2-Allyl-1-hexanol (13). An oven-dried round-bottom flask with a two necked adapter and condenser was placed under nitrogen and on an ice bath. $LiAlH_4$ (1M in THF, 0.80 g, 21.0 mmol, 21.0 mL) was added to the oven-dried flask. In a separate flask a mixture of 2-Allyl-hexanoate (12) (1.3 g, 7.04 mmol) in THF (50 mL) was made under nitrogen. The 2-Allyl-hexanoate (12) in THF solution was added to the flask containing $LiAlH_4$ dropwise. The reaction flask was heated to reflux at 40℃ for two hours. The reaction was then quenched by creating a slurry of 6M HCl (35 mL) in ice (70 g) and the reaction mixture was slowly poured over the slurry. The resulting mixture was extracted with diethyl ether (3x with 35 mL). The organic layers were then combined and washed with brine (35 mL) before being dried over $MgSO_4$ concentrated under vacuum. 2-Allyl-1-hexanol (4) (0.88 g, 6.19 mmol, 89% crude) was obtained as a colorless liquid. ^{1}H NMR (400 MHz, CDCl3) δ 5.82 (ddt, J = 17.2, 10.1, 7.2 Hz, 1H), 5.22 – 4.83 (m, 2H), 3.80 – 3.70 (m, 1H), 3.56 (dd, J = 5.6, 4.1 Hz, 2H), 2.03 (s, 3H), 1.68 – 1.46 (m, 2H), 1.45 – 1.09 (m, 4H), 0.97 (d, J = 6.6 Hz, 3H).

Mono(2-allylhexyl) phthalate (14). A mixture containing 2-allyl-1-hexanol (13) (0.29 g, 2 mmol), phthalic anhydride (0.30 g, 2 mmol), and pyridine (0.2 mL) was made in a round-bottom flask and heated to reflux at 120℃ for three hours. The reaction was then allowed to stir overnight. The reaction mixture was diluted with H_2O (15 mL) and extracted with diethyl ether (3x with 15 mL). The organic layers were combined and washed twice with 3M HCl (15 mL) before being dried over $MgSO_4$ and concentrated under vacuum. The resulting mixture of crystals and liquid was dry loaded into a column and purified using flash column chromatography in hexanes/ethyl acetate with a gradient of 12% ethyl acetate for 1 CV, 12-100% for 10 CV, and 100% for 2 CV. Mono(2-allylhexyl) phthalate (0.33 g, 1.14 mmol, 58%) was obtained as a white crystalline solid. ^{1}H NMR (400 MHz, CDCl3) δ 8.04 (dd, J =

5.8, 2.9 Hz, 1H), 7.96 (dd, J = 5.8, 3.0 Hz, 4H), 5.78 (dd, J = 17.1, 8.9 Hz, 1H), 5.12 – 4.88 (m, 2H), 4.25 (t, J = 5.0 Hz, 2H), 2.15 (d, J = 7.6 Hz, 3H), 1.92 – 1.79 (m, 2H), 1.27 (q, J = 10.1, 6.7 Hz, 4H), 1.00 (t, J = 7.6 Hz, 3H).

2cx-MMHP (9). Mono(2-allylhexyl) phthalate (14) (0.22 g, 0.76 mmol), $NaIO_4$ (0.67 g, 3.10 mmol) and $RuCl_3$ hydrate (3.46 mg, 0.017 mmol) were combined in a round-bottom flask. CCl4 (1.5 mL), CH_3CN (1.5 mL), and H_2O (2.3 mL) were added and the reaction flask was fitted to a septum and allowed to stir overnight. The reaction mixture was diluted with dichloromethane (10 mL) and H_2O (23 mL) and extracted with dichloromethane (3x with 10 mL). The organic layers were combined, dried over $MgSO_4$, and concentrated under vacuum. The product was then purified with flash column chromatography dichloromethane/methanol plus 0.5% acetic acid with 2% methanol for 1 CV, followed by a gradient of 2-20% methanol for 10 CV, followed by 20% methanol for 2 CV. 2cx-MMHP (0.14 g, 0.45 mmol, 54%) was obtained as a viscous, rose-colored liquid. ^{1}H NMR (400 MHz, CDCl3) δ 8.38 (s, 2H), 7.89 (d, J = 7.6 Hz, 1H), 7.68 (d, J = 7.5 Hz, 1H), 7.64 – 7.51 (m, 2H), 4.43 (dd, J = 10.9, 4.2 Hz, 2H), 2.55 (dd, J = 15.8, 6.9 Hz, 2H), 2.31 (tt, J = 12.6, 6.7 Hz, 3H), 1.62 – 1.14 (m, 4H), 0.89 (t, J = 7.1 Hz, 3H).

Diethyl (3-butenyl)ethyl malonate (16). A round-bottom flask and stir bar were dried in the oven and cooled under nitrogen. NaH (60% dispersion in mineral oil, 0.58 g, 14.4 mmol) was added and the flask was fitted with a septum before placing under nitrogen. THF (45 mL) was added and the flask was placed on an ice bath. The flask was cooled for 15 minutes before adding diethyl ethylmalonate (2.26 g, 2.25 mL, 12 mmol). After stirring 30 minutes on ice, 4-bromo-1-butene (2.43 g, 1.83 mL, 18 mmol) was added and the reaction flask was removed from the ice bath and the nitrogen was turned off. NaI (0.90 g, 6 mmol) was added

and the reaction was placed under a condenser with a drying tube containing glass wool and anhydrous calcium sulfate placed on top. The reaction was refluxed at 65℃ overnight. The reaction was quenched with H_2O (50 mL) and extracted with diethyl ether (3x with 20 mL). The organic layers were combined, dried over $MgSO_4$, and concentrated under vacuum. The resulting liquid was then purified with flash column chromatography in hexanes/ethyl acetate using a gradient of 5% ethyl acetate for 1 CV, 5-40% ethyl acetate for 10 CV, and 40% ethyl acetate for 2 CV. Diethyl (3-butenyl)ethyl malonate (8) (2.82 g, 11.6 mmol, 79%) was obtained. ^{1}H NMR (400 MHz, CDCl3) δ 5.78 (ddt, J = 16.0, 11.1, 5.6 Hz, 1H), 4.99 (dd, J = 29.6, 13.7 Hz, 2H), 4.18 (q, J = 7.1 Hz, 4H), 2.62 (d, J = 7.1 Hz, 7H), 1.95 (d, J = 7.6 Hz, 2H), 1.44 – 1.19 (m, 6H).

2-Ethyl-5-hexenoate (17). Diethyl (3-butenyl)ethyl malonate (16) (2.00 g, 8.25 mmol) was added to a round-bottom flask with a stir bar. DMSO (21 mL), LiCl (1.05 g, 24.8 mmol), and H_2O (0.35 mL) were combined with diethyl (3-butenyl)ethyl malonate (16) and the flask was heated to 180℃ with stirring. The flask was heated for 16 hours and allowed to stir overnight. The reaction was quenched with H_2O (75 mL) before extracting with hexanes (3x with 50 mL). The organic layers were combined and washed with brine (75 mL) and dried over $MgSO_4$. The organic layers were then concentrated under vacuum. The resulting liquid was purified using flash column chromatography in hexanes/ethyl acetate with 5% ethyl acetate for 1 column volume (CV) followed by a gradient of 5-40% ethyl acetate for 10 CV and a final 40% ethyl acetate for 2 CV. 2-Ethyl-5-hexenoate (0.20 g, 1.17 mmol, 14%) was obtained as a dark brown liquid. ^{1}H NMR (400 MHz, CDCl3) δ 5.93 – 5.59 (m, 1H), 5.24 – 4.77 (m, 2H), 2.40 (t, J = 7.2 Hz, 2H), 2.15 – 1.86 (m, 2H), 1.74 – 1.66 (m, 7H), 1.27 (d, J = 3.3 Hz, 3H).

2-Ethyl-5-hexen-1-ol (18). An oven-dried three-necked round-bottom flask with a condenser and stir bar placed under nitrogen and in an ice bath. $LiAlH_4$ (1M in THF, 0.13 g, 3.52 mmol, 3.50 mL) was added to the three-necked round-bottom flask. A mixture of 2-Ethyl-5-hexenoate (17) (0.20 g, 1.17 mmol) in THF (8.80 mL) was created in a separate round-bottom flask before being added to the three-necked flask dropwise. The three-necked reaction flask was then removed from the ice bath and heated to 40°C for two hours with stirring. The reaction was allowed to stir overnight. The reaction was quenched by creating a slurry of 6M HCl (6 mL) in ice (12 g) and the reaction mixture was slowly poured over the slurry. The resulting mixture was extracted with diethyl ether (3x with 6 mL). The organic layers were then combined and washed with brine (6 mL) before being dried over $MgSO_4$ concentrated under vacuum. 2-Ethyl-5-hexenol (0.18 g, 1.40 mmol, 79% crude) was obtained. ^{1}H NMR (400 MHz, CDCl3) δ 6.19 – 5.71 (m, 1H), 5.24 – 4.91 (m, 2H), 3.81 – 3.66 (m, 1H), 3.60 – 3.50 (m, 2H), 2.35 – 1.99 (m, 3H), 1.51 – 1.34 (m, 4H), 1.03 – 0.77 (m, 2H).

Mono(2-ethyl-5-hexenyl) phthalate (19). A mixture containing 2-ethyl-5-hexenol (18) (0.18 g, 1.4 mmol), phthalic anhydride (0.21 g, 1.4 mmol), and pyridine (0.15 mL) was made in a round-bottom flask and heated to reflux at 120°C for two hours. The reaction was then allowed to stir overnight. The reaction mixture was diluted with H_2O (10 mL) and extracted with diethyl ether (3x with 10 mL). The organic layers were combined and washed twice with 3M HCl (10 mL) before being dried over $MgSO_4$ and concentrated under vacuum. The resulting crystalline solid was dry loaded into a column and purified using flash column chromatography in hexanes/ethyl acetate using a gradient of 12% ethyl acetate for 1 CV, 12-100% ethyl acetate for 10 CV, and 100% ethyl acetate for 2 CV. Mono(2-ethyl-5-hexenyl)

phthalate (0.24 g, 0.87 mmol, 81%) was obtained as a white crystalline solid. ^{1}H NMR (400 MHz, CDCl3) δ 8.07 (dd, J = 5.6, 3.1 Hz, 1H), 7.72 – 7.60 (m, 4H), 5.87 – 5.80 (m, 1H), 5.02 (dd, J = 28.8, 13.8 Hz, 2H), 4.31 (d, J = 5.6 Hz, 2H), 2.14 (q, J = 7.4 Hz, 3H), 1.60 – 1.38 (m, 4H), 0.96 (t, J = 7.5 Hz, 3H).

5oxo-MEHP (7). A mixture of DMF (2.10 mL) and H_2O (0.30 mL) was made and half of the solution was added to a round-bottom flask containing mono(2-ethyl-5-hexenyl) phthalate (19) (0.24 g, 0.87 mmol) and a stir bar. $PdCl_2$ (1.70 mg, 0.0087 mmol) and p-benzoquinone (0.10 g, 0.96 mmol) were dissolved in the remaining DMF/H_2O. The $PdCl_2$ and p-benzoquinone mixture in DMF/H_2O was added to the flask containing mono(2-ethyl-5-hexenyl) phthalate (19). The reaction was stirred at room temperature overnight. The reaction was quenched with 3M HCl (6 ml) and extracted with diethyl ether (3x with 10 mL). The organic layers were combined, washed with brine (6 mL), dried over $MgSO_4$, and concentrated under vacuum. 5oxo-MEHP (0.22 g, 0.75 mmol, 86% crude) was obtained as a mixture of orange-colored crystals and liquid. ^{1}H NMR (400 MHz, CDCl3) δ 8.01 (s, 1H), 7.55 – 7.52 (m, 4H), 4.11 (d, J = 7.1 Hz, 2H), 2.99 (d, J = 1.3 Hz, 3H), 2.88 (s, 2H), 2.04 (s, 2H), 1.19 (t, J = 7.0 Hz, 6H).

5-Iodo-1-pentene (24). Sodium iodide (10.0 g, 66.8 mmol) was dissolved in acetone (36 mL) in a round-bottom flask. 5-Bromo-1-pentene (5.96 g, 40 mmol, 4.73 mL) was added to the flask. The mixture was heated to 50°C with stirring for one hour. Fractional distillation was used to distill off the acetone, leaving the product behind. Once only the product remained in the flask, DI H_2O (20 mL) was added to the flask. The product was then extracted with ethyl ether (3x with 20 mL). The organic layers were combined and washed sequentially with H_2O (20 mL), saturated sodium sulfite (20 mL), and brine (20 mL). The

organic layers were then dried with $MgSO_4$ and concentrated under vacuum. 5-Iodo-1-pentene (7.47 g, 38.1 mmol, 95% crude) was obtained as a light-yellow liquid. Stored in a refrigerator at 8 ℃.

Diethyl (3-pentenyl)ethyl malonate (20). A round-bottom flask and stir bar were dried in the oven and cooled under nitrogen. NaH (60% dispersion in mineral oil, 0.29 g, 7.2 mmol) was added and the flask was fitted with a septum before placing under nitrogen. THF (23 mL) was added and the flask was placed on an ice bath. The flask was cooled for 15 minutes before adding diethyl ethylmalonate (1.13 g, 1.12 mL, 6 mmol). After stirring 30 minutes on ice, 5-bromo-1-pentene (1.34 g, 1.07 mL, 9 mmol) was added and the reaction flask was removed from the ice bath and the nitrogen was turned off. NaI (0.45 g, 3 mmol) was added and the reaction was placed under a condenser with a drying tube containing glass wool and anhydrous calcium sulfate placed on top. The reaction was refluxed at 65℃ overnight. The reaction was quenched with H_2O (25 mL) and extracted with diethyl ether (3x with 10 mL). The organic layers were combined, dried over $MgSO_4$, and concentrated under vacuum. Diethyl (3-pentenyl)ethyl malonate (20) (1.46 g, 5.70 mmol, 94% crude) was obtained as a yellow-orange liquid.

ethyl 2-ethyl-6-heptenoate (21a). Diethyl (3-pentenyl)ethyl malonate (20) (1.35 g, 5.27 mmol) was added to a round-bottom flask with a stir bar. DMSO (13.4 mL), LiCl (0.67 g, 15.8 mmol), and H_2O (0.23 mL) were combined with diethyl (3-pentenyl)ethyl malonate and the flask was heated to 180℃ with stirring. The flask was heated for 15 hours and allowed to stir overnight. The reaction was quenched with H_2O (47 mL) before extracting with hexanes (3x with 30 mL). The organic layers were combined and washed with brine (47 mL) and dried over $MgSO_4$. The organic layers were then concentrated under vacuum. The resulting

liquid was purified using flash column chromatography in hexanes/ethyl acetate with 5% ethyl acetate for 1 column volume (CV) followed by a gradient of 5-40% ethyl acetate for 10 CV and a final 40% ethyl acetate for 2 CV. Ethyl 2-ethyl-6-heptenoate (0.22 g, 1.19 mmol, 10%) was obtained as a viscous dark brown liquid.

ethyl 2-ethyl-6-heptenoate (21b). Ethyl butyrate (1.17g, 10.0 mmol) was mixed with THF (20 mL) under nitrogen in a round-bottom flask containing a stir bar and fitted with a septum. The reaction flask was placed in an acetone bath and cooled to -78℃ for 15 minutes. NaHMDS (12 mL) was added and allowed to react for 30 minutes while in the acetone bath. 5-Iodo-1-pentene (24) (3.92 g, 20 mmol, 2.45 mL) was added to the reaction flask and the flask was removed from the acetone bath. The reaction was allowed to stir overnight. The reaction mixture was quenched with 1M HCl (50 mL) and extracted with ethyl ether (3x with 50 mL). The organic layers were combined and dried over $MgSO_4$ before being concentrated under vacuum. The resulting liquid was purified using flash column chromatography in hexanes ethyl acetate with 5% ethyl acetate for 1 CV followed by a gradient of 5-40% ethyl acetate for 10 CV and a final 40% ethyl acetate for 2 CV. Ethyl 2-ethyl-6-heptenoate (1.17 g, 6.34 mmol, 63%) was obtained as a transparent liquid. ^{1}H NMR (400 MHz, CDCl3) δ 5.77 (ddd, J = 17.0, 10.2, 6.6 Hz, 1H), 5.05 – 4.90 (m, 2H), 4.16 (dq, J = 14.0, 7.0 Hz, 2H), 2.36 (t, J = 7.2 Hz, 1H), 2.06 (q, J = 6.8 Hz, 2H), 1.44 – 1.17 (m, 9H), 0.97 (d, J = 6.6 Hz, 3H).

2-ethyl-6-hepten-1-ol (22). An oven-dried three-necked round-bottom flask with a condenser and stir bar placed under nitrogen and in an ice bath. $LiAlH_4$ (1M in THF, 0.31 g, 8.14 mmol, 8.14 mL) was added to the three-necked round-bottom flask. A mixture of ethyl 2-ethyl-6-heptenoate (21b) (0.50 g, 2.71 mmol) in THF (20 mL) was created in a separate

round-bottom flask before being added to the three-necked flask dropwise. The three-necked reaction flask was then removed from the ice bath and heated to 40℃ for two hours with stirring. The reaction was allowed to stir overnight. The reaction was quenched by creating a slurry of 6M HCl (14 mL) in ice (25 g) and the reaction mixture was slowly poured over the slurry. The resulting mixture was extracted with diethyl ether (3x with 15 mL). The organic layers were then combined and washed with brine (15 mL) before being dried over $MgSO_4$ concentrated under vacuum. 2-ethyl-6-heptenol (0.35 g, 2.46 mmol, 86% crude) was obtained. ^{1}H NMR (400 MHz, CDCl3) δ 5.40 (s, 1H), 5.09 – 4.86 (m, 2H), 3.81 (s, 1H), 3.25 (d, J = 6.7 Hz, 2H), 2.04 (d, J = 50.9 Hz, 2H), 1.49 (d, J = 1.5 Hz, 1H), 1.20 (s, 6H), 0.90 (d, J = 6.7 Hz, 3H).

Mono(2-ethyl-6-heptenyl) phthalate (23). A mixture containing 2-ethyl-6-heptenol (22) (0.32 g, 2.25 mmol), phthalic anhydride (0.36 g, 2.25 mmol), and pyridine (0.21 mL) was made in a round-bottom flask and heated to reflux at 120℃ for two hours. The reaction was then allowed to stir overnight. The reaction mixture was diluted with H_2O (10 mL) and extracted with diethyl ether (3x with 10 mL). The organic layers were combined and washed twice with 3M HCl (10 mL) before being dried over $MgSO_4$ and concentrated under vacuum. The resulting crystalline solid was dry loaded onto a column and purified using flash column chromatography using hexanes/ethyl acetate with a gradient of 12% ethyl acetate for 1 CV, 12-100% ethyl acetate for 10 CV, and 100% ethyl acetate for 2 CV. Mono(2-ethyl-6-heptenyl) phthalate (0.47 g, 1.62 mmol, 49%) was obtained as a white crystalline solid. ^{1}H NMR (400 MHz, CDCl3) δ 7.88 – 7.74 (m, 1H), 7.54 – 7.39 (m, 4H), 5.70 (td, J = 10.2, 5.2 Hz, 1H), 4.17 (dd, J = 5.7, 3.3 Hz, 2H), 1.97 (s, 3H), 1.78 – 1.52 (m, 6H), 1.18 (t, J = 7.2 Hz, 3H).

5cx-MEPP (8). Mono(2-ethyl-6-heptenyl) phthalate (23) (0.30 g, 1.03 mmol), $NaIO_4$ (0.90 g, 4.22 mmol) and $RuCl_3$ hydrate (4.71 mg, 0.023 mmol) were combined in a round-bottom flask. CCl4 (2.0 mL), CH_3CN (2.0 mL), and H_2O (3.1 mL) were added and the reaction flask was fitted to a septum and allowed to stir overnight. The reaction mixture was diluted with dichloromethane (11 mL) and H_2O (24 mL) and extracted with dichloromethane (3x with 11 mL). The organic layers were combined, dried over $MgSO_4$, and concentrated under vacuum. The product was then purified with flash column chromatography dichloromethane/methanol plus 0.5% acetic acid with 2% methanol for 1 CV, followed by a gradient of 2-20% methanol for 10 CV, followed by 20% methanol for 2 CV. 5cx-MEPP (0.21 g, 0.54 mmol, 35%) was obtained as a viscous, purple-black liquid. ^{1}H NMR (400 MHz, CDCl3) δ 7.85 – 7.75 (m, 1H), 7.66 – 7.59 (m, 1H), 7.58 – 7.42 (m, 2H), 4.26 – 4.11 (m, 2H), 2.33 (t, J = 7.4 Hz, 2H), 1.67 – 1.59 (m, 10H).

Thermal Shift Assay Protocol

The TSAs were carried out using the melt curve function of a QuantStudio 3 qRT-PCR. A stock solution of PPARγ LBD of 0.5 µg/µL in 50 mM Tris HCl, 100 mM NaCl, 1 mM TCEP, and 20% glycerol at pH 8.0 was made and stored at -80°C. A fresh solution of the PPARγ ligand rosiglitazone of 1 mM in DMSO was created each time the assay was performed. SYPRO Orange 5000X dye was diluted with DI H_2O to 80X stock each time the assay was performed. A 96-well plate was used in the assays and wells were filled to 20 µL total solution containing 0.1 M phosphate buffer at pH 7.0, DI H_2O, SYPRO Orange dye, PPARγ LBD, and the ligand of interest. A no protein control (NPC) and ligand only control (LOC) were used to ensure accuracy of the melt curve and to ensure that there were no

ligand-dye interactions or impurities in the buffer that would cause fluorescence in the control wells. In the NPC wells, 0.1 M phosphate buffer (5 µL), SYPRO Orange dye (2.5 µL, 10X concentration), and DI H_2O (12.5 µL) were mixed by pipetting up and down several times. In LOC wells, 0.1 M phosphate buffer (5.0 µL), SYPRO Orange dye (2.5 µL, 10X final concentration), DI H_2O (10.5 µL), and the ligand of interest (2.0 µL, 0.2 mM final concentration) were added. In the reaction wells, PPARγ LBD (3.0 µL, 2.0 µM final concentration) was added along with the ligand of interest (varying concentrations), and 0.1 M phosphate buffer (5.0 µL), SYPRO Orange dye (2.5 µL, 10X final concentration), were mixed and DI H_2O was added until a total volume of 20 µL was reached. The 96-well plate was then sealed and centrifuged at 800 g for 1 minute. The QuantStudio 3 qRT-PCR was set using the following parameters:

Experiment Type: Melt Curve
Reagents: Other
Ramp: Standard
Reporter: SYPRO Orange
Quencher: None
Passive Reference: None
Ramp Mode: Continuous
Thermal Profile: Step 1 – 25°C, 2 minutes, 1.6°C/s
Step 2 – 99°C, 2 minutes, 0.05°C/s
Optical Filters: Excitation – x4(580 ±10)
Emission – m4(623±14)

Targets were set for all wells in use and the melt curve experiment was run. The melt curve results were analyzed using Excel, and the melt temperature for each well in which a melt curve was obtained was estimated by taking the first derivative of the fluorescence emission with respect to temperature.[25]

References

(1) Blount, B. C.; Silva, M. J.; Caudill, S. P.; Needham, L. L.; Pirkle, J. L.; Sampson, E. J.; Lucier, G. W.; Jackson, R. J.; Brock, J. W. Levels of Seven Urinary Phthalate Metabolites in a Human Reference Population. *Environ. Health Perspect.* **2000**, *108* (10), 979–982.

(2) Ito, Y.; Kamijima, M.; Nakajima, T. Di(2-Ethylhexyl) Phthalate-Induced Toxicity and Peroxisome Proliferator-Activated Receptor Alpha: A Review. *Environ. Health Prev. Med.* **2019**, *24* (1), 47.

(3) Kastner, J.; Cooper, D. G.; Marić, M.; Dodd, P.; Yargeau, V. Aqueous Leaching of Di-2-Ethylhexyl Phthalate and "Green" Plasticizers from Poly(Vinyl Chloride). *Science of The Total Environment* **2012**, *432*, 357–364. https://doi.org/10.1016/j.scitotenv.2012.06.014.

(4) Koch, H. M.; Preuss, R.; Angerer, J. Di(2-Ethylhexyl)Phthalate (DEHP): Human Metabolism and Internal Exposure - an Update and Latest Results. *Int. J. Androl.* **2006**, *29* (1), 155–165.

(5) Wassenaar, P. N. H.; Legler, J. Systematic Review and Meta-Analysis of Early Life Exposure to Di(2-Ethylhexyl) Phthalate and Obesity Related Outcomes in Rodents. *Chemosphere* **2017**, *188*, 174–181.

(6) Hurst, C. H.; Waxman, D. J. Activation of PPAR and PPAR by Environmental Phthalate Monoesters. *Toxicol. Sci.* **2003**, *74* (2), 297–308.

(7) Testa, C.; Nuti, F.; Hayek, J.; De Felice, C.; Chelli, M.; Rovero, P.; Latini, G.; Papini, A. M. Di-(2-Ethylhexyl) Phthalate and Autism Spectrum Disorders. *ASN Neuro* **2012**, *4* (4), AN20120015.

(8) Gore, A. C.; Chappell, V. A.; Fenton, S. E.; Flaws, J. A.; Nadal, A.; Prins, G. S.; Toppari, J.; Zoeller, R. T. Executive Summary to EDC-2: The Endocrine Society's Second Scientific Statement on Endocrine-Disrupting Chemicals. *Endocr. Rev.* **2015**, *36* (6), 593–602.

(9) Choi, K.; Joo, H.; Campbell, J. L.; Clewell, R. A.; Andersen, M. E.; Clewell, H. J. In Vitro Metabolism of Di(2-Ethylhexyl) Phthalate (DEHP) by Various Tissues and Cytochrome P450s of Human and Rat. *Toxicol. in Vitro* **2012**, *26* (2), 315–322.

(10) Ito, Y.; Yokota, H.; Wang, R.; Yamanoshita, O.; Ichihara, G.; Wang, H.; Kurata, Y.; Takagi, K.; Nakajima, T. Species Differences in the Metabolism of Di(2-Ethylhexyl)

Phthalate (DEHP) in Several Organs of Mice, Rats, and Marmosets. *Arch. Toxicol.* **2005**, *79* (3), 147–154.

(11) Coleman, M. *Human Drug Metabolism: An Introduction*, Second Edition.; Wiley-Blackwell: Chichester, West Sussex, UK, 2010.

(12) Kato, K.; Silva, M. J.; Reidy, J. A.; Hurtz, D.; Malek, N. A.; Needham, L. L.; Nakazawa, H.; Barr, D. B.; Calafat, A. M. Mono(2-Ethyl-5-Hydroxyhexyl) Phthalate and Mono-(2-Ethyl-5-Oxohexyl) Phthalate as Biomarkers for Human Exposure Assessment to Di-(2-Ethylhexyl) Phthalate. *Environ. Health Perspect.* **2004**, *112* (3), 327–330.

(13) Preuss, R.; Koch, H. M.; Angerer, J. Biological Monitoring of the Five Major Metabolites of Di-(2-Ethylhexyl)Phthalate (DEHP) in Human Urine Using Column-Switching Liquid Chromatography–Tandem Mass Spectrometry. *J. Chromatogr. B* **2005**, *816*, 269–280.

(14) Koch, H. M.; Bolt, H. M.; Preuss, R.; Angerer, J. New Metabolites of Di(2-Ethylhexyl)Phthalate (DEHP) in Human Urine and Serum after Single Oral Doses of Deuterium-Labelled DEHP. *Arch. Toxicol.* **2005**, *79* (7), 367–376.

(15) Chauvigné, F.; Menuet, A.; Lesné, L.; Chagnon, M.; Chevrier, C.; Regnier, J.; Angerer, J.; Jégou, B. Time- and Dose-Related Effects of Di-(2-Ethylhexyl) Phthalate and Its Main Metabolites on the Function of the Rat Fetal Testis in Vitro. *Environ. Health Perspect.* **2009**, *117* (4), 515–521.

(16) Casals-Casas, C.; Feige, J. N.; Desvergne, B. Interference of Pollutants with PPARs: Endocrine Disruption Meets Metabolism. *Int. J. Obes.* **2008**, *32* (S6), S53–S61.

(17) Tyagi, S.; Sharma, S.; Gupta, P.; Saini, A.; Kaushal, C. The Peroxisome Proliferator-Activated Receptor: A Family of Nuclear Receptors Role in Various Diseases. *J Adv Pharm Tech Res* **2011**, *2* (4), 236.

(18) Liberato, M. V.; et. al. Medium Chain Fatty Acids Are Selective Peroxisome Proliferator Activated Receptor (PPAR) γ Activators and Pan-PPAR Partial Agonists. *PLoS ONE* **2012**, *7* (5), e36297.

(19) Feige, J. N.; Gelman, L.; Rossi, D.; Zoete, V.; Métivier, R.; Tudor, C.; Anghel, S. I.; Grosdidier, A.; Lathion, C.; Engelborghs, Y.; Michielin, O.; Wahli, W.; Desvergne, B. The Endocrine Disruptor Monoethyl-Hexyl-Phthalate Is a Selective Peroxisome

Proliferator-Activated Receptor γ Modulator That Promotes Adipogenesis. *J. Biol. Chem*. **2007**, *282* (26), 19152–19166.

(20) Lanners, S.; Norouzi-Arasi, H.; Khiri, N.; Hanquet, G. Solvent- and Structure-Dependent Regioselectivity in the Boron-Mediated Aldol Reaction of 2-(1,3-Dioxolan-2-Yl)Ethyl Ketones. *Eur. J. Org. Chem*. **2007,** *2007* (24), 4065–4075.

(21) McDaniel, K. Synthesis of Oxidative Metabolites of Di(2-Ethylhexyl) Phthalate. Eagle Scholar, University of Mary Washington, 2017.

(22) Gottleib, H. E.; Kotylar, V.; Nudelman, A. NMR Chemical Shifts of Common Laboratory Solvents as Trace Impurities. *J. Org. Chem.* **1997**, *62* (21), 7512-7515.

(23) Krapcho, A. P.; Weimaster, J. F.; Eldrige, J. M.; Jahngen, E.; Lovey, A.; Stephens, W. Synthetic Applications and Mechanism Studies of the Decarbalkoxylations of Geminal Diesters and Related Systems Effected in Dimethyl Sulfoxide by Water and/or by Water with Added Salts. *J. Org. Chem.* **1978**, *43* (1), 138–147.

(24) Cao, M.; Yesilcimen, A.; Wasa, M. Enantioselective Conia-Ene-Type Cyclizations of Alkynyl Ketones through Cooperative Action of B(C 6 F 5) 3 , N -Alkylamine and a Zn-Based Catalyst. *J. Am. Chem. Soc*. **2019**, *141* (10), 4199–4203.

(25) Smith, T. E.; Richardson, D. P.; Truran, G. A.; Belecki, K.; Onishi, M. Acylation, Diastereoselective Alkylation, and Cleavage of an Oxazolidinone Chiral Auxiliary. *J. Chem. Educ.* **2008**, *85* (5), 695.

(26) Grøftehauge, M. K.; Hajizadeh, N. R.; Swann, M. J.; Pohl, E. Protein–Ligand Interactions Investigated by Thermal Shift Assays (TSA) and Dual Polarization Interferometry (DPI). *Acta Crystallogr D Biol Crystallogr* **2015**, *71* (1), 36–44.

(27) Sviben, D.; Bertoša, B.; Hloušek-Kasun, A.; Forcic, D.; Halassy, B.; Brgles, M. Investigation of the Thermal Shift Assay and Its Power to Predict Protein and Virus Stabilizing Conditions. *J. Pharmaceut. Biomed.* **2018**, *161*, 73–82.

(28) Pantoliano, M. W.; Petrella, E. C.; Kwasnoski, J. D.; Lobanov, V. S.; Myslik, J.; Graf, E.; Carver, T.; Asel, E.; Springer, B. A.; Lane, P.; et al. High-Density Miniaturized Thermal Shift Assays as a General Strategy for Drug Discovery. *J. Biomol. Screen.* **2001**, *6* (6), 429–440.

(29) Gorania, M.; Seker, H.; Haris, P. Predicting a Proteins Melting Temperature from Its Amino Acid Sequence. In *2010 Annual International Conference of the IEEE Engineering in Medicine and Biology*; 2010.

(30) Niesen, F. H.; Berglund, H.; Vedadi, M. The Use of Differential Scanning Fluorimetry to Detect Ligand Interactions That Promote Protein Stability. *Nat. Protoc.* **2007**, *2* (9), 2212–2221.

(31) Huynh, K.; Partch, C. L. Analysis of Protein Stability and Ligand Interactions by Thermal Shift Assay. *Curr. Protoc. Protein Sci.* **2015**, *79* (1).

(32) Lecka-Czernik, B.; Ackert-Bicknell, C.; Adamo, M. L. Activation of Peroxisome Proliferator-Activated Receptor γ (PPARγ) by Rosiglitazone Suppresses Components of the Insulin-Like Growth Factor Regulatory System in Vitro and in Vivo. *Endocrinol.* **2007**, *148* (1), 903–911.

(33) Nunez, D.; Slunt, K. Optimization of a Ligand Binding Assay for Peroxisome Proliferator-Activated Receptors [Poster]. Presented at the University of Mary Washington Research and Creativity Day, Fredericksburg, VA, April 22, 2016.

(34) *QuantStudio™ 3 and 5 Real-Time PCR Systems INSTALLATION, USE, AND MAINTENANCE.* Life Technologies, Carlsbad, CA, 2015.

(35) Ribeiro Filho, H. V.; et. al. Screening for PPAR Non-Agonist Ligands Followed by Characterization of a Hit, AM-879, with Additional No-Adipogenic and Cdk5-Mediated Phosphorylation Inhibition Properties. *Front. Endocrinol*. **2018**, *9*, 11.

(36) Chênevert, R.; Pelchat, N.; Morin, P. Lipase-Mediated Enantioselective Acylation of Alcohols with Functionalized Vinyl Esters: Acyl Donor Tolerance and Applications. *Tetrahedron: Asymmetry* **2009**, *20* (10), 1191–1196.

Appendix A. NMR Spectra

Figure 19. 400 MHz ^{1}H NMR spectrum of purified diethyl allylbutylmalonate **(11)** in $CDCl_3$

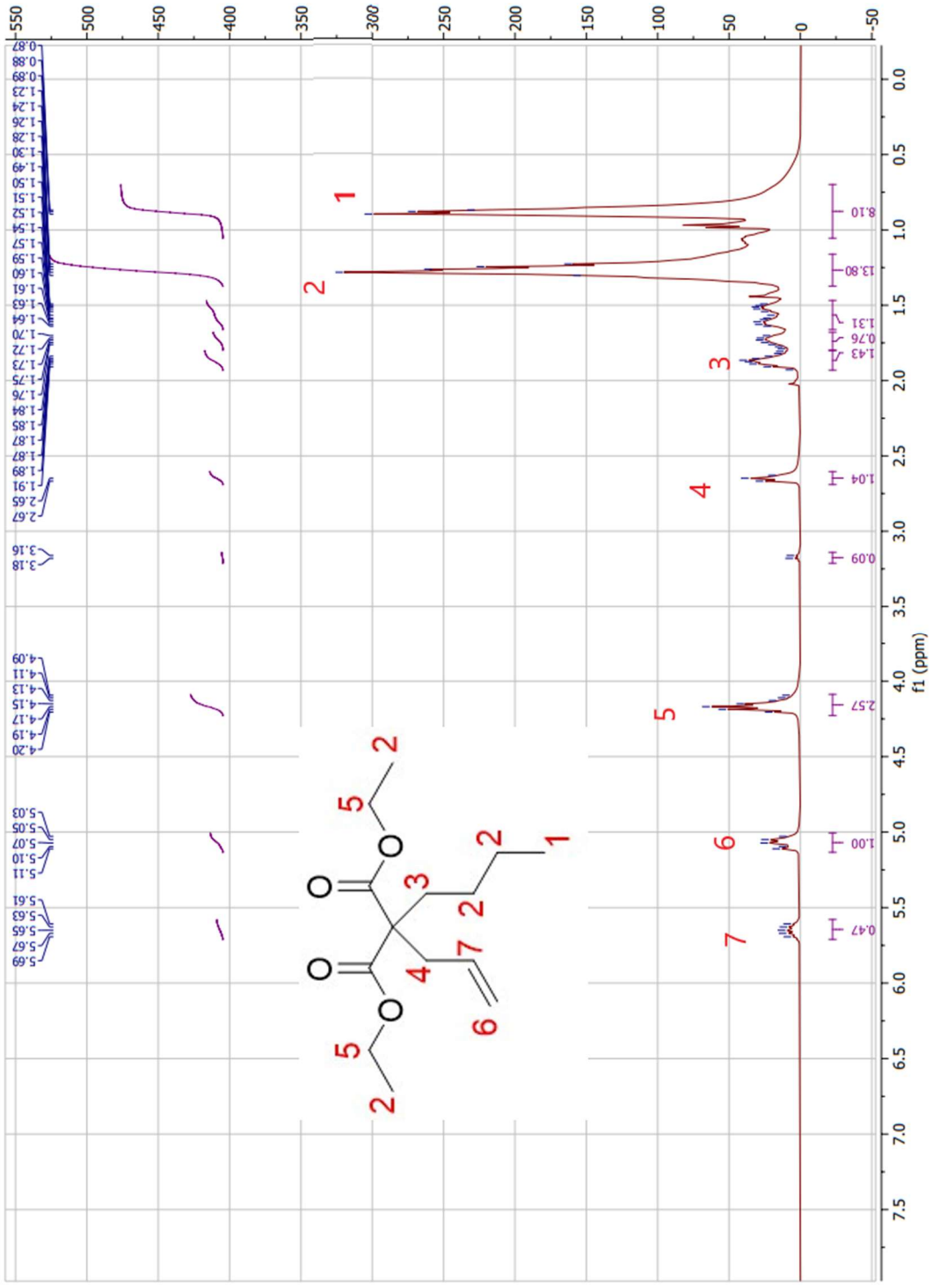

Figure 20. 400 MHz ^{1}H NMR spectrum of purified 2-allylhexanoate (12) in $CDCl_3$

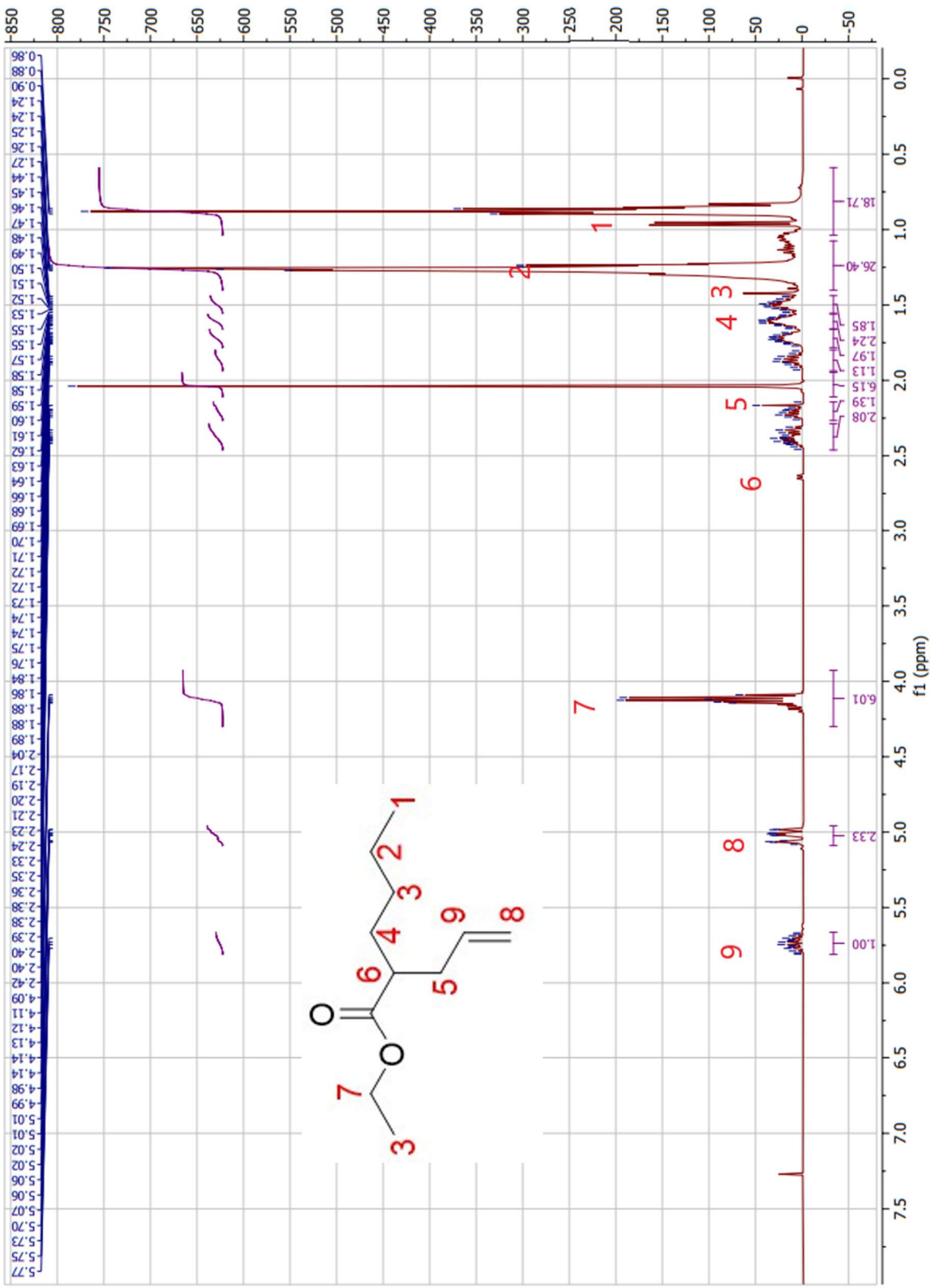

Figure 21. 400 MHz ^{1}H NMR of purified 2-allylhexanol (13) in $CDCl_3$

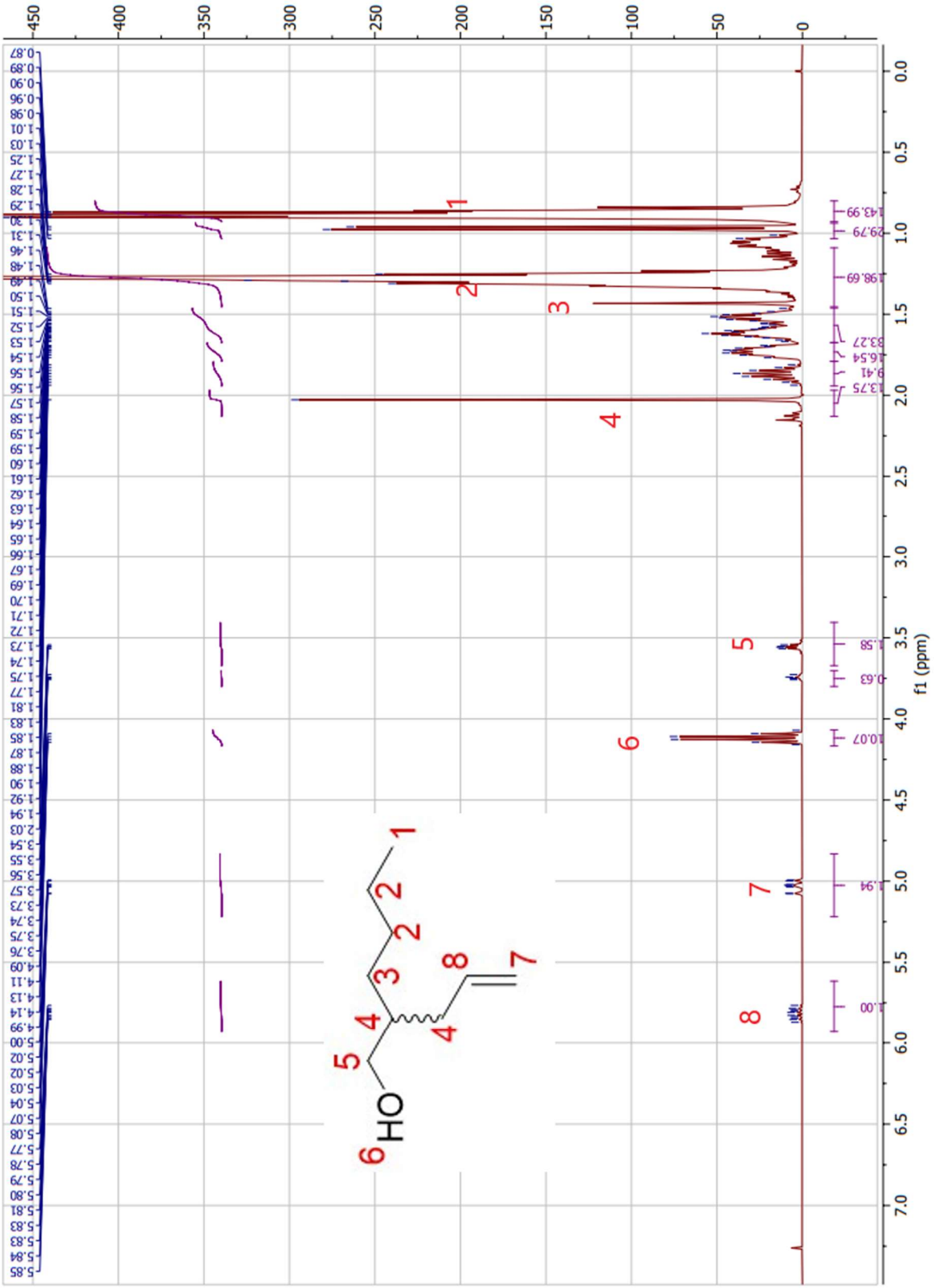

Figure 22. 400 MHz ^{1}H NMR of purified mono(2-allylhexyl) phthalate (14) in $CDCl_3$

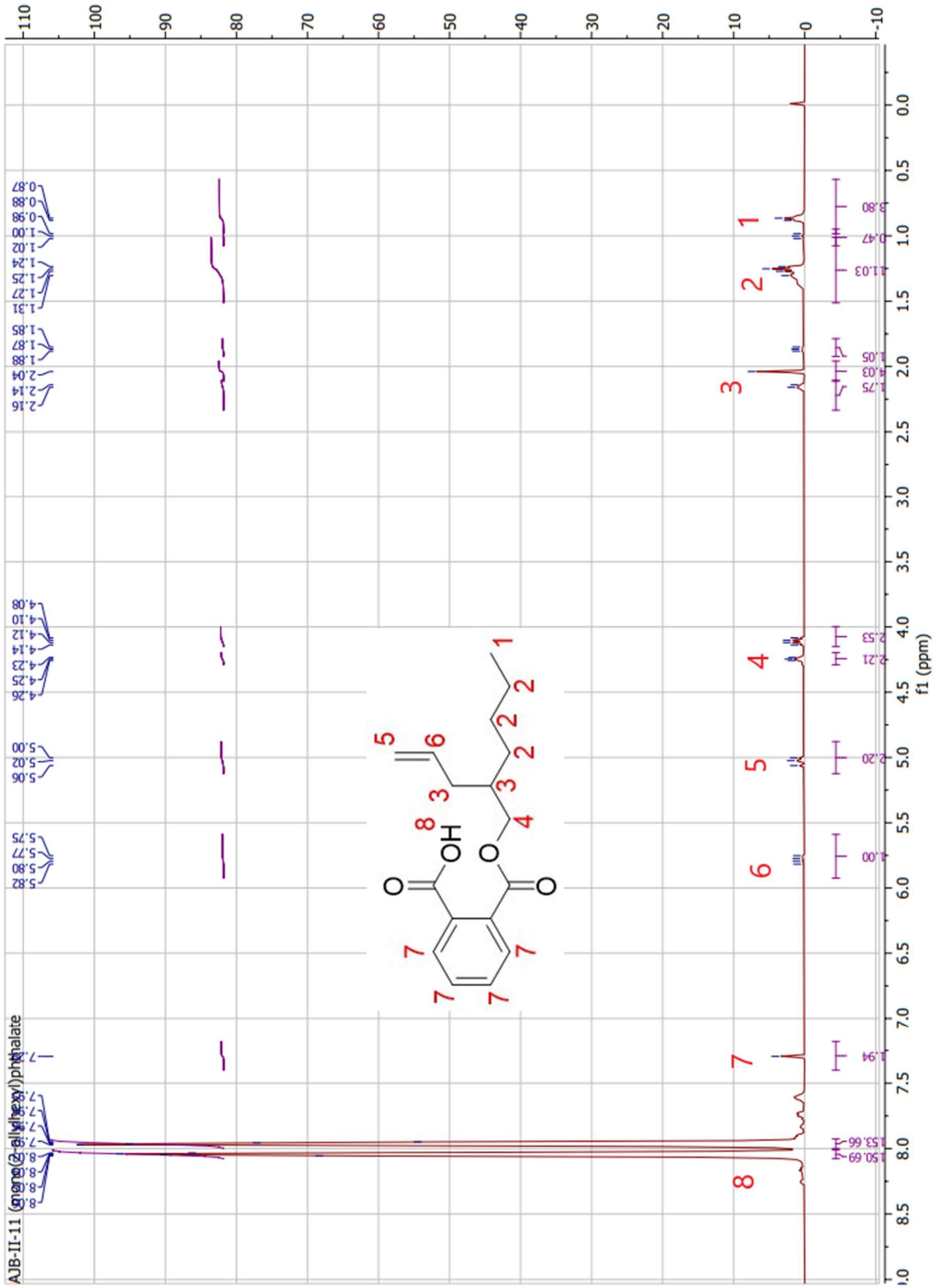

Figure 23. 400 MHz ^{1}H NMR of purified 2cx-MMHP (9) in $CDCl_3$

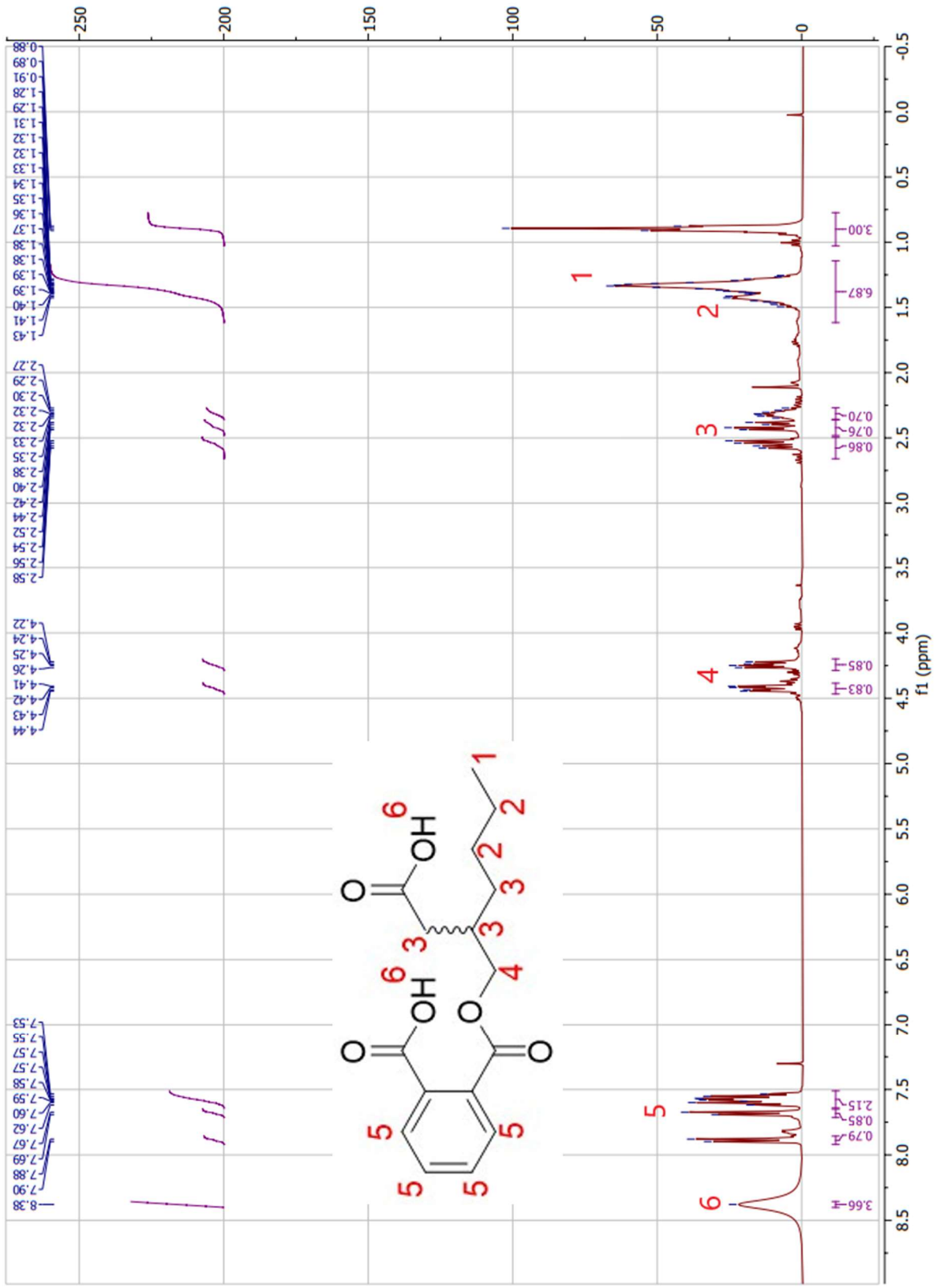

Figure 24. 400 MHz ^{1}H NMR of purified diethyl (3-butenyl)ethyl malonate (16) in $CDCl_3$

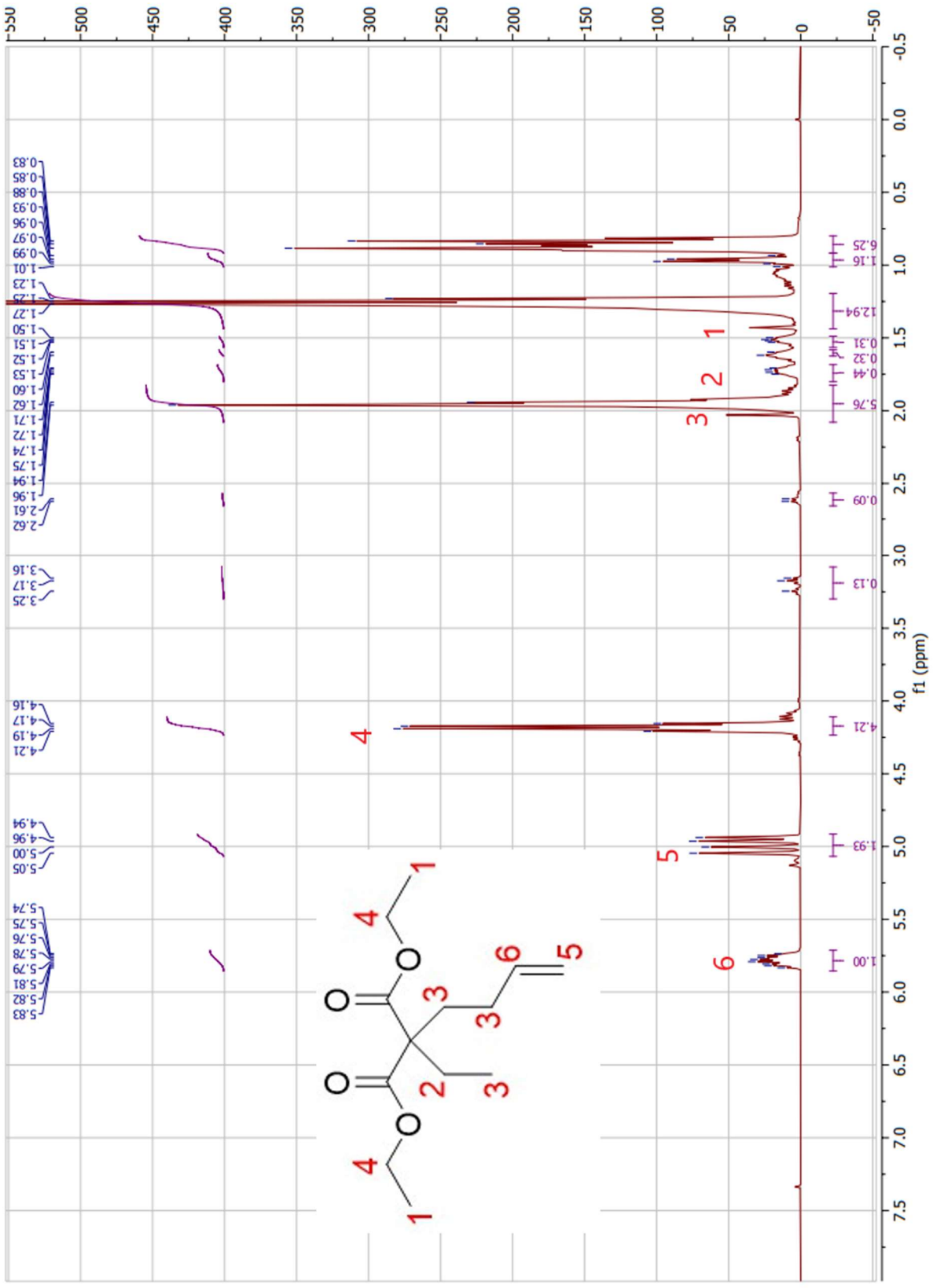

Figure 25. 400 MHz ^{1}H NMR of purified 2-ethyl-5-hexenoate (17) in $CDCl_3$

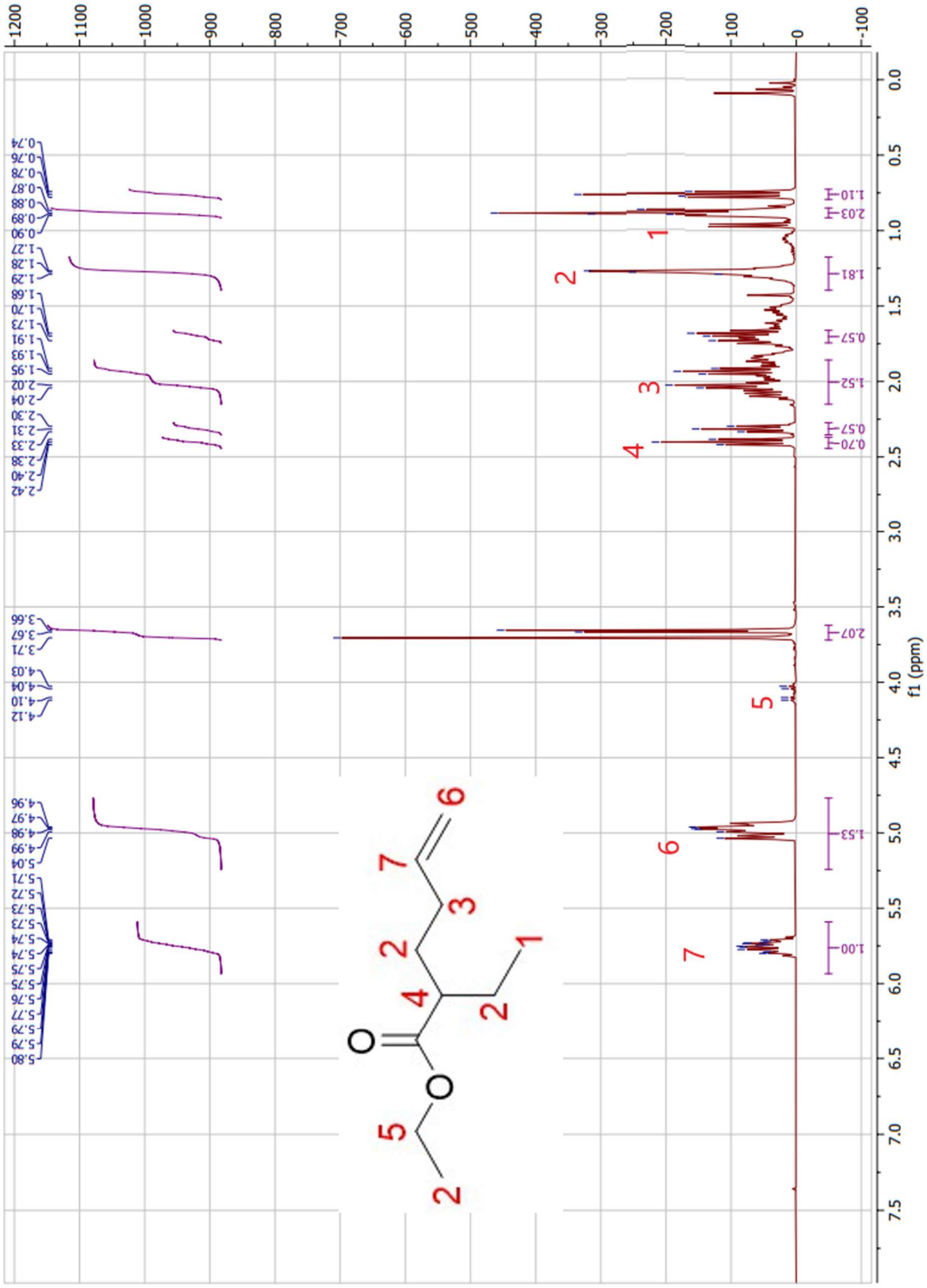

Figure 26. 400 MHz ^{1}H NMR of purified 2-ethyl-5-hexenol (18) in $CDCl_3$

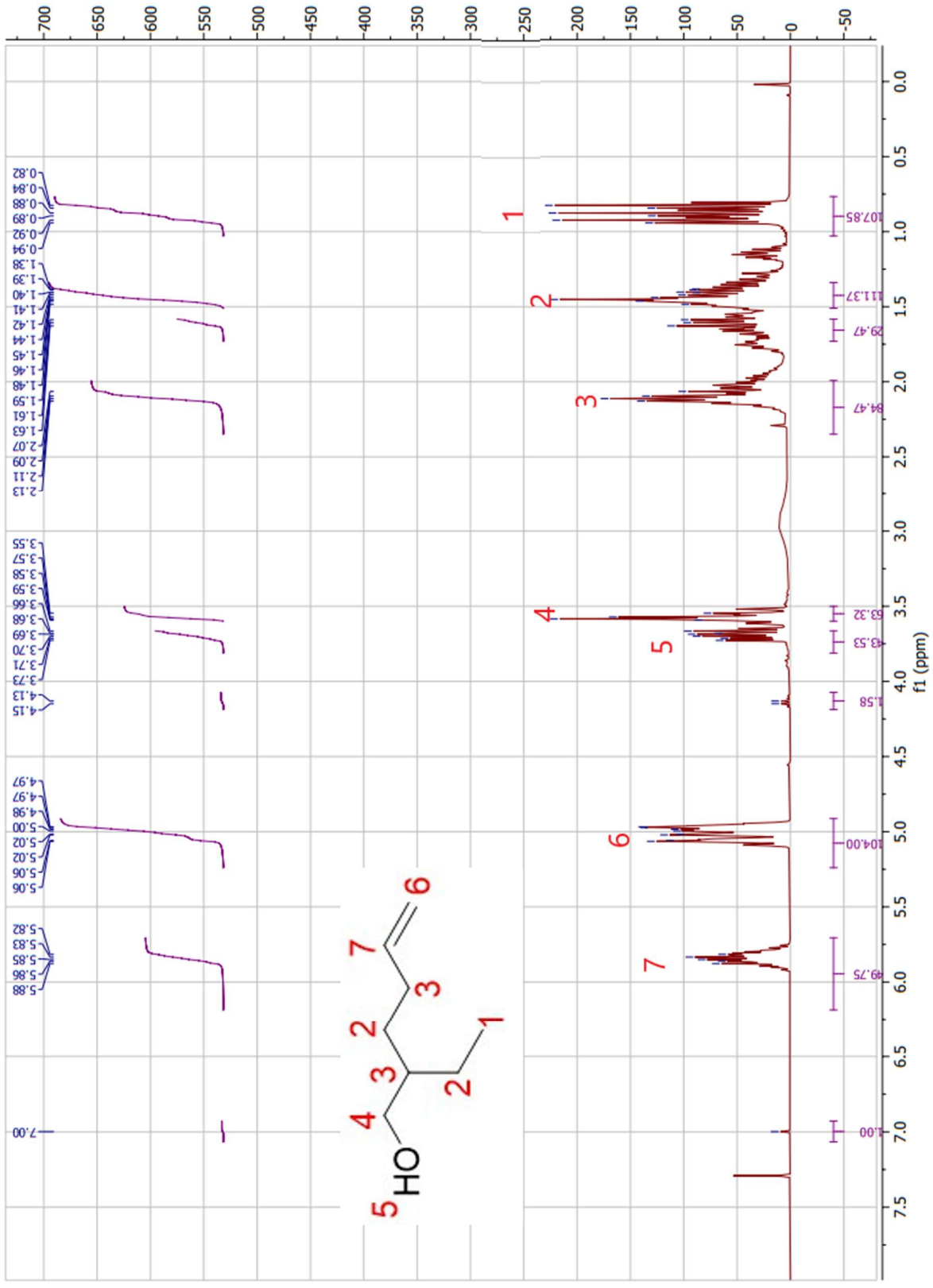

Figure 27. 400 MHz ^{1}H NMR of purified mono(2-ethyl-5-hexenyl) phthalate (19) in $CDCl_3$

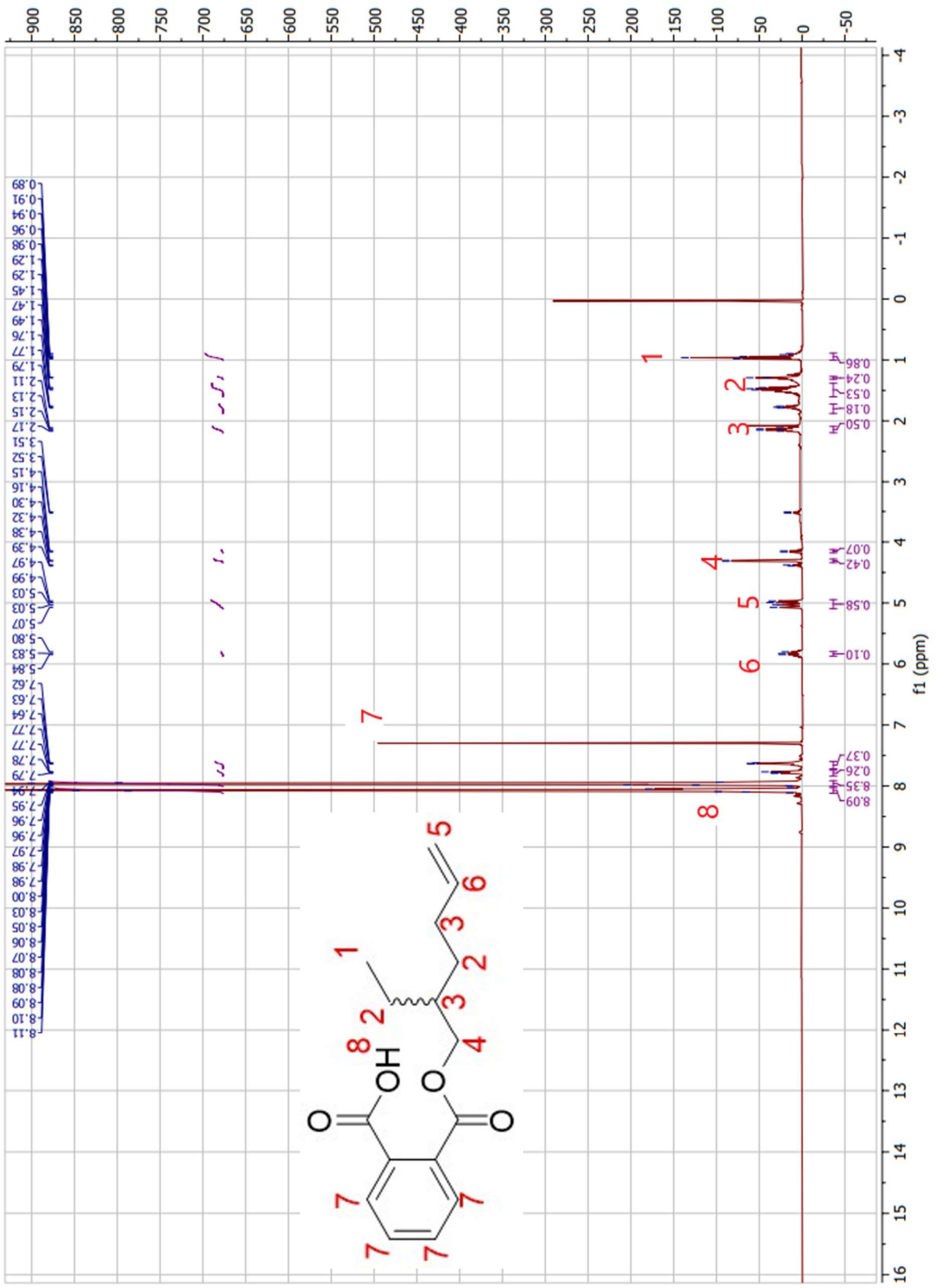

Figure 28. 400 MHz ^{1}H NMR of purified 5oxo-MEHP (7) in $CDCl_3$

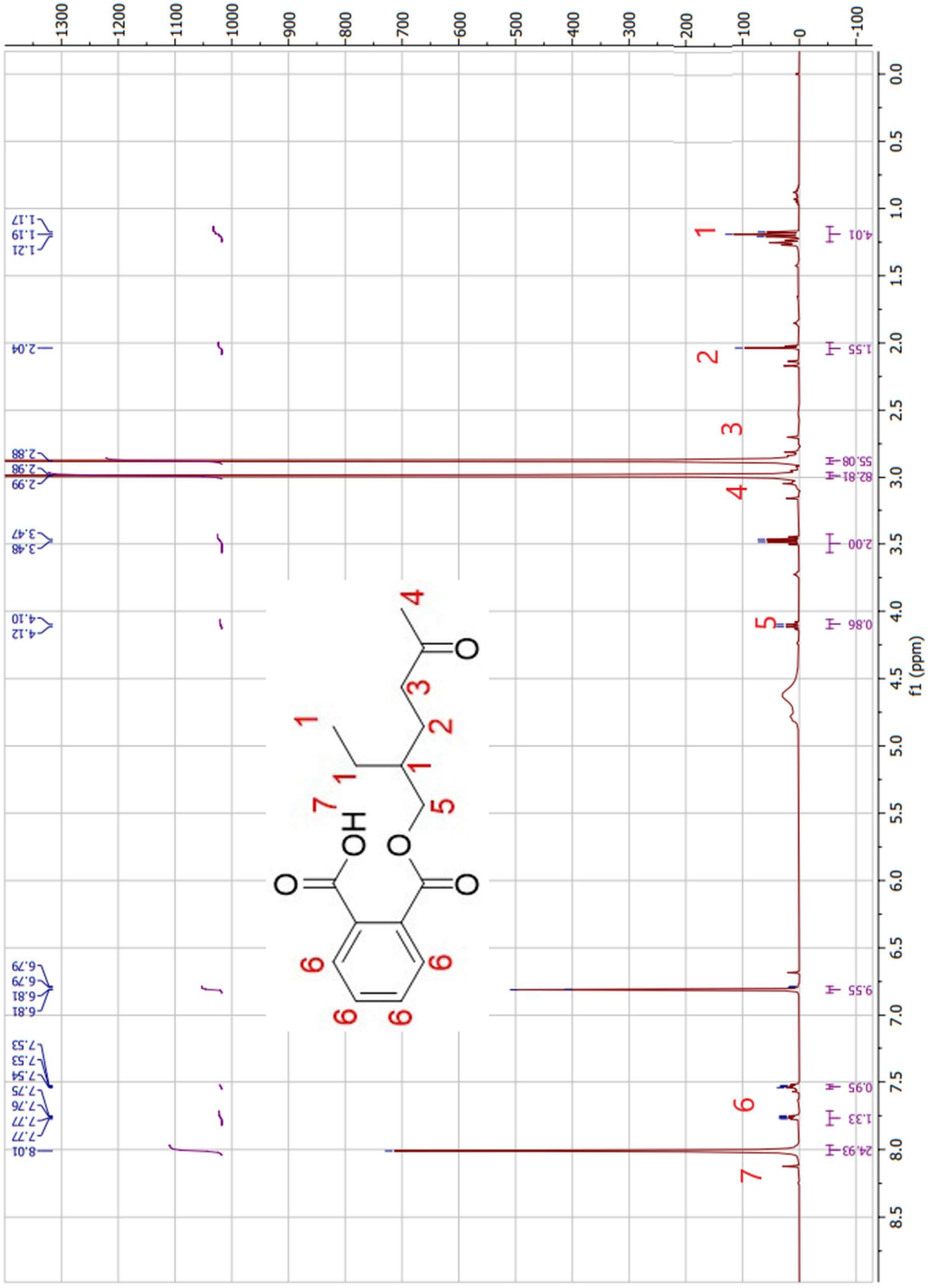

Figure 29. 400 MHz ^{1}H NMR of purified ethyl 2-ethyl-6-heptenoate (21b) in $CDCl_3$

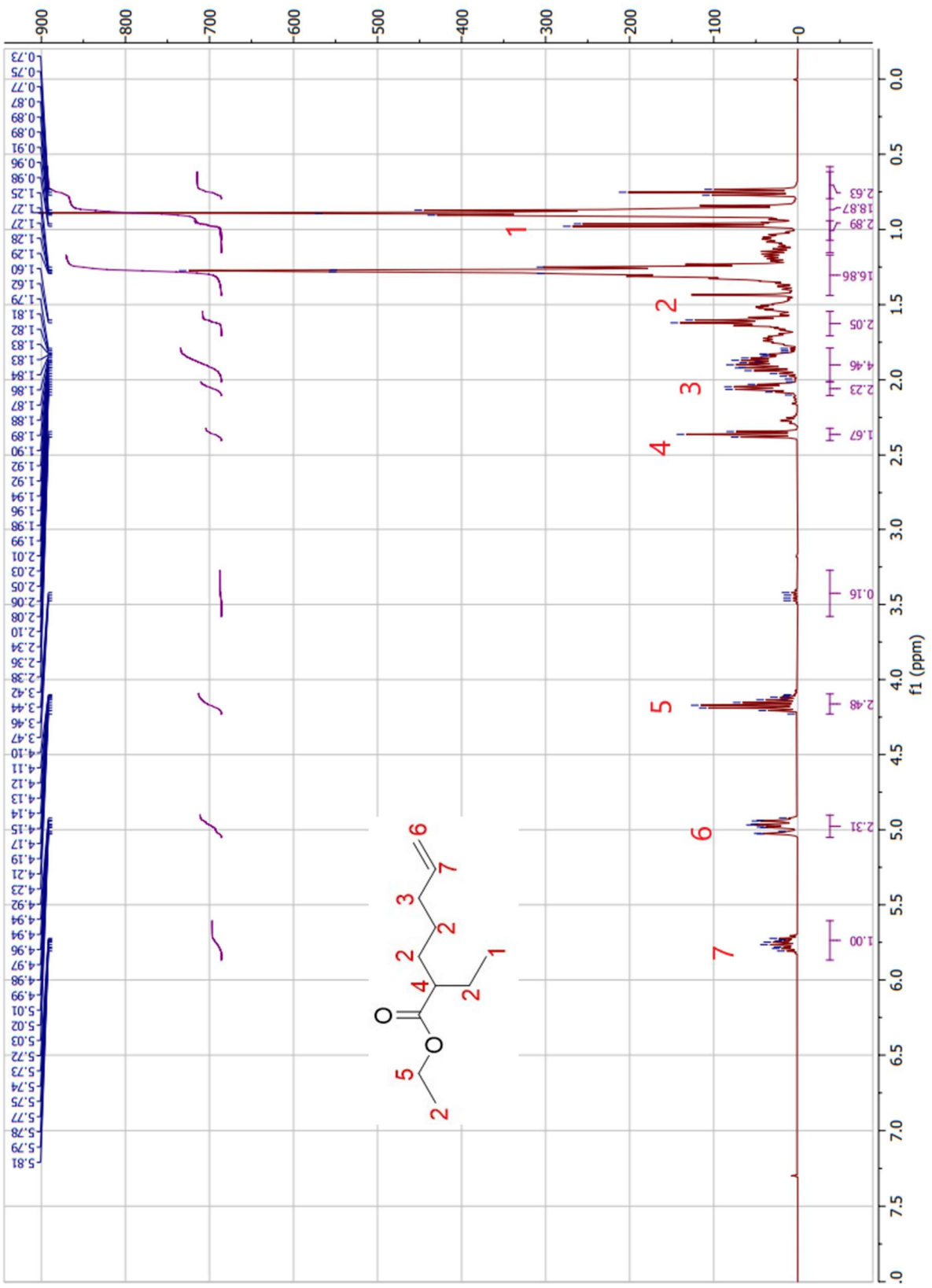

Figure 30. 400 MHz ^{1}H NMR of purified 2-ethyl-6-heptenol (22) in $CDCl_3$

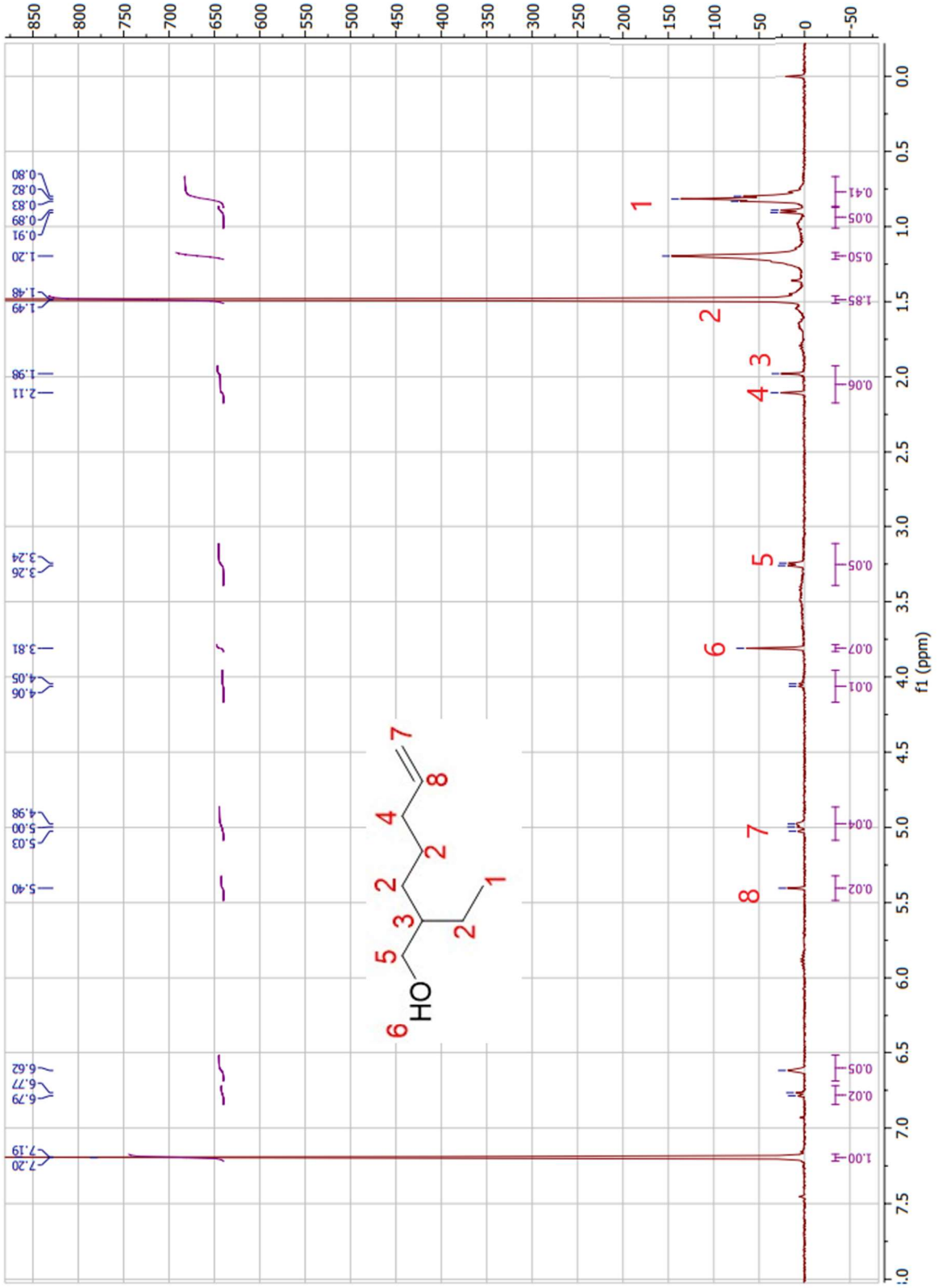

Figure 31. 400 MHz ^{1}H NMR of purified mono(2-ethyl-6-heptenyl) phthalate (23) in $CDCl_3$

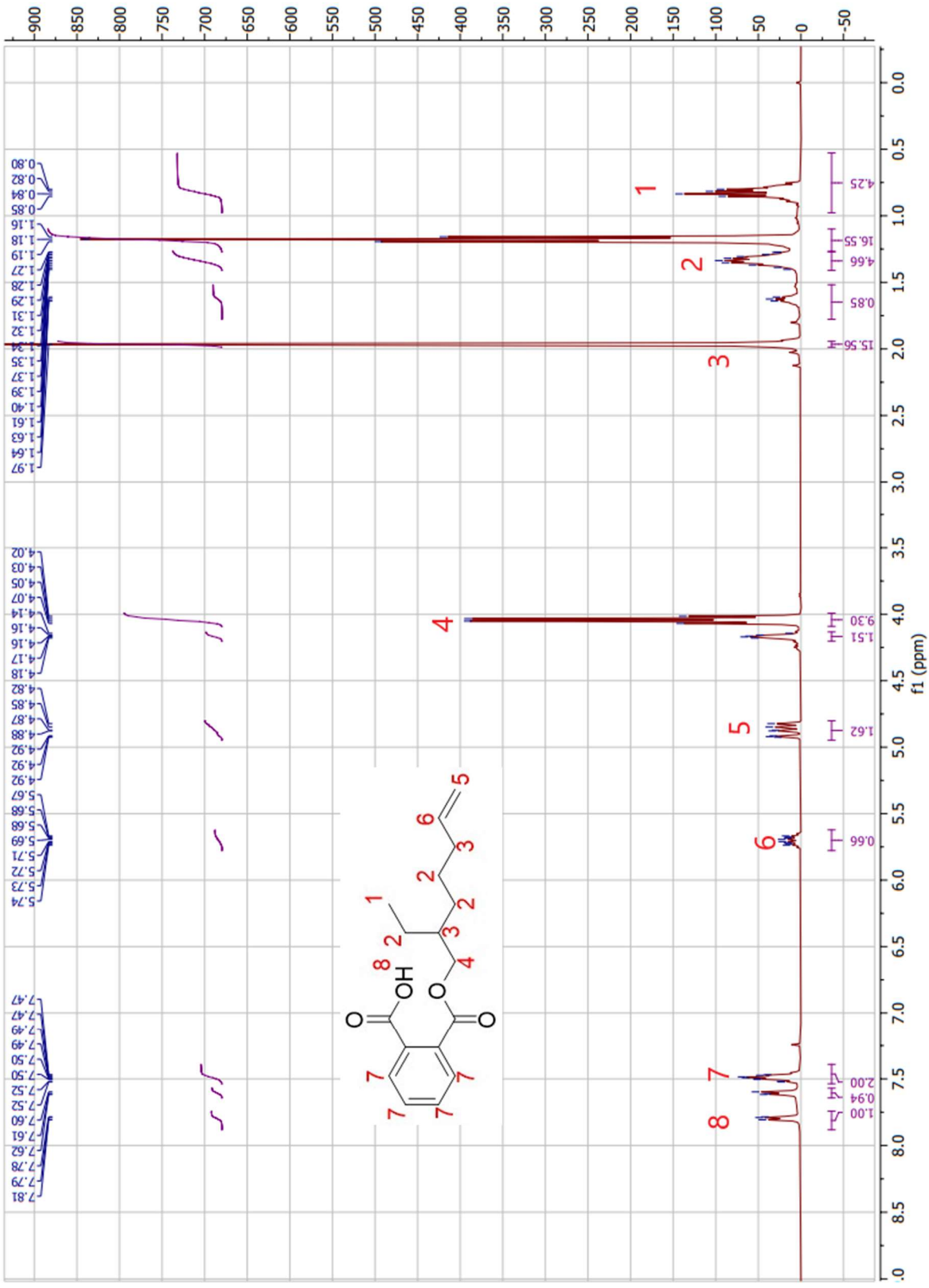

Figure 32. 400 MHz ^{1}H NMR of purified 5cx-MEPP (8) in $CDCl_3$

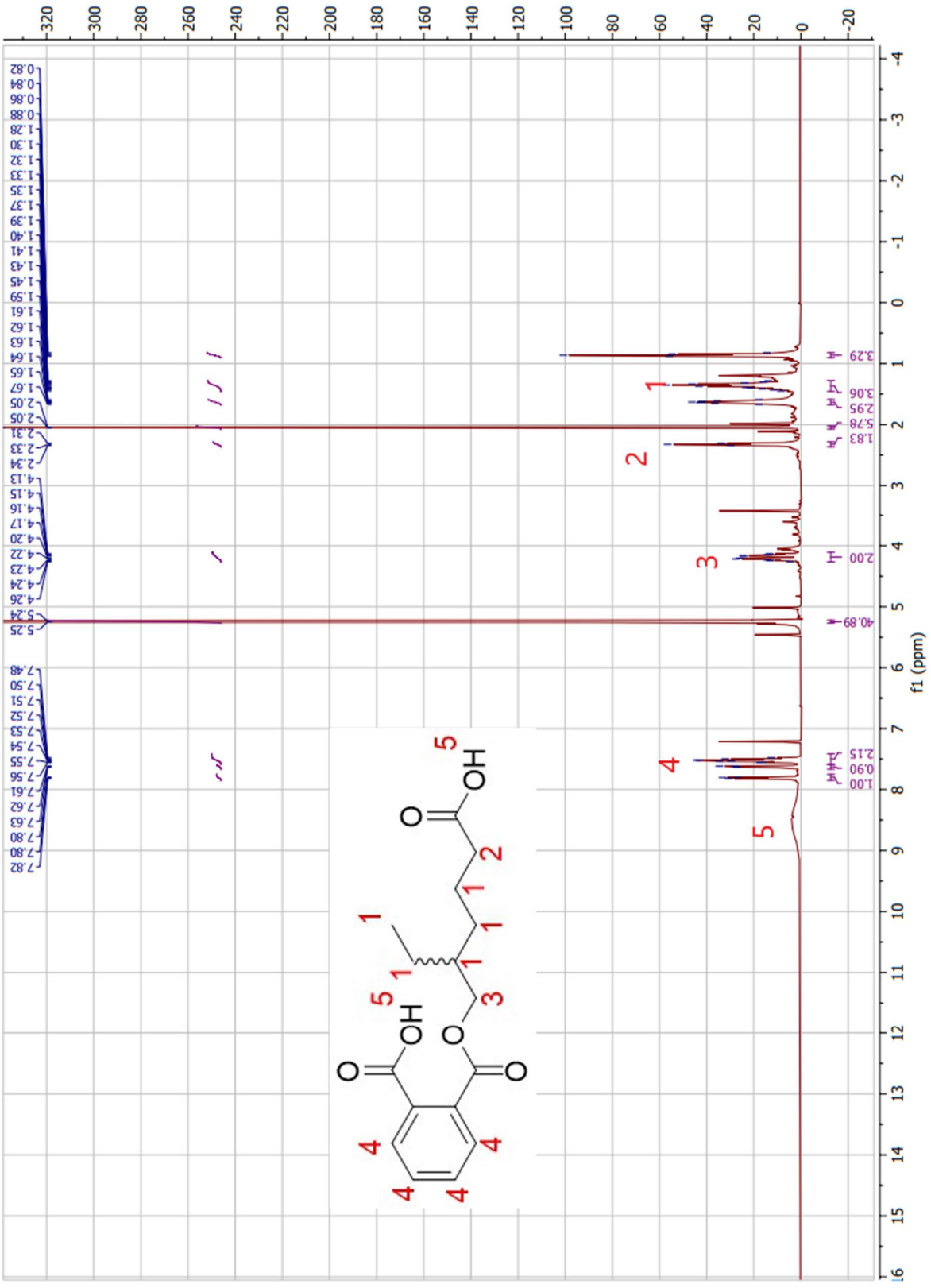

Appendix B. GC-MS Spectra

Figure 33. GC-MS of crude diethyl allylbutylmalonate (11)

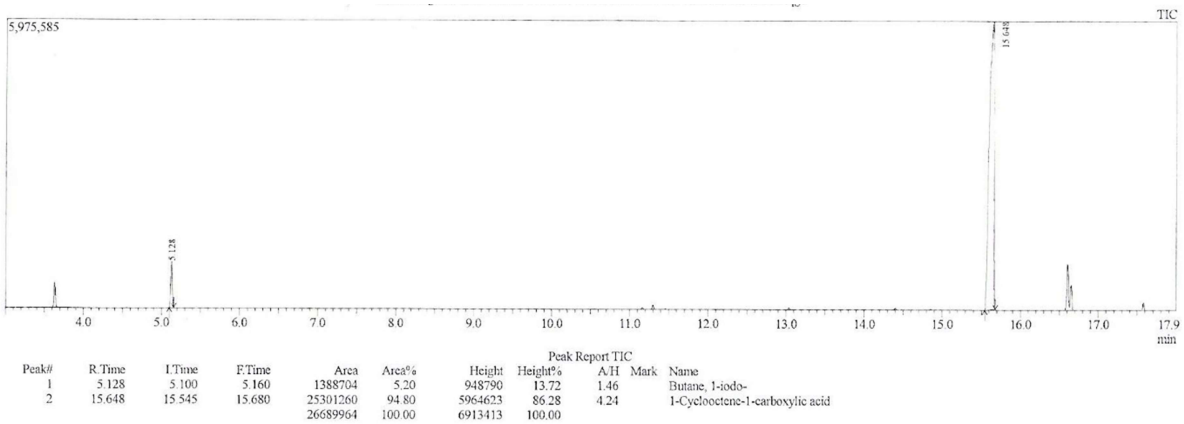

Peak Report TIC

Peak#	R.Time	I.Time	F.Time	Area	Area%	Height	Height%	A/H	Mark	Name
1	5.128	5.100	5.160	1388704	5.20	948790	13.72	1.46		Butane, 1-iodo-
2	15.648	15.545	15.680	25301260	94.80	5964623	86.28	4.24		1-Cyclooctene-1-carboxylic acid
				26689964	100.00	6913413	100.00			

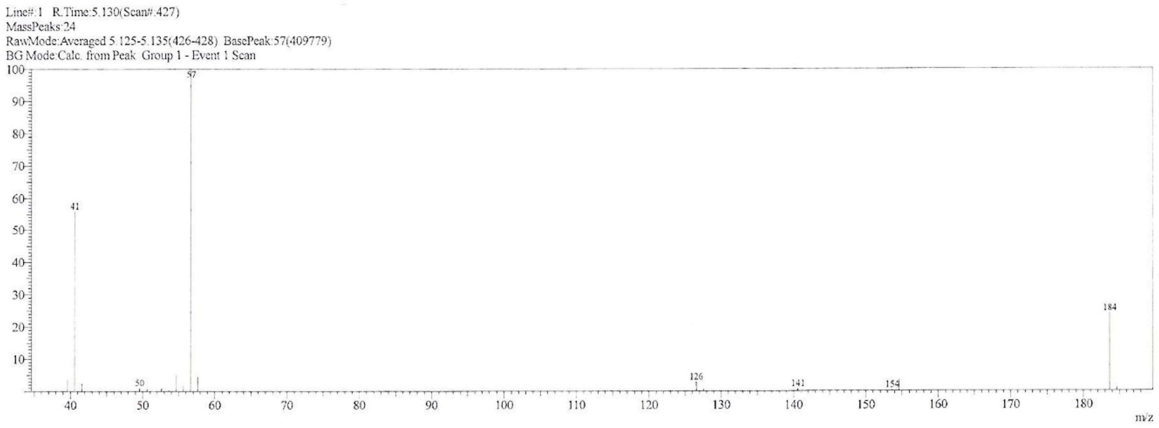

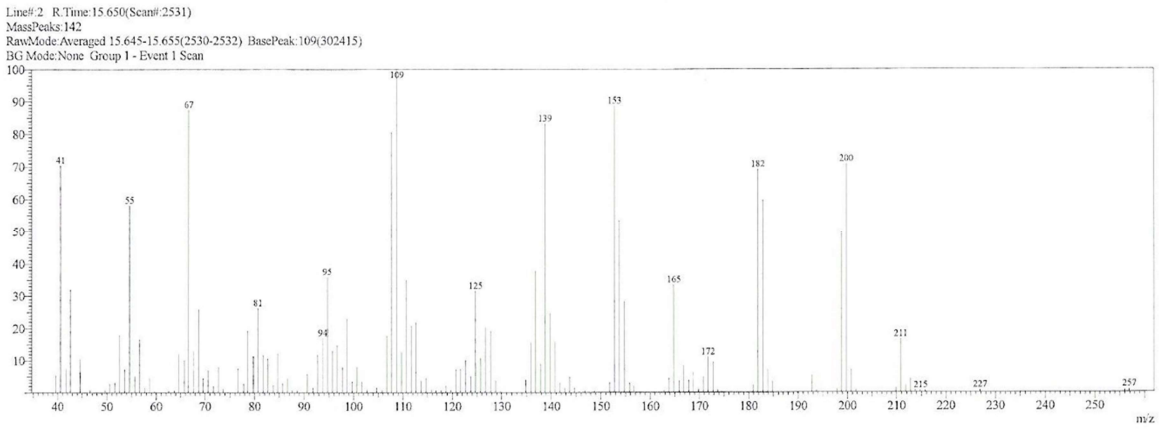

Figure 34. GC-MS of crude 2-allylhexanoate (12)

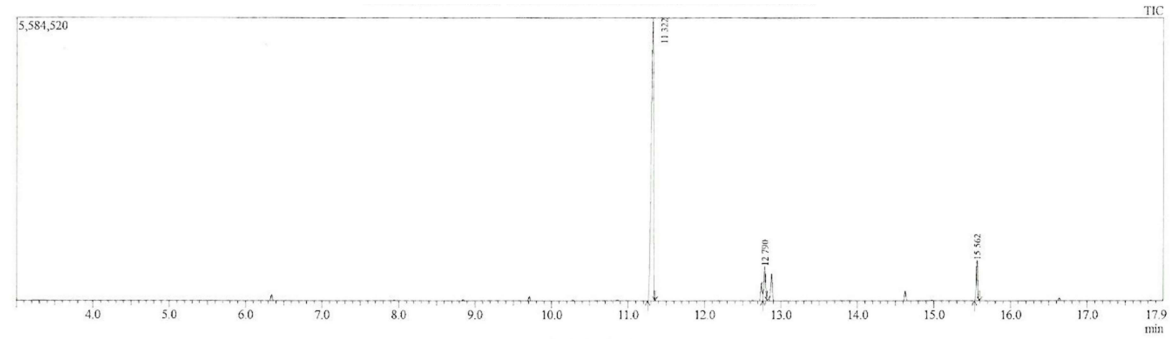

Peak Report TIC

Peak#	R.Time	I.Time	F.Time	Area	Area%	Height	Height%	A/H	Mark	Name
1	11.322	11.255	11.355	12809308	85.46	5582680	79.20	2.29		6-Ethyl-3-(1-methylethyl)tetrahydro(2H)pyran
2	12.790	12.765	12.825	1069940	7.14	676227	9.59	1.58	V	Propan-2-ol, 1-(2-isopropyl-5-methylcyclohex
3	15.562	15.530	15.595	1110056	7.41	790267	11.21	1.40		1-Cyclooctene-1-carboxylic acid
				14989304	100.00	7049174	100.00			

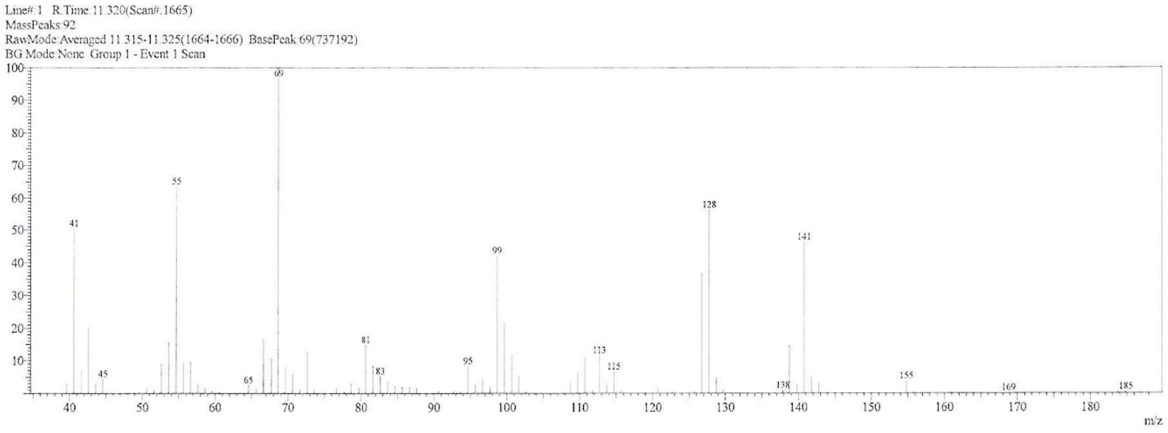

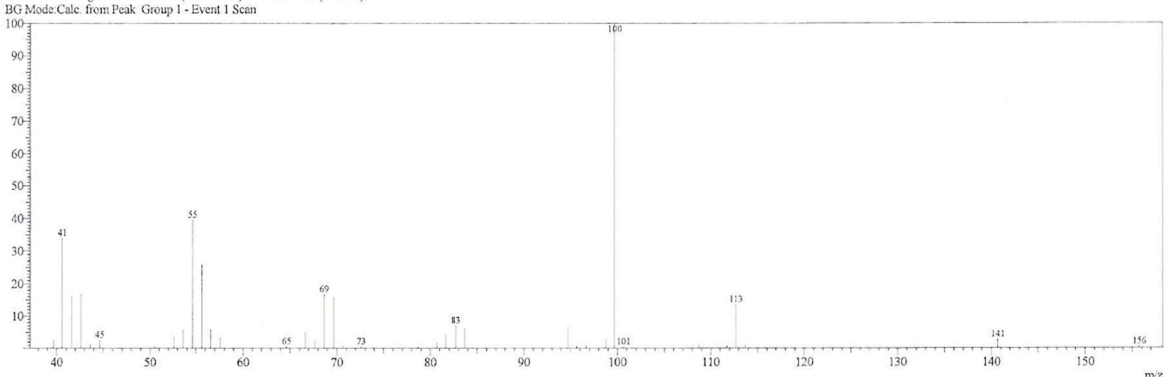

Line#:3 R.Time:15.560(Scan#:2513)
MassPeaks:96
RawMode:Averaged 15.555-15.565(2512-2514) BasePeak:109(40512)
BG Mode:None Group 1 - Event 1 Scan

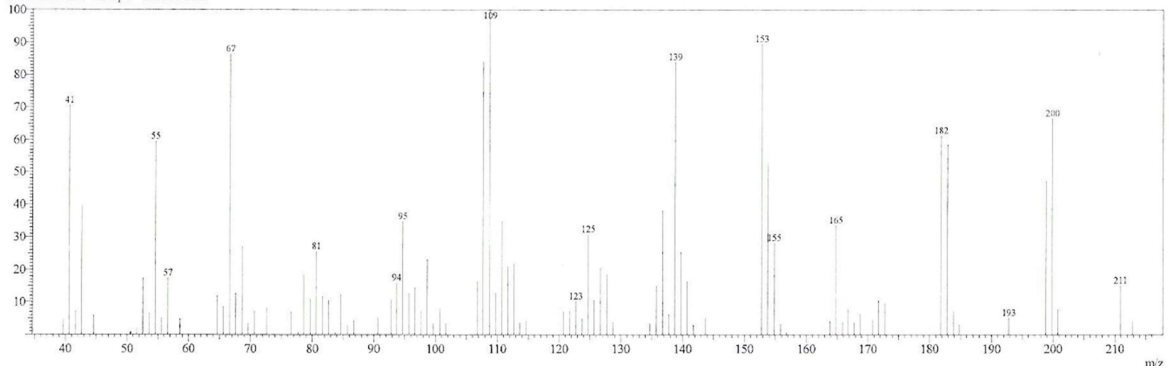

Figure 35. GC-MS of crude 2-allylhexanol (13)

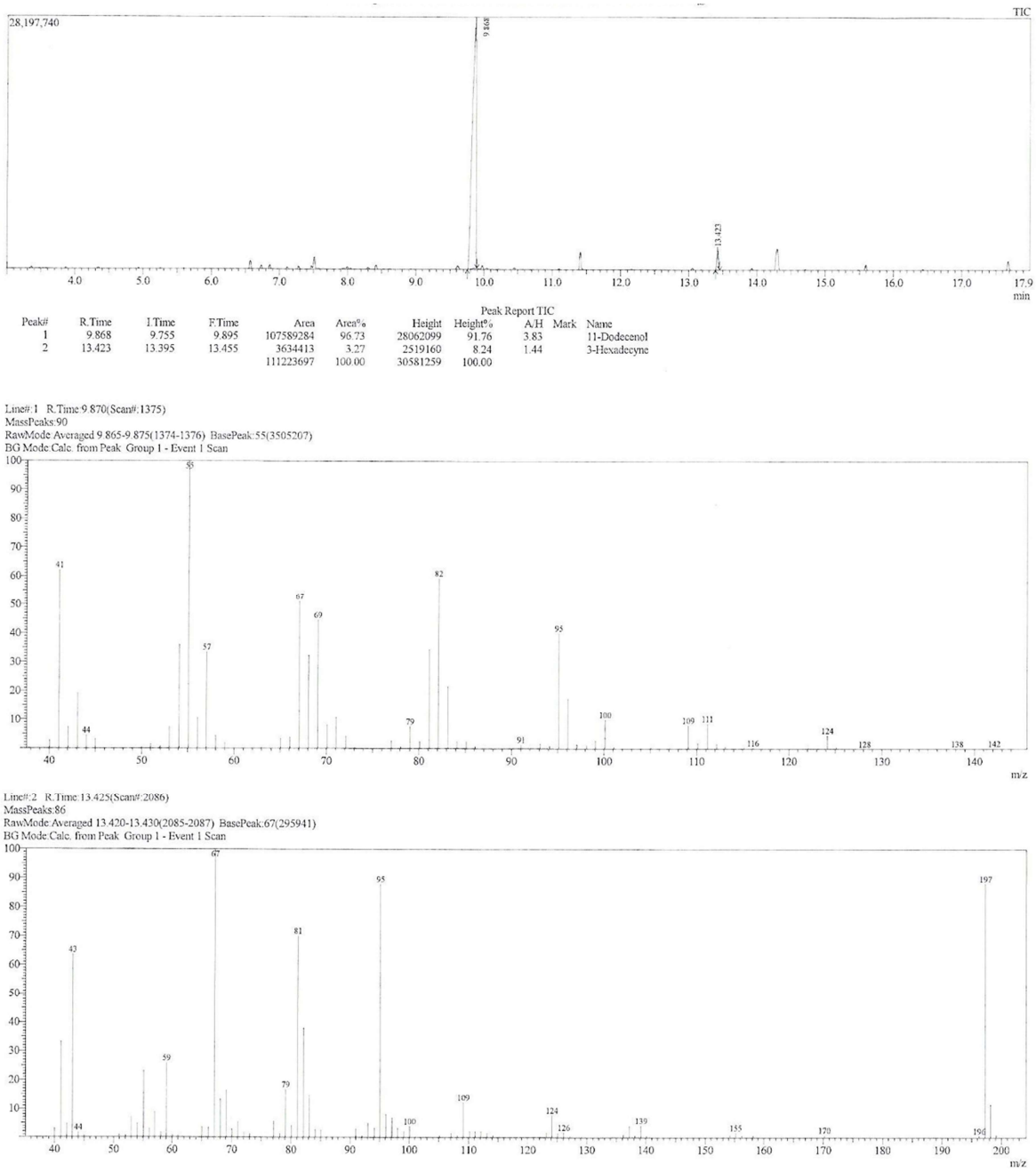

Peak Report TIC

Peak#	R.Time	I.Time	F.Time	Area	Area%	Height	Height%	A/H	Mark	Name
1	9.868	9.755	9.895	107589284	96.73	28062099	91.76	3.83		11-Dodecenol
2	13.423	13.395	13.455	3634413	3.27	2519160	8.24	1.44		3-Hexadecyne
				111223697	100.00	30581259	100.00			

Line#:1 R.Time:9.870(Scan#:1375)
MassPeaks:90
RawMode:Averaged 9.865-9.875(1374-1376) BasePeak:55(3505207)
BG Mode:Calc. from Peak Group 1 - Event 1 Scan

Line#:2 R.Time:13.425(Scan#:2086)
MassPeaks:86
RawMode:Averaged 13.420-13.430(2085-2087) BasePeak:67(295941)
BG Mode:Calc. from Peak Group 1 - Event 1 Scan

Figure 36. GC-MS of crude diethyl (3-butenyl)ethylmalonate (16)

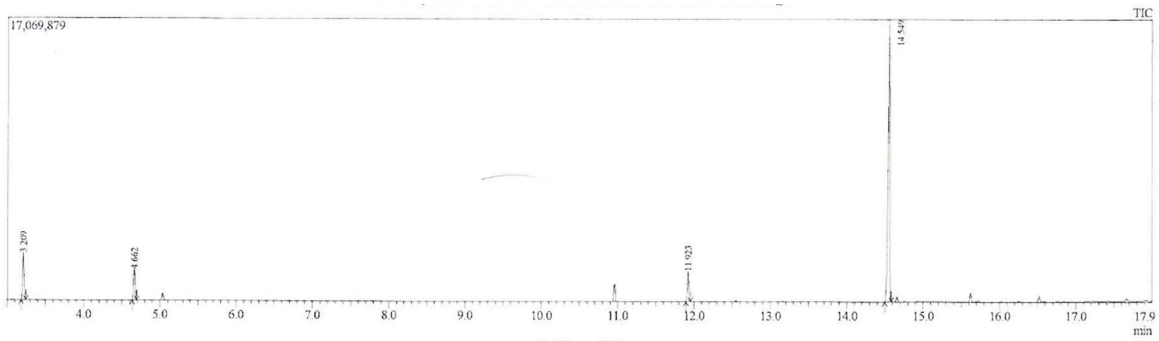

Peak Report TIC

Peak#	R.Time	I.Time	F.Time	Area	Area%	Height	Height%	A/H	Mark	Name
1	3.209	3.180	3.245	3744834	10.16	2812420	11.98	1.33		1-Butene, 4-bromo-
2	4.662	4.635	4.695	2659747	7.21	1845331	7.86	1.44		1-Butene, 4-iodo-
3	11.923	11.895	11.955	2504401	6.79	1783197	7.59	1.40		Allyl thiopropionate
4	14.549	14.500	14.585	27965279	75.84	17044106	72.57	1.64		Diethyl diethylmalonate
				36874261	100.00	23485054	100.00			

Line#:1 R.Time:3.210(Scan#:43)
MassPeaks:37
RawMode:Averaged 3.205-3.215(42-44) BasePeak:55(1613211)
BG Mode:Calc. from Peak Group 1 - Event 1 Scan

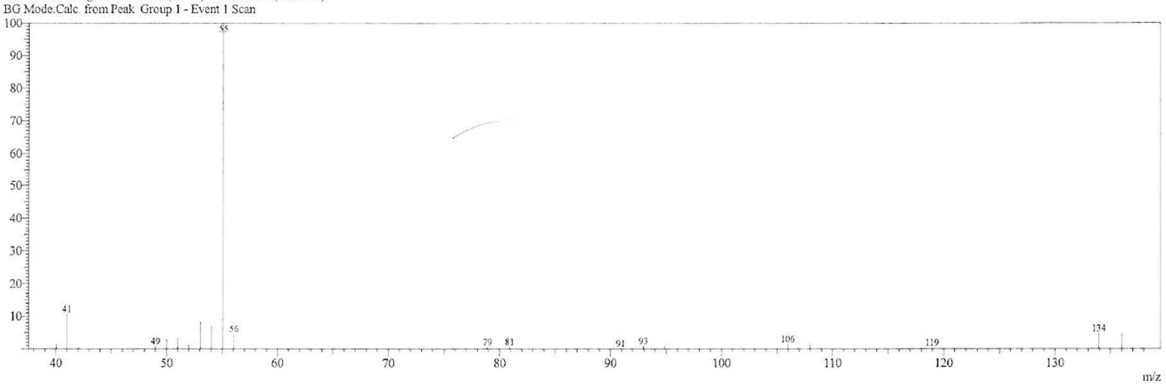

Line#:2 R.Time:4.660(Scan#:333)
MassPeaks:24
RawMode:Averaged 4.655-4.665(332-334) BasePeak:55(1159767)
BG Mode:Calc. from Peak Group 1 - Event 1 Scan

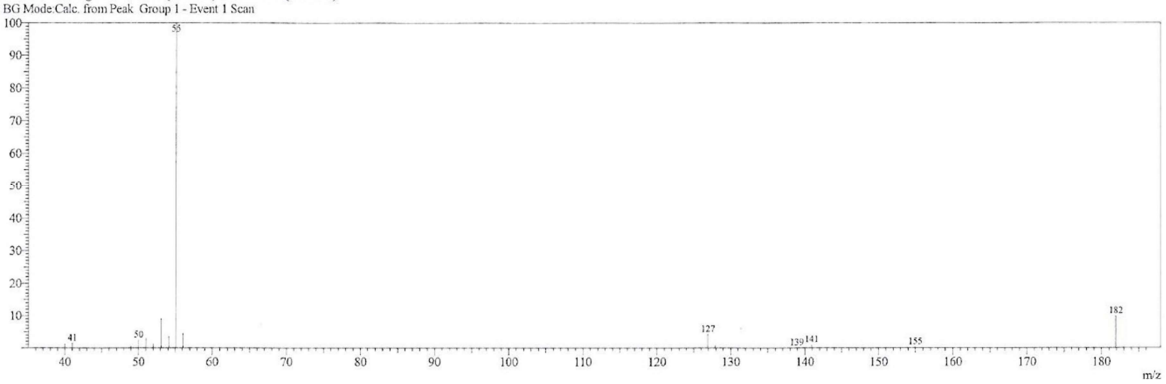

Line#:3 R.Time:11.925(Scan#:1786)
MassPeaks:49
RawMode:Averaged 11.920-11.930(1785-1787) BasePeak:57(963980)
BG Mode:Calc. from Peak Group 1 - Event 1 Scan

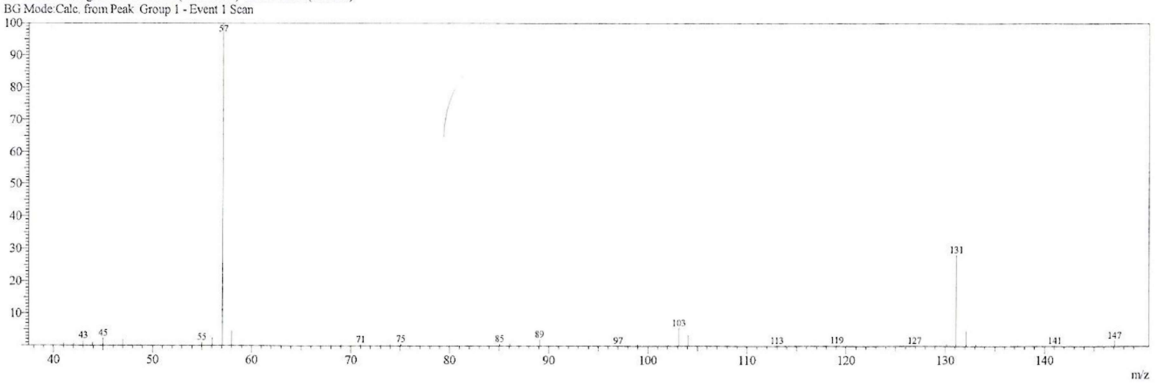

Line#:4 R.Time:14.550(Scan#:2311)
MassPeaks:143
RawMode:Averaged 14.545-14.555(2310-2312) BasePeak:173(1607839)
BG Mode:Calc. from Peak Group 1 - Event 1 Scan

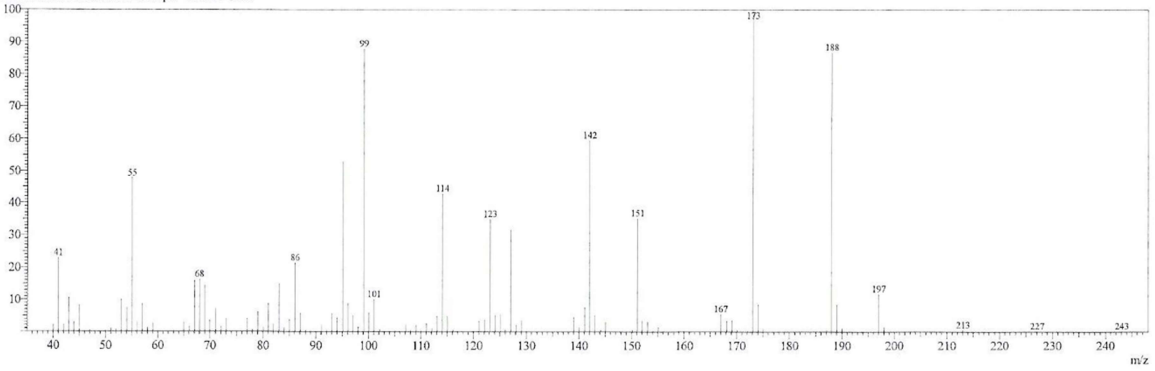

Figure 37. GC-MS of crude 2-ethyl-5-hexenoate (17)

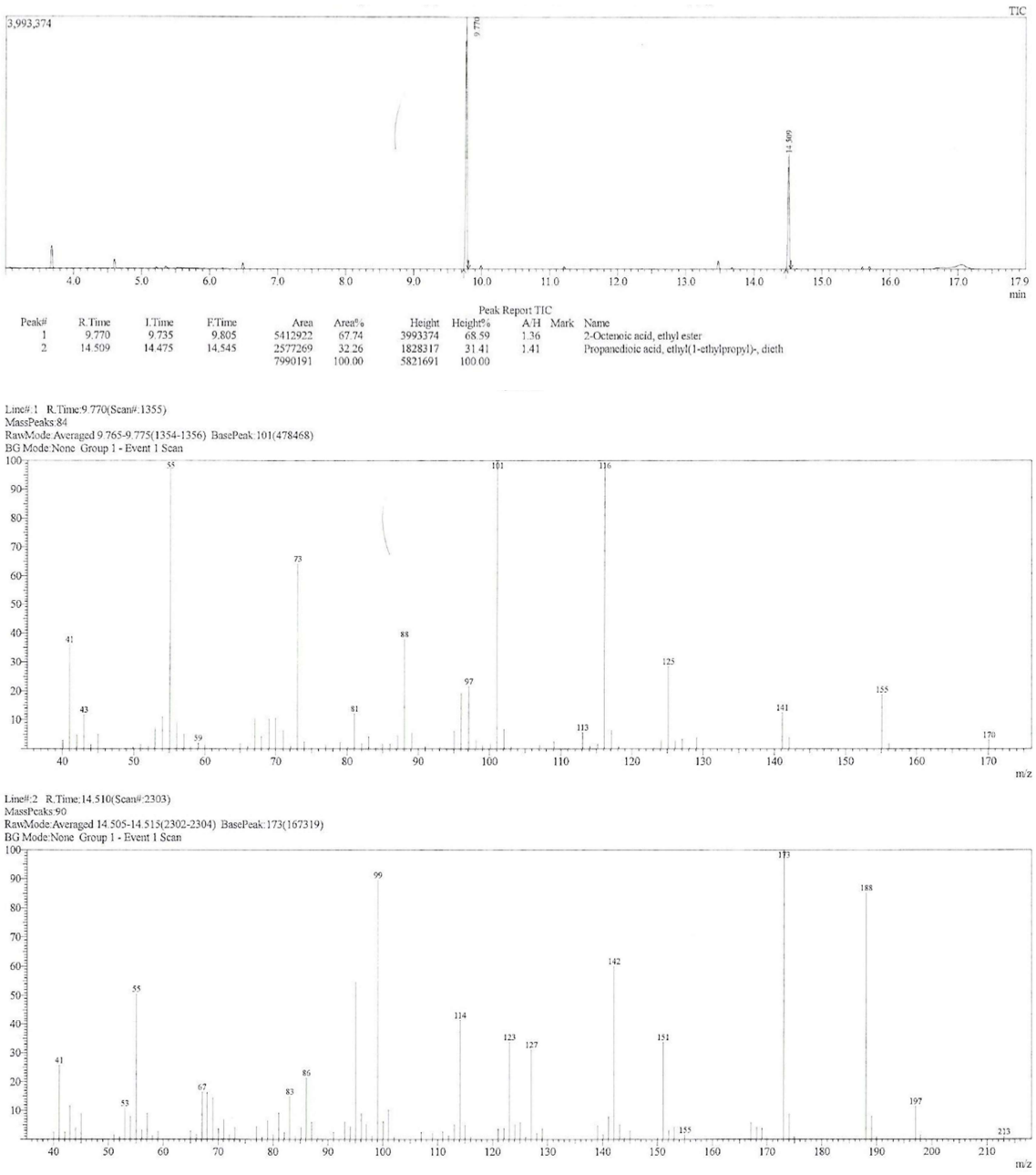

Peak Report TIC

Peak#	R.Time	I.Time	F.Time	Area	Area%	Height	Height%	A/H	Mark	Name
1	9.770	9.735	9.805	5412922	67.74	3993374	68.59	1.36		2-Octenoic acid, ethyl ester
2	14.509	14.475	14.545	2577269	32.26	1828317	31.41	1.41		Propanedioic acid, ethyl(1-ethylpropyl)-, dieth
				7990191	100.00	5821691	100.00			

Line#:1 R.Time:9.770(Scan#:1355)
MassPeaks:84
RawMode:Averaged 9.765-9.775(1354-1356) BasePeak:101(478468)
BG Mode:None Group 1 - Event 1 Scan

Line#:2 R.Time:14.510(Scan#:2303)
MassPeaks:90
RawMode:Averaged 14.505-14.515(2302-2304) BasePeak:173(167319)
BG Mode:None Group 1 - Event 1 Scan

Figure 38. GC-MS of crude 2-ethyl-5-hexenol (18)

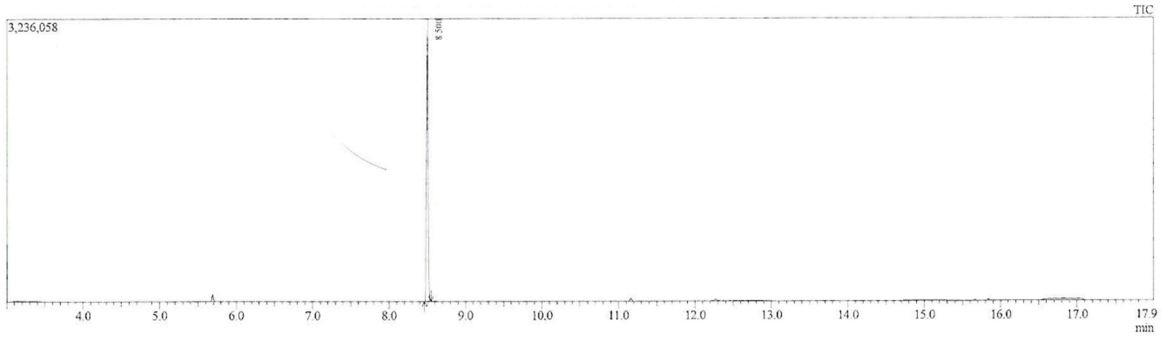

Peak Report TIC

Peak#	R.Time	I.Time	F.Time	Area	Area%	Height	Height%	A/H	Mark	Name
1	8.500	8.465	8.550	4463709	100.00	3231288	100.00	1.38		9-Decen-1-ol
				4463709	100.00	3231288	100.00			

Spectrum

Line#:1 R.Time:8.500(Scan#:1101)
MassPeaks:56
RawMode:Averaged 8.495-8.505(1100-1102) BasePeak:55(421029)
BG Mode:None Group 1 - Event 1 Scan

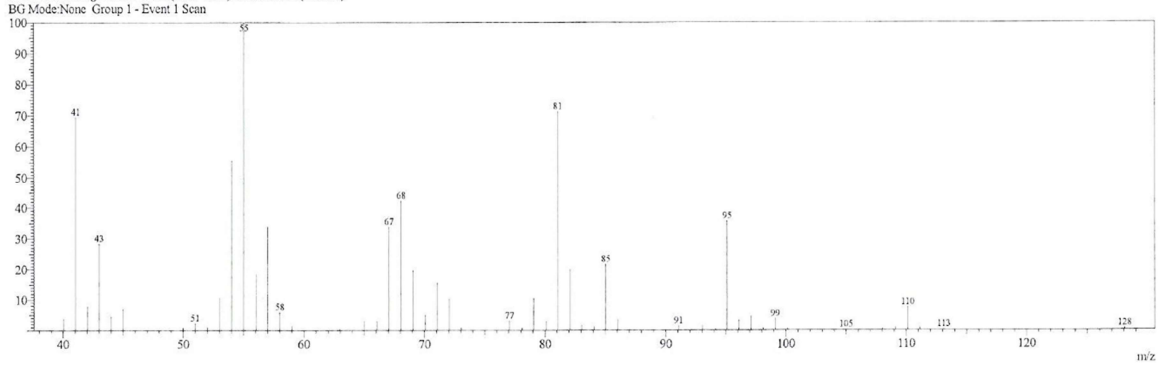

Figure 39. GC-MS of crude diethyl (3-pentenyl)ethylmalonate (20)

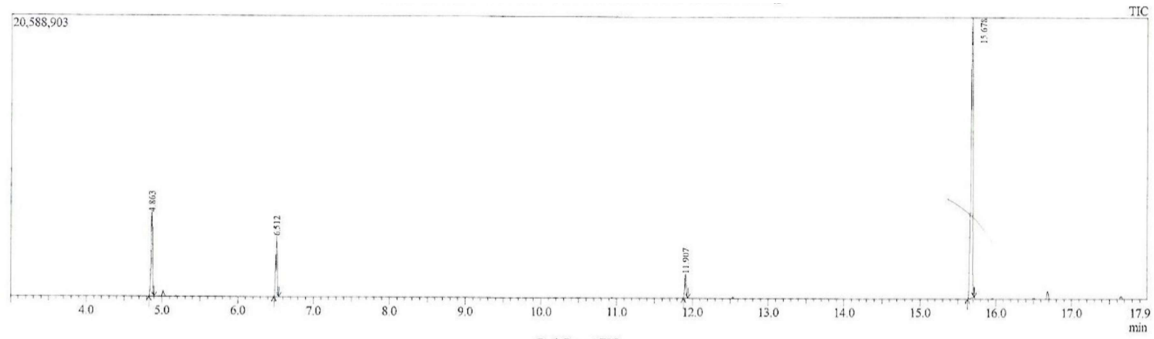

Peak Report TIC

Peak#	R.Time	I.Time	F.Time	Area	Area%	Height	Height%	A/H	Mark	Name
1	4.863	4.830	4.900	8807156	17.30	6175433	18.82	1.43		1-Pentene, 5-bromo-
2	6.512	6.480	6.545	6288517	12.35	4409763	13.44	1.43		Cyclopentane, iodo-
3	11.907	11.880	11.940	2328489	4.57	1724185	5.26	1.35		Malic acid, 2-ethyl-, dimethyl ester
4	15.678	15.630	15.715	33482450	65.77	20495293	62.48	1.63		2-Decenedioic acid, diethyl ester
				50906612	100.00	32804674	100.00			

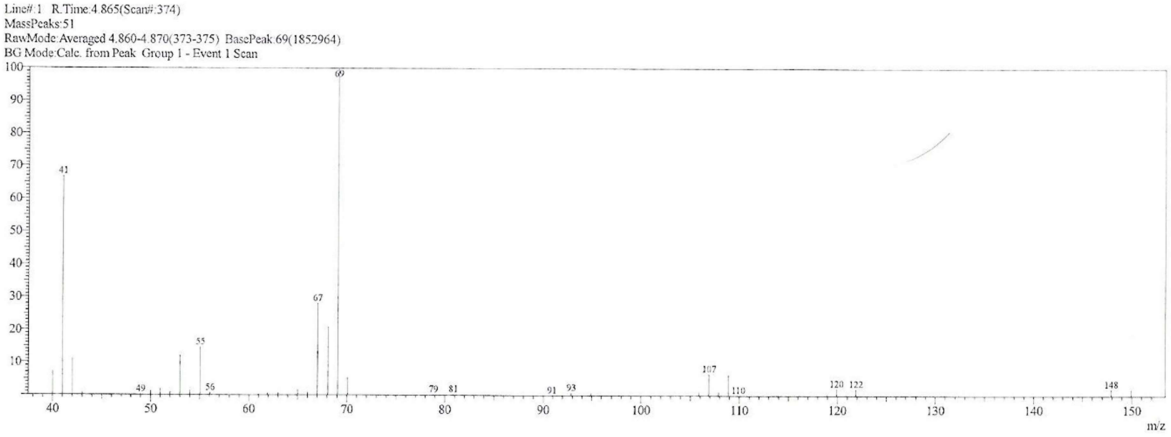

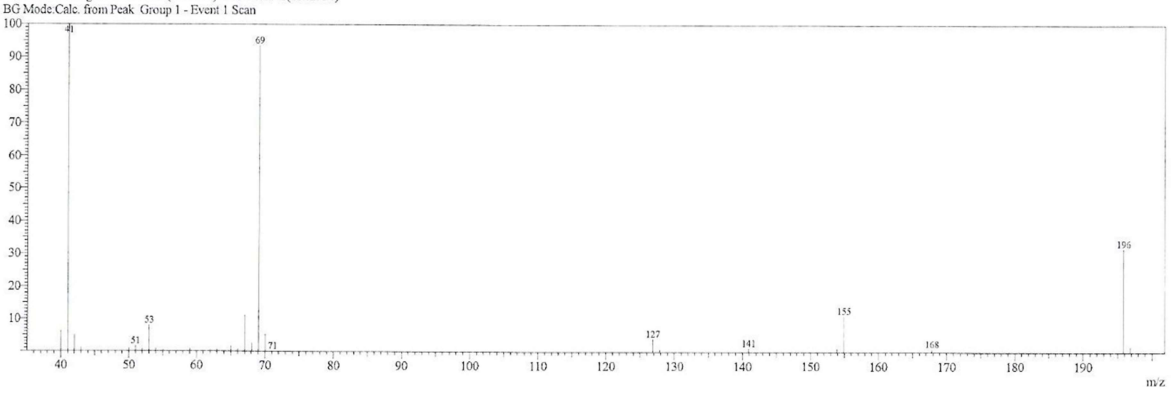

Line#:3 R.Time:11.905(Scan#:1782)
MassPeaks:49
RawMode:Averaged 11.900-11.910(1781-1783) BasePeak:57(880017)
BG Mode:Calc. from Peak Group 1 - Event 1 Scan

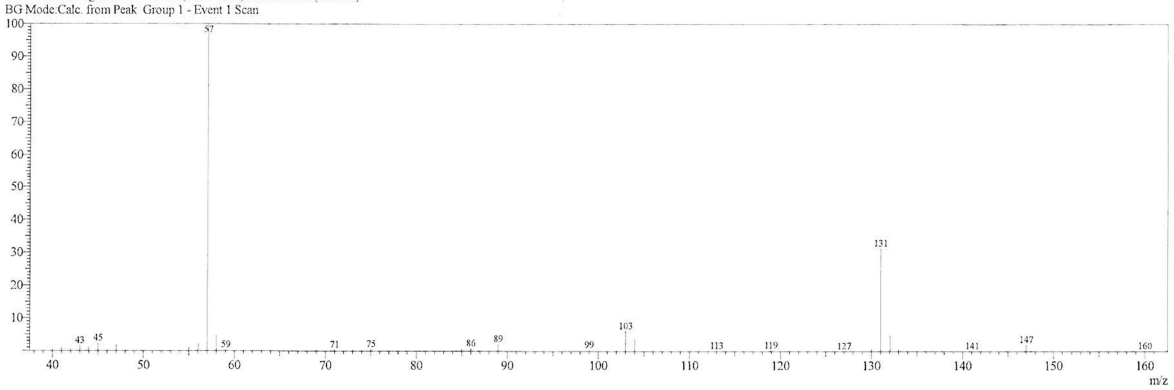

Line#:4 R.Time:15.680(Scan#:2537)
MassPeaks:163
RawMode:Averaged 15.675-15.685(2536-2538) BasePeak:109(1222198)
BG Mode:Calc. from Peak Group 1 - Event 1 Scan

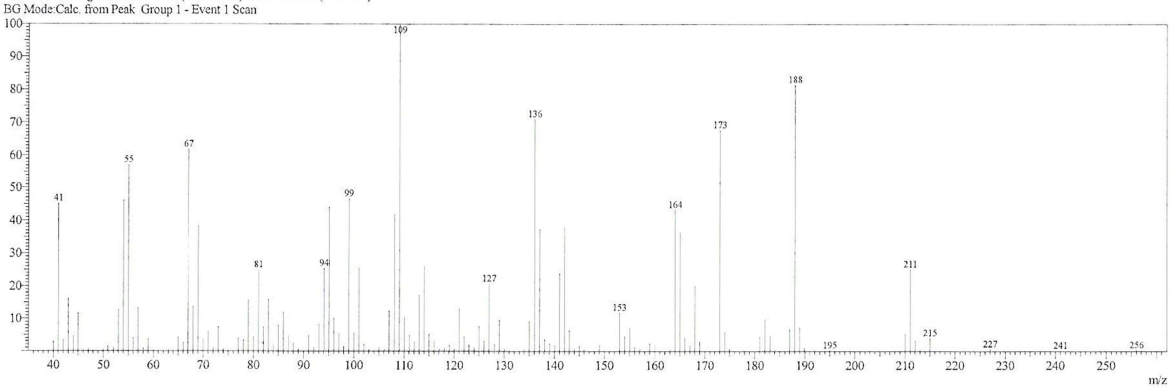

Figure 40. GC-MS of crude ethyl 2-ethyl-6-heptenoate (21b)

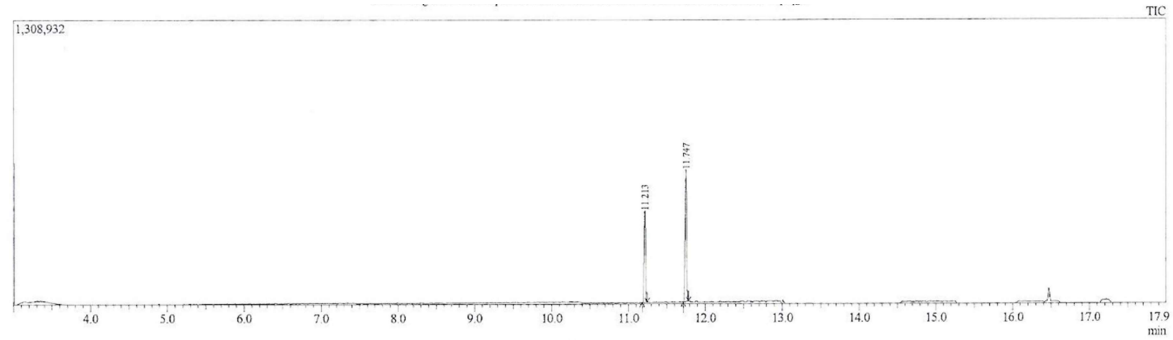

Peak Report TIC

Peak#	R.Time	I.Time	F.Time	Area	Area%	Height	Height%	A/H	Mark	Name
1	11.213	11.180	11.245	576954	40.86	421511	40.94	1.37		Hexanoic acid, 2-ethyl-, ethyl ester
2	11.747	11.715	11.785	835199	59.14	607962	59.06	1.37		2-Ethyl-n-butyric acid ethyl ester
				1412153	100.00	1029473	100.00			

Line#:1 R.Time:11.215(Scan#:1644)
MassPeaks:50
RawMode:Averaged 11.210-11.220(1643-1645) BasePeak:116(70608)
BG Mode:Calc. from Peak Group 1 - Event 1 Scan

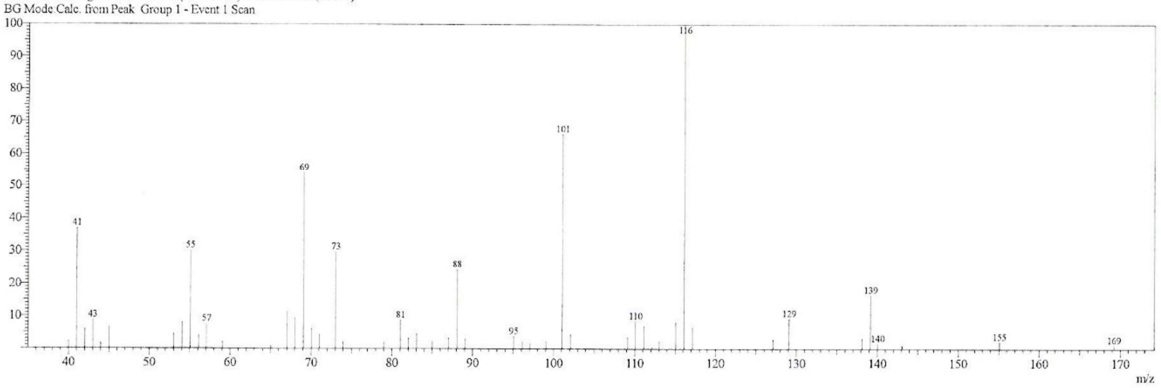

Line#:2 R.Time:11.745(Scan#:1750)
MassPeaks:40
RawMode:Averaged 11.740-11.750(1749-1751) BasePeak:71(157952)
BG Mode:Calc. from Peak Group 1 - Event 1 Scan

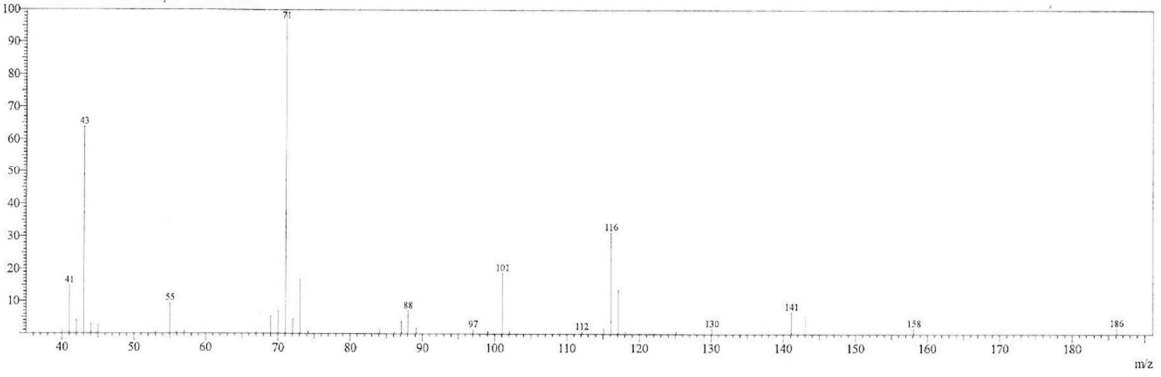

Figure 41. GC-MS of crude 2-ethyl-6-hepten-1-ol (22)

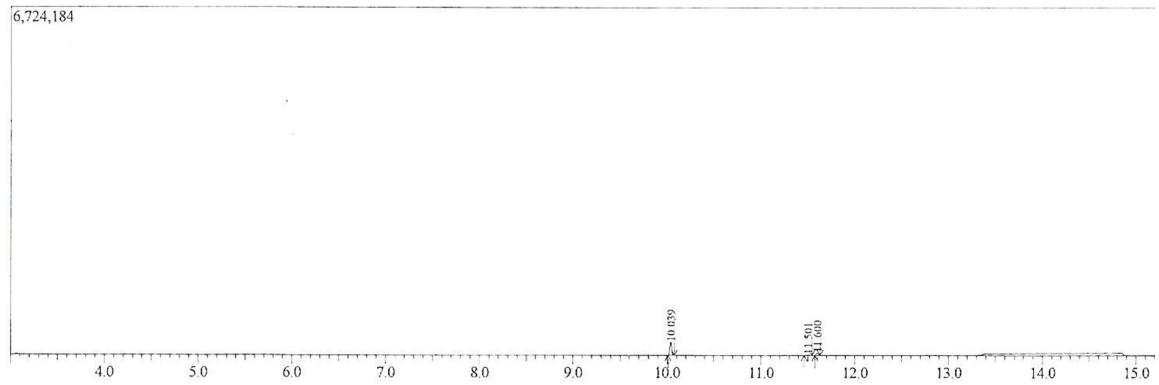

Peak Report TIC

Peak#	R.Time	I.Time	F.Time	Area	Area%	Height	Height%	A/H	Mark	Name
1	10.039	10.010	10.080	348633	79.22	254936	81.11	1.37	MI	3-Nonen-1-ol, (E)-
2	11.501	11.460	11.545	22118	5.03	13658	4.35	1.62	MI	1,3-Propanediol, 2,2-dimethyl-
3	11.600	11.575	11.630	69312	15.75	45714	14.54	1.52	MI	1,3-Hexanediol, 2-ethyl-
				440063	100.00	314308	100.00